HIGH RESOLUTION INTERFEROMETRIC MEASUREMENTS OF RESIDUAL STRAINS IN COMPOSITES

by

Joosik Lee

Dissertation submitted to the Faculty of the
Virginia Polytechnic Institute and State University
in partial fulfillment of the requirements for the degree of

DOCTOR OF PHILOSOPHY

in

Engineering Mechanics

APPROVED:

R. Czarnek, Chairman

N. E. Dowling

D. T. Mook

J. Morton

R. H. Plaut

December, 1990

Blacksburg, Virginia

HIGH RESOLUTION INTERFEROMETRIC MEASUREMENTS OF RESIDUAL STRAINS IN COMPOSITES

by

Joosik Lee

Committee Chairman : Robert Czarnek

Engineering Mechanics

(ABSTRACT)

As composites have been more widely accepted as structural materials, residual stresses in them have become a more serious issue. Various experimental methods have been developed and used to measure residual strains in different kinds and shapes of materials. The anisotropic and heterogeneous nature of composites and the complexity of residual stresses, however, pose limitations on current techniques. Those techniques lack the sensitivity or spatial resolution that is required for the measurement of local deformation of composites on a ply-by-ply basis, or give point-by-point and averaged information. Also they are incapable of resolving the complexity of combined effect of different residual stress components. In order to measure residual strains more effectively, a new method of measuring them is required.

Moire interferometry combined with the cut-and-sectioning method has been developed for effective measurement of residual strains in fiber-reinforced composites. This optical technique provided the capability of studying separately the effect of each component of residual stresses. It also allowed the

determination of high-sensitivity full-field deformation information. This approach was applied to thick composite cylinders for measuring residual strains. The results showed a strong influence of curing procedure on residual stresses.

Also, in order to determine residual strains on a within-the-ply basis, a new high-resolution data reduction procedure has been developed. This procedure enhanced the resolution of the existing data reduction technique without losing qualitative information. The combination of both aforementioned techniques provided an effective tool for measuring residual strains of composite materials. The technique is illustrated in an investigation of the effect of stacking sequence on residual strains in flat composite panels.

ACKNOWLEDGEMENTS

The author wishes to express his sincere appreciation to Prof. Robert Czarnek , the chairman of the committee, for his assistance and guidance during the course of this research. Prof. Czarnek has shared with the author his intelligent ideas and invaluable experiences on the technical issues of this work. Also his deep concern and consideration on non-technical matters are greatly appreciated.

In addition, the author thanks

- his committee members for their participation and guidance,
- Shih-Yung Lin for running a FEM program and other fellow students Ray Boeman, Bongtae Han, Peter Ifju, and Jau-Je Wu for their cooperation and friendship,
- Vicky Czarnek for her constant concern and friendship,
- his parents and parents-in-law whose support and inspiration were indispensable for the author to complete his work,
- his wife, Myungsook, for her patience, understanding, and encouragement throughout his graduate career, and his two sons, Kyungseop and Wonseop, who have spiritually strengthened the author with their smiles.

Research presented in this dissertation was sponsored by the following agencies:

- Research on residual stress measurements in thick composite cylinders was sponsored by Office of Naval Research under University Research Initiative program.

- Research on high resolution data reduction method for interferometric measurements was sponsored by Defence Advanced Research Project Agency and National Science Foundation Science and Technology Center at Virginia Polytechnic Institute and State University.

- Development of the mesh generating program and research on residual stress measurements using moire interferometry and high resolution data reduction technique was sponsored by National Science Foundation Science and Technology Center at Virginia Polytechnic Institute and State University.

Their sponsorship is gratefully acknowledged.

TABLE OF CONTENTS

Page

ABSTRACT ii

ACKNOWLEDGEMENTS iv

LIST OF TABLES viii

LIST OF FIGURES ix

PART 1 : INTRODUCTION

1.1 Motivation 1

1.2 Literature Review 3

1.3 A New Approach 13

1.4 Moire Interferometry 13

1.5 Objectives 17

PART 2 : RESIDUAL STRAINS IN THICK COMPOSITE CYLINDERS

2.1 Introduction 19

2.2 Specimens 20

2.3 Experimental Procedure 23

2.4 Results and Discussion 25

2.5 Summary and Conclusions 46

PART 3 : A NEW PROCEDURE FOR HIGH RESOLUTION DATA REDUCTION

3.1 Introduction 51

3.2 Fringe Pattern Recording and Data Extraction 53

3.3 A New Algorithm 56

Page

3.4 Nonuniform Mesh Generator....66

3.5 Summary....69

PART 4 : HIGH RESOLUTION MEASUREMENT OF RESIDUAL STRAINS IN COMPOSITE PLATES

4.1 Introduction....71

4.2 Specimens and Experimental Procedure....72

4.3 Results and Discussion....73

4.4 Summary....96

PART 5 : CLOSURE

5.1 Summary and Conclusions....99

5.2 Recommendations....102

REFERENCES....103

VITA....108

LIST OF TABLES

Page

Table 2.1 Comparison of residual strains for two different specimens, one with 3 curing stages and the other with 4 curing stages. (a) After the release of the hoop stresses. (b) After the release of the axial stresses. The minimum and the maximum values of strains are separated by a slash. 49

Table 4.1 Comparison of (a) residual strains and (b) the maximum transverse stresses for specimens with different stacking sequences. Note that the residual strains have signs opposite to the measured strains. The minimum and the maximum values of strains are separated by a slash. 97

LIST OF FIGURES

Page

Figure 1.1 Basic two beam moire interferometer. 14

Figure 1.2 A three-mirror, four-beam moire interferometer. 16

Figure 2.1 Specimen configuration and details of the cuts. (a) Stage 1 (b) Stage 2 (c) Stage 3 22

Figure 2.2 U and V fringe patterns representing the deformation of the first specimen due to the bending produced by cutting it open. 27

Figure 2.3 Residual strain distribution in the first specimen due to the open cut 29

Figure 2.4 U and V displacement fields of the first specimen due to the release of the hoop stresses. The concentration of fringes on the V pattern corresponds to high shear zone near the edge of the cut 30

Figure 2.5 (a) Normal strain distribution in specimen #1 due to the release of the hoop stresses. The blank and the shaded rectangles represent 90° and 0° plies, respectively. 31

(b) Shear strain distribution in specimen #1 due to the release of the hoop stresses. The blank and the shaded rectangles represent 90° and 0° plies, respectively. 32

Figure 2.6 (a) Coordinate system of a laminate. (b) The interaction of plies near the edge of a cut. 34

Figure 2.7 Shapes of a laminate (a) before and (b) after a cut was made. The deformed shape is exaggerated. 35

Figure 2.8 U and V displacement patterns of the first specimen due to the release of the axial stresses. 37

Figure 2.9 U and V patterns representing the deformation of the second specimen due to the bending produced by the open cut 38

Page

Figure 2.10 U and V patterns of the second specimen representing the deformation field resulting from the combined effect of global bending and local stress variations. 40

Figure 2.11 (a) Distribution of the normal strains through the thickness of the cylinder wall due to the combined effect of global bending and local stress variations. The blank and the shaded rectangles represent 90° and 0° plies, respectively..... 41

(b) Distribution of the shear strain through the thickness of the cylinder wall due to the combined effect of global bending and local stress variations. The blank and the shaded rectangles represent 90° and 0° plies, respectively..... 42

Figure 2.12 U and V patterns representing the deformation of the second specimen due to the release of the hoop stresses..... 43

Figure 2.13 (a) Normal strain distribution through the thickness of the cylinder wall due to the release of the hoop stresses. The blank and the shaded rectangles represent 90° and 0° plies, respectively..... 44

(b) Shear strain distribution through the thickness of the cylinder wall due to the release of the hoop stresses. The blank and the shaded rectangles represent 90° and 0° plies, respectively..... 45

Figure 2.14 U and V patterns representing the deformation of the second specimen due to the release of the axial stresses. 47

Figure 3.1 Distribution of exposure energy across an interference fringe pattern for three different exposure times. Strips at the bottom of the figure demonstrate the corresponding fringe pattern recorded in high-contrast photographic process..... 54

Figure 3.2 (a) Conventionally recorded fringe pattern representing the horizontal displacement field on a surface of a cantilever beam loaded in bending..... 58

(b) Overexposed moire fringe pattern representing the horizontal displacement field on a surface of a cantilever beam loaded in bending..... 59

Page

(c) Moire fringe pattern representing the horizontal displacement field on a surface of a cantilever beam loaded in bending recorded with overexposed carrier pattern of rotation....60

(d) Moire fringe pattern representing the horizontal displacement field on a surface of a cantilever beam loaded in bending recorded with overexposed carrier pattern of extension....61

Figure 3.3 Electronically generated contour map of U displacement field with standard contour interval of 417 nm. 64

Figure 3.4 Electronically generated contour map of U displacement field with contour interval of 41.7 nm. 65

Figure 3.5 Electronically generated mesh for the epoxy cantilever beam. 67

Figure 4.1 U and V displacement patterns for $[0_4/90_4/0_4/90_4/0_4]$ specimen after the residual stresses are released. 75

Figure 4.2 (a) U and (b) V displacement patterns for $[0_4/90_4/0_4/90_4/0_4]$ specimen after carrier fringes of extension were added. 76

Figure 4.3 A nonuniform mesh produced for data analysis of the specimen with stacking sequence of $[0_4/90_4/0_4/90_4/0_4]$....77

Figure 4.4 (a) Computer generated U-displacement pattern showing a good agreement with the original fringe patterns. Contour interval is 83.4 nm and the original fringes are highlighted by thicker lines. 78

(b) Computer generated V-displacement pattern showing a good agreement with the original fringe patterns. Contour interval is 83.4 nm and the original fringes are highlighted by thicker lines. 79

Figure 4.5 (a) Contour map of the measured normal strain ε_x for $[0_4/90_4/0_4/90_4/0_4]$ specimen with a contour interval of 250 μm/m. 81

Page

(b) Contour map of the measured normal strain ε_y for $[0_4/90_4/0_4/90_4/0_4]$ specimen with a contour interval of 250 μm/m. 82

(c) Contour map of the measured interlaminar shear strain γ_{xy} for $[0_4/90_4/0_4/90_4/0_4]$ specimen with a contour interval of 500 μm/m. 83

Figure 4.6 Formation of σ_x at the edge of a cut. 84

Figure 4.7 (a) Contour map and (b) the distribution along A-A' of the transverse stress in a 90° ply . The maximum value was obtained at the edge of the cut 86

Figure 4.8 U and V displacement patterns for $[0_2/90_2/0_2/90_2/0_2]_s$ specimen after the residual stresses are released. 87

Figure 4.9 (a) Contour map of the measured normal strain ε_x for $[0_2/90_2/0_2/90_2/0_2]_s$ specimen with a contour interval of 250 μm/m. 88

(b) Contour map of the measured normal strain ε_y for $[0_2/90_2/0_2/90_2/0_2]_s$ specimen with a contour interval of 250 μm/m. 89

(c) Contour map of the measured interlaminar shear strain γ_{xy} for $[0_2/90_2/0_2/90_2/0_2]_s$ specimen with a contour interval of 500 μm/m. 90

Figure 4.10 U and V displacement patterns for $[0_2/90_2/0_2/90_2/0_2]$ specimen after the residual stresses are released. 92

Page

Figure 4.11 (a) Contour map of the measured normal strain ε_x for $[0_2/90_2/0_2/90_2/0_2]$ specimen with a contour interval of 250 μm/m. 93

(b) Contour map of the measured normal strain ε_y for $[0_2/90_2/0_2/90_2/0_2]$ specimen with a contour interval of 250 μm/m. 94

(c) Contour map of the measured interlaminar shear strain γ_{xy} for $[0_2/90_2/0_2/90_2/0_2]$ specimen with a contour interval of 500 μm/m. 95

PART 1 : INTRODUCTION

1.1 Motivation

Residual stresses introduced during the manufacturing process can be one of the most important factors in determining structural integrity. Residual stresses can be either beneficial or detrimental, depending upon their distribution with respect to the service-induced stresses. In some cases, residual stresses are produced intentionally to improve the structural performance of a material. For instance, it is well known that shot-peening enhances the fatigue life of metals. Also, in general, stresses in the opposite direction to service-induced stresses may increase the allowable design stress. Steel-reinforced concrete with pre-stressed steel bars is a good example. In other cases, however, residual stresses are unavoidable and undesirable. They can result from a manufacturing process such as machining, drawing, welding, casting, or heat treatment. In fiber-reinforced composite materials, residual stresses are produced during curing, especially at the peak temperature and during the cooling part of the curing process, due to the solidification of the matrix material and different coefficients of thermal expansion (CTE) in the fibers and in the matrix. In laminated fibrous composites, different fiber orientations in different plies are another factor that produce residual stresses. While residual stresses are sometimes negligible, they are usually significant enough so that, when neglected in design, they can cause failure of a structural member below the designed load or prior to the

designed life of the member. When the magnitudes and the directions of residual stresses are not known, they can be accounted for by using a safety factor. An unnecessarily large safety factor, however, makes the structure over-designed, that is, over-strengthened, over-priced and, more importantly, over-weight.

By forming composites, the material properties such as strength, stiffness, corrosion resistance, wear resistance, appearance, weight, fatigue life, temperature-dependent behavior, thermal insulation, thermal conductivity, and acoustic insulation can be improved [1]. An additional advantage is that composite materials can be tailored to efficiently meet design requirement of structural members in various applications. Among those mentioned above, the high strength-to-weight and stiffness-to-weight ratios are the most important aspects of composites, which have made fiber-reinforced composites very useful in weight-sensitive applications such as aircraft and space structures.

As composites have been more widely accepted as structural materials, residual stresses in them have become a more serious issue. The residual stresses in fiber-reinforced composite materials are a function of many parameters such as constituent material properties, stacking sequence and orientation of plies, fiber content, and curing temperature [2]. Chamis [2] pointed out that the residual stresses can reach values comparable to the transverse strength of a ply and thus induce matrix cracking of the plies in a laminate. Residual stresses in each ply are equilibrated with interlaminar shear stresses transmitted, near free edges, from adjacent plies and may result in delamination.

Residual stresses are divided into two categories, micro residual stresses and macro residual stresses [3]. Micro residual stresses are produced due to the different CTE's of the constituents such as, for instance, fibers and matrix in fiber-reinforced composites. The solidification of matrix materials also contributes to the production of micro residual stresses. Macro residual stresses, on the other hand, arise from the different CTE's in the longitudinal and in the transverse directions of plies. Therefore, macro residual stresses exist in those composites which have plies oriented at different angles. Macro residual stresses are also produced due to fiber tension. The magnitude and distribution of macro residual stresses are dependent on the size, shape, and stacking sequence of the laminates. Residual deformations are measured as a combined effect of all different components of residual stresses which exist in a material, and the effect of each component should be quantified separately.

Various experimental methods have been developed and used to measure residual strains in different kinds and shapes of materials, including composite materials. The anisotropic and heterogeneous nature of composites and the complexity of residual stresses, however, give limitations on current techniques. In order to measure residual strains more effectively, a new method of measuring them seems to be required.

1.2 Literature Review

Over the decades, many researchers have developed various experimental techniques for measuring residual strains. Some of the techniques were initially developed for conventional isotropic and homogeneous materials and

modified later for non-conventional materials such as composites. Some others were developed solely for composite materials. Since it is neither practical nor desirable to include all of them here, only the widely-used techniques are reviewed in the next few sections.

1.2.1 Hole-Drilling [4-17]

One of the most popular methods is hole-drilling. In this technique, the residual strains produced when residual stresses are relieved by drilling a hole into a structural member are measured in the vicinity of the hole. An electrical-resistance strain-gage rosette is a common tool for measuring the relieved residual strains, while some other approaches using photoelasticity or brittle coatings can be used. Using analytical and/or empirical methods, the residual stresses can be calculated from information about the magnitude and the direction of the measured residual strains and material properties.

The method was first proposed by Mathar in 1933 [4]. He suggested that "initial stresses", as he called them, in structural members could be determined by drilling a circular hole in them and measuring the resulting deformations. He used a mechanical extensometer to measure diametral changes of a drilled hole. Then he assumed that the distribution of residual stresses was uniform through the thickness of a specimen and used Kirsch's solution to calculate the residual stresses from the measured deformation. Mathar pointed out that, in a plate which is thick relative to the size of a hole, the diametral change of the hole had a limiting value since the stresses relieved at some distance below the surface had no appreciable effect on the deformation at the surface. He also

showed that, in order to determine the residual stresses, the depth of the holes need be only 1.5 to 2 times their diameter. In his analysis, Mathar considered only the cases of simple tension or simple compression.

The extensometer was replaced with electrical-resistance wire strain gages later by Soete and Vancrombrugge [5], measuring strains directly around the hole. Using the strain gages, they avoided the vibration problem that Mathar's extensometer suffered from during the drilling operation. They determined the residual stresses in both butt and fillet welds. In their analysis, Soete and Vancrombrugge assumed that the materials were infinite relative to the size of the hole, elastic, and isotropic. They also assumed the state of plane stress in that stresses do not vary with depth below the surface of the specimens.

Kelsey [6] developed a procedure for using the hole drilling method where the residual stresses varied with depth below the surface of specimen. The method involved determination of the relationship between surface strain and hole depth for a known uniform stress field, and then correlating these data with those obtained by drilling a hole in a known non-uniform stress field, for instance, pure bending. He showed that non-uniform stresses can be evaluated to a depth below the surface of about one-half the hole diameter. The directions as well as the magnitudes of the principal residual stresses were obtained.

Bert et al. developed a method for determining the principal residual stresses and directions in rectangularly orthotropic materials [7] and applied it to glass-fiber-reinforced plastic [8]. Whereas Rendler and Vigness [9] showed

that, for relatively thick isotropic materials, the strain change vs. the ratio of drill depth to drill diameter was the same for the different drill diameters, Bert et al. observed that the same similitude did not exist for their thin composite specimens. Bert et al. suggested that, for relatively thin materials, each combination of thickness and hole diameter must be calibrated.

Nawwar et al. [10] presented a modified hole-drilling technique for measuring residual stresses in sheet and thin-plate materials. The new method eliminated the necessity for calibration of each experimental hole-gage assembly and extended the range of measurement to stresses close to the yield strength. Using the technique, Nawwar and Shewchuk [11] measured stress gradients in a biaxial-residual-stress field by taking a series of point measurements and evaluating the stress profile. They considered the effects of hole location, the interaction between holes, and the redistribution of stress due to hole drilling.

Although the hole-drilling strain-gage method has been used successfully in many applications over the years and recently adapted as an ASTM standard [12] and an industrial technique [13], it has some disadvantages. For instance, a hole should be drilled at the center of the strain-gage rosette. A tiny misalignment of the strain-gage rosette with respect to the hole produces quite significant errors. Ajovalasit [14] showed that 10% of the hole radius off-center yields, depending on the state of stress, up to about 25% stress-measurement error. In addition to that, Sandifer and Bowie [15] pointed out that even a protective-coating technique can greatly affect data reliability. McDonach et al. [16] overcame the difficulties associated with the use of strain-gage rosettes,

such as inaccuracies caused by off-center holes, by utilizing moire interferometry. They measured the in-plane displacements produced by drilling a hole in a T-butt weld. Nelson and McCrickerd [17] used holography instead. Although the hole-drilling method combined with moire interferometry and holography gave full-field displacement information around the hole and solved some of the difficulties related to strain gages, its inherent nature of giving average strain over the thickness of the specimens prevents it from measuring deformation on a ply-by-ply basis and detecting local nonuniformities inside the composite structures.

1.2.2 Layer-Removal [18-25]

A method of determining the residual stresses in cylinders, called the boring-out method, was developed by Sachs [18], in which residual strains developed on the outer surface of the specimen when the inner surface is mechanically removed are measured. The residual stresses in the material removed are then determined by the theory of elasticity. He assumed that the principal axes of residual stress coincided with the principal axes of the cylinder and the material was elastically isotropic. Lambert [19] extended Sachs' theory for the case where the residual stresses are antisymmetric, i.e., the stress state left by plastic bending of the cylinder. With a similar technique to the boring-out method, the residual strains in the inner surface can be measured while layers on the outer surface are removed. This makes the procedure for determining residual stresses in cylindrical specimens complete.

The mechanical method for removing material from the surfaces of the cylinders alters, to some extent, the residual stress distribution. Srinivasan et al. [20] showed that electrochemical machining (ECM) offers an excellent method of removing metal without altering residual stresses. Rasty and Hartley [21] used ECM for measuring residual stresses in Zircaloy-4 that is used extensively as nuclear fuel cladding in light water reactor cores. Olson and Bert [22] and Voyiadjis et al. [23] extended previous analyses of residual stresses to the case in which the material exhibits cylindrical elastic anisotropy, i.e., the principal axes of anisotropy are parallel to the principal axes of the cylinder. The analysis by Voyiadjis et al. also determined the residual shear stress in the wall of the tube. Voyiadjis and Hartley [24] further extended their previous analysis for cylindrically orthotropic materials, in that solutions were obtained for an n-layered tube. In their analysis they assumed that constituents of the tube were homogeneous within each layer and elastically orthotropic with different elastic constants. Toombes et al. [25] measured residual strains on the inner surface of graphite/epoxy tubes by mechanically machining the outer surface of the tubes. They used the analysis by Voyiadjis et al. [23] to obtain the hoop, axial and radial residual stresses. In the data reduction, they accounted for the change in the lamina modulus with respect to the radius.

As in the hole-drilling technique, only averaged information about deformation through the thickness of the cylindrical specimens is obtained in the layer-removal method.

1.2.3 Photoelasticity [26-29]

Photoelasticity is a well known optical technique for measuring stresses [26]. When a polarized light enters into a photoelastic material, which is optically isotropic when free of stress and becomes optically anisotropic when stressed, the light is separated into two linearly polarized beams of light. Since the refractive index for one polarization is different from that for the other, which is called double refraction, the phase shift occurs between two light waves. Due to this phase difference, an interference pattern is obtained. Stresses are then determined from the stress-optic law that relates the principal stress difference to the fringe orders of the photoelastic fringe pattern.

While photoelasticity has been widely used in numerous applications, it is not viable for measurement of composites because it is restricted to transparent materials [27,28] or homogeneous materials in cases where a photoelastic model of a real structure can be made [29]. Although a photoelastic coating can be utilized to study opaque materials, its low sensitivity and low resolution are a significant drawback.

1.2.4 Acoustical Techniques [30-36]

In this category, two different techniques are reviewed, one normally used with Rayleigh surface waves for surface residual stress measurement, the other with transverse shear waves for residual stress measurement inside the materials. In this work, the former is simply called the ultrasonic method and the latter acoustoelasticity as to differentiate from the former.

The ultrasonic method utilizes the fact that the velocity of an ultrasonic wave propagating in a material changes with applied stress. The method involves inducing an ultrasound wave with frequencies varying from a few hundred kilohertz to several megahertz into the specimen and measuring its velocity change with stress. For measuring residual stresses, Rayleigh surface waves are normally used. The velocity of the surface wave is determined by measuring the time for the wave to travel the gage length defined by the distance between the receiving and the transmitting transducers. Residual stresses for a given material are then calculated by measuring the relative change in the travel time as a function of applied stress. Since an ultrasound wave of shorter wavelength penetrates deeper below the surface of a material, one can measure the subsurface stresses and the stress gradient normal to the surface by varying the frequencies of the wave.

The acoustoelastic technique is based on the principle that an acoustically isotropic material becomes anisotropic when stressed. Since ultrasound waves have some properties of electromagnetic waves such as polarization, reflection, transmission, diffraction and interference, the ultrasonic similitude to visible light can be utilized for measuring residual stress, i.e., the ultrasound wave is split into two linearly polarized waves when it enters the material, and propagates along the principal directions with different velocities. By using the stress-acoustical law which says that the velocity difference between the two principal waves is directly proportional to the difference of the two principal stresses [30], the residual stresses can be determined provided that the material properties are known. While both longitudinal and transverse shear waves can be used

for regular stress measurements, the latter with frequencies of typically 2 to 10 MHz are normally used for residual stress measurement.

The method of acoustoelasticity has been widely used to determine residual stresses in metals with various shapes. Fukuoka et al. measured residual stresses in a patch-welded circular disk made of mild steel [31] and in a wide-flanged rolled beam [32]. Noronha and Wert [33] applied the acoustoelastic analysis to a section of a steel I-beam. Whereas elastic behavior of materials was assumed in most of the previous work, Johnson [34] pointed out that the plastic deformation caused changes in acoustic response to various degrees depending upon the materials and, therefore, careful acoustic characterization of the material was necessary for precise stress determination. He introduced the acoustoelastic theory for elastic-plastic materials [35]. Lu [36] used Johnson's theory to determine the residual stresses in aluminum specimens and stated that further development of the ultrasonic technique for elastic-plastic material was needed.

Although the acoustical techniques are very useful in some applications due to their nondestructive nature, they have many drawbacks that make their usage limited. First, they give average stress over a certain depth below the surface of a specimen in the ultrasonic method and over the thickness of a specimen in acoustoelasticity . Secondly, they have low resolution. Thirdly, it is very difficult to separate the effects on velocity changes of stress from those of material inhomogeneity and anisotropy. The acoustical techniques are, therefore, not suitable for applications to laminated composite materials where ply-by-ply or within-the-ply analysis is desired.

1.2.5 The Embedded Strain Gage Method [37-41]

Daniel et al. [37] embedded strain gages to measure subsurface strains in laminated composite materials. In this method strain gages were aligned relative to the fibers and laid down between plies without using any adhesive. Then the assembled specimens were cured in an autoclave and the residual strains produced at the peak temperature and during the cooling part of the curing procedure were measured. The heating part seemed to produce no residual strains. It was shown that conventional strain gages, when a patch of scrim cloth was removed, do not produce local thickening of the specimen, do not change the average material properties, and do not reduce the strength of the specimen. To compare strains during curing with those due to purely thermal expansion, the specimens were subjected to a thermal cycle from room temperature to the curing temperature and back down to room temperature. The results indicated that residual stresses induced during the curing process are primarily caused by different CTE's of the different plies. This technique was used for measuring residual strains in composite materials with various kinds of fiber and matrix systems such as boron/epoxy and glass/epoxy [38], graphite/polyimide [39], graphite/kevlar/epoxy and graphite/S-glass/epoxy [40], and woven glass/epoxy systems [41].

The embedded strain gage method is very useful in measuring subsurface strains between the laminae as well as surface strains and, therefore, predicting failure of a composite structure. It is, however, unable to provide either the

information of deformation in the direction perpendicular to the laminae or that within the lamina. Furthermore, it only gives average strains.

1.3 A New Approach

The above mentioned experimental techniques have been used successfully in many applications. However, they do not allow us to measure residual strains on a ply-by-ply basis. Neither do they separate combined effects of residual-stress components. The new method, i.e., moire interferometry combined with the cut-and-sectioning technique, provides an effective way of measuring residual strains. It offers full field measurement of residual deformation of composites at a micro or a sub-ply* as well as a macro level, detects local non-uniformities and imperfections, and separates the combined effects of different components of residual stresses.

1.4 Moire Interferometry

Moire interferometry is an optical method which provides whole-field information of in-plane surface displacements [42]. It is based on two beam interference. A high-frequency diffraction grating is replicated on the specimen surface and deforms together with it. The specimen grating is illuminated by two mutually coherent collimated beams of laser light as illustrated in Figure 1.1. Their +1 and -1 diffraction orders carry information about the deformation of the specimen grating. The diffracted beams interfere, producing

---

* The level of the measurements depends on the size of fiber. For instance, the deformation around a graphite fiber (7 μm in diameter) can not be measured while that around a boron fiber (100 μm in diameter) can since the spatial resolution of the measurements is about 10 to 15 μm.

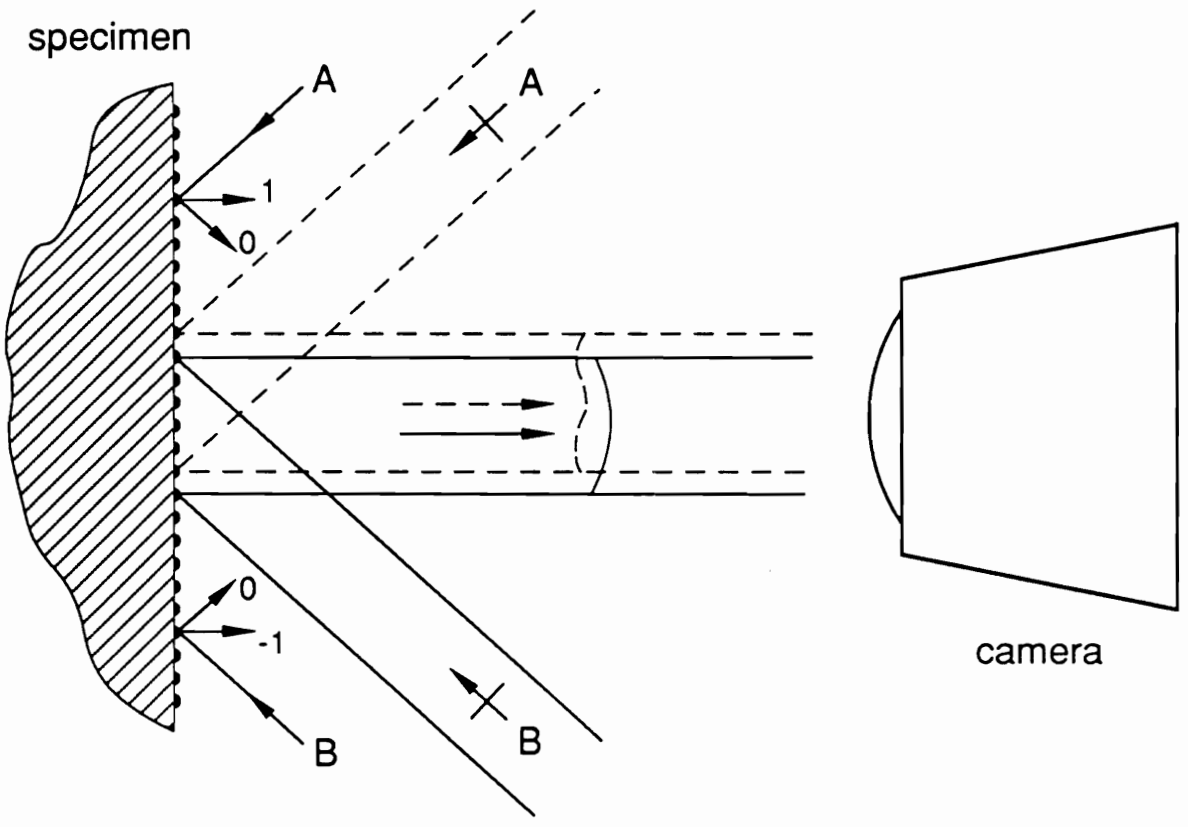

Figure 1.1 Basic two beam moire interferometer.

an interference fringe pattern. This pattern is a contour map of in-plane displacements in the direction perpendicular to the grating lines. Consequently, in the x-y plane, the grating lines parallel to the x axis yield a displacement pattern in the y direction, V, and similarly those parallel to the y axis produce an x displacement component, U. In practice a three-mirror, four-beam interferometer [43,44] is used, providing two orthogonal components of in-plane displacements simultaneously. Figure 1.2 shows a diagram of the interferometer used in this work.

The governing equations for U and V are

$$U = \frac{\lambda}{2\sin\theta} N_x \qquad V = \frac{\lambda}{2\sin\theta} N_y \tag{1.1}$$

where N_x and N_y are the fringe orders of the U and V fringe patterns, respectively, λ is the wavelength of the light used and 2θ is the angle of intersection of the two illuminating beams. A fringe order is defined as a number assigned to a fringe and is equal to the measured parameter divided by a contour interval.

Normal and shear strains are then calculated from the following strain-displacement relations;

$$\varepsilon_x = \frac{\partial U}{\partial x} = \frac{\lambda}{2\sin\theta}\frac{\partial N_x}{\partial x} \qquad \varepsilon_y = \frac{\partial V}{\partial y} = \frac{\lambda}{2\sin\theta}\frac{\partial N_y}{\partial y} \tag{1.2a}$$

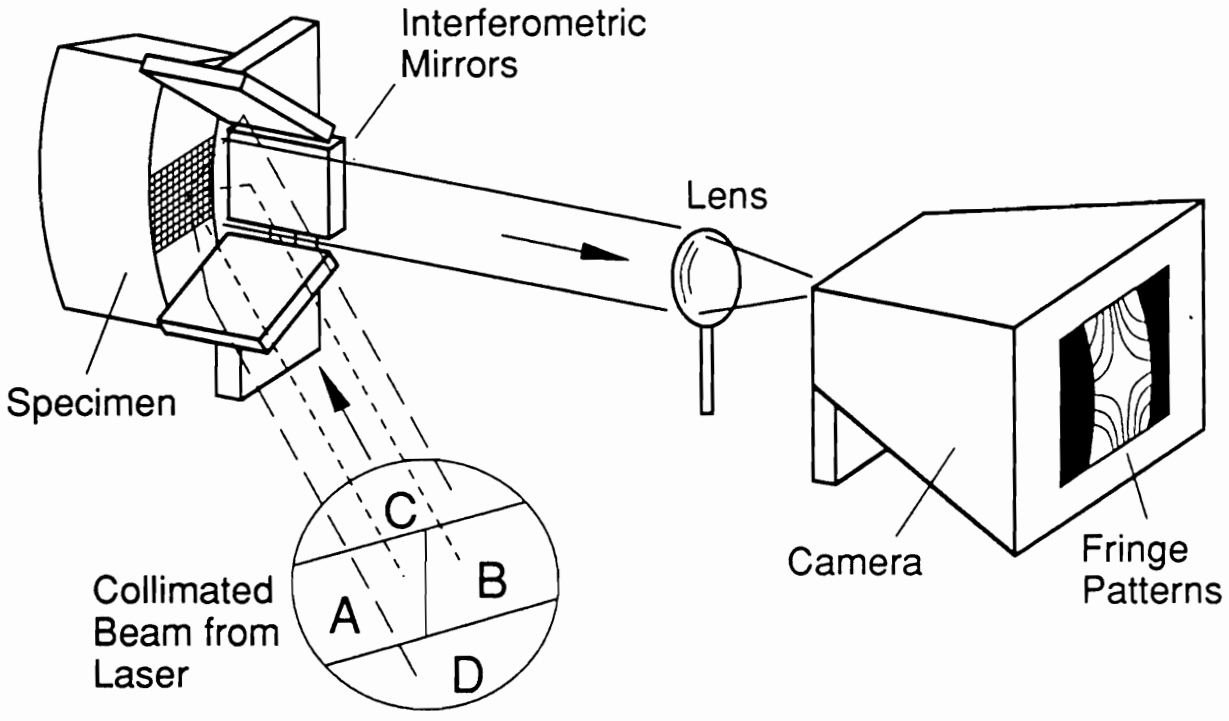

Figure 1.2 A three-mirror, four-beam moire interferometer.

$$\gamma_{xy} = \frac{\partial U}{\partial y} + \frac{\partial V}{\partial x} = \frac{\lambda}{2\sin\theta}\left[\frac{\partial N_x}{\partial y} + \frac{\partial N_y}{\partial x}\right] \qquad (1.2b)$$

The sensitivity of the measurements is $\lambda/(2\sin\theta)$ and, with the standard configuration used at VPI&SU, is equal to 0.417 μm per fringe order.

1.5 Objectives

The objective of this work was to experimentally determine residual strains introduced during manufacturing process in composite materials. This includes developing a new test method and measuring residual strains. Moire interferometry was chosen as a measuring tool for the high-sensitivity, high-resolution, high-contrast and full field information that it can provide. This work is focused on macro residual stresses and/or the corresponding residual deformations since they are much more critical in designing structures than micro residual stresses.

The main objective of the second part was to develop a new technique for effective measurement of residual strains. The residual strains introduced to thick graphite/epoxy composite cylinders during the manufacturing process were studied by utilizing the new approach, the cut-and-sectioning method combined with moire interferometry. The detailed procedure of the method is described. The development of a new data reduction procedure is presented in Part 3. An example of the application of the new algorithm to an isotropic and homogeneous material is included. The new algorithm enhanced the

resolution of measurement of regular moire interferometry without losing qualitative information of deformation. In Part 4, the new procedure for high-resolution data reduction described in Part 3 is applied to obtain the distribution of residual strains in graphite/epoxy composite plates. Specimens with three different stacking sequences were tested to study the effects of size and stacking sequences of plies on residual strains.

PART 2 : RESIDUAL STRAINS IN THICK COMPOSITE CYLINDERS

2.1 Introduction

Composite cylinders have been widely used for various engineering applications such as airplanes, submarines, missiles and other space structures because, in addition to high stiffness-to-weight and high strength-to-weight ratios of general composite structures, they offer high torsional and bending stiffness per unit weight. They also eliminate the free-edge problem which exists in other structures.

Residual stresses in thick composite cylinders are a more serious issue than those in flat composite plates because of their shape. Also, in general, the thicker the composite structures, the larger the residual stresses. Recently attempts by the composite industry to fabricate thick composite cylinders have resulted in frequent failures during or after curing process because of the residual stresses produced by the difference between the curing temperature and room temperature. Space structures operate in very low temperatures so the residual stresses will be a lot greater. The temperature could be as low as about -150°C (-238°F), and the difference between this and the curing temperature is about twice as large as that between room temperature and the curing temperature. Manufacturers, therefore, usually make thick composite cylinders in a few stages to prevent them from premature failure. The procedure consists of a few repetitions of lay-up and curing. In other words, a lay-up with a

thickness of a fraction of the total desired thickness is made and cured. Another lay-up is made and cured. This procedure is repeated until the total desired thickness is achieved. The procedure is, however, usually based on the trial-and-error method and there is no extensive data, neither analytical nor experimental, that can make the procedure more reliable and effective. A lot of experimental and analytical work on the residual stresses and strains has been performed in recent years. All the analytical work, however, requires assumptions and/or approximations, and the experimental work lacks the sensitivity that is required for local measurement of deformation on a ply-by-ply basis. Additionally, neither analytical nor experimental work was found to include the effect of curing stops. Hence the necessity arises for developing a new tool for effectively measuring residual strains, especially in thick composite cylinders that include a few curing stages.

The objective of this part was to experimentally study the residual deformation introduced in thick composite cylinders during the manufacturing process. Measurements at the sub-ply level are desired to analyze the residual deformation of thick composites. In order to achieve this goal, moire interferometry combined with the cut-and-sectioning technique is selected.

2.2 Specimens

2.2.1 Specimen #1

The first specimen was a 25.4 mm (1 in) wide ring with an outside diameter of 203 mm (8 in) and a wall thickness of 15.2 mm (0.6 in). It was cut out of a composite cylinder. The material was a cross-ply graphite/epoxy

composite with the fibers oriented along the hoop (90°) and the axial (0°) directions in a $[90_2/0]_{29}/90_2$ sequence. The composite was cured in three stages at approximately 1/2t, 3/4t and t, where t is the thickness of the cylinder, measured from the inner wall.

The specimen was manufactured by Hitco, Inc. of Gardena, California. The fibers were of the Celion 6K type and epoxy system E707 was used as the matrix. The cylinder was prepared by pre-preg filament winding in the hoop direction and hand installed in the axial direction. The fiber tension was 22.24 to 35.58 N/tow (5 to 8 lbs/tow), and the tow/ply thickness was 0.188 mm (0.0074 in) in the hoop direction and 0.14 mm (0.0055 in) in the axial direction.

In order to minimize the instability of the specimens due to moisture and temperature changes during the experiment, they were stored in the laboratory for a few weeks where the tests were performed. Additionally all the gratings were replicated in the same testing laboratory. The experiment for each specimen was completed in 24 hours to avoid time-dependent deformations. The geometry and the dimensions of the specimens are shown in Figure 2.1(a). The locations of diffraction gratings and strain gages are also included in the figure.

2.2.2 Specimen #2

The second specimen had the same geometry as the first one. It was made by the same manufacturer with the same types of fibers and epoxy system. The difference was in the number of plies and in the curing stages.

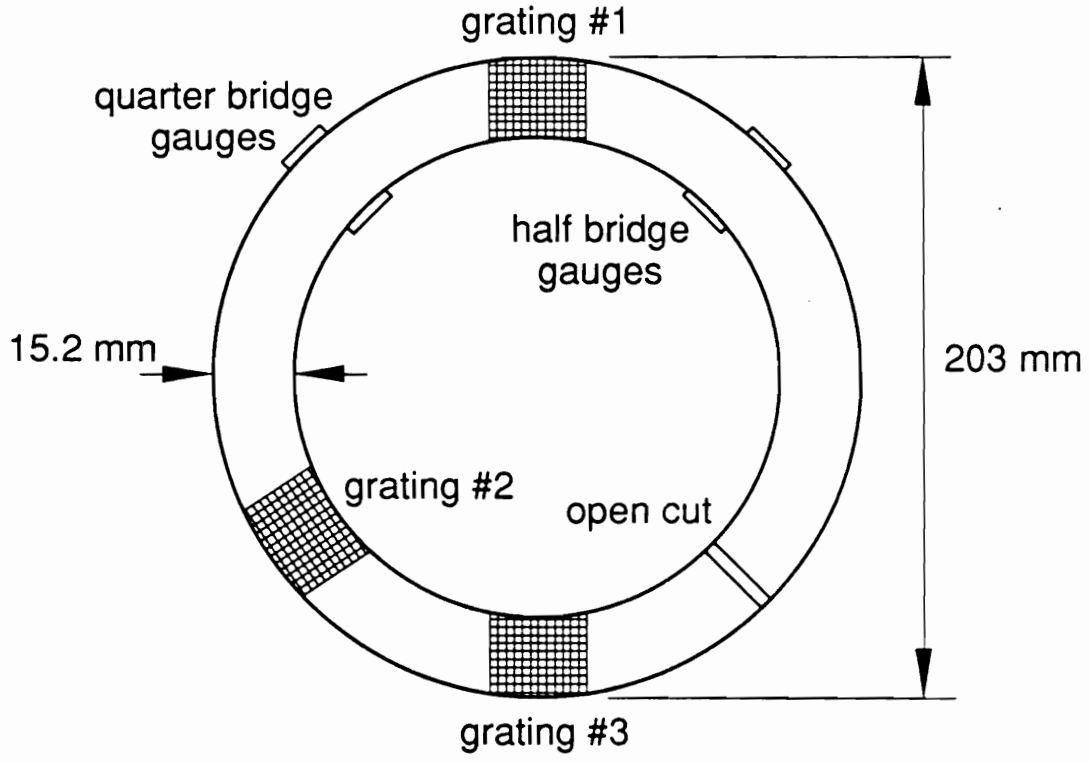

(a)

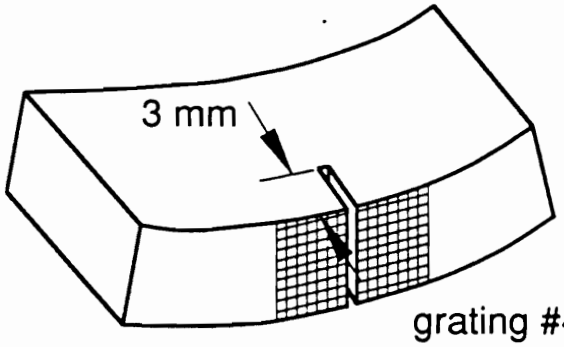

(b)

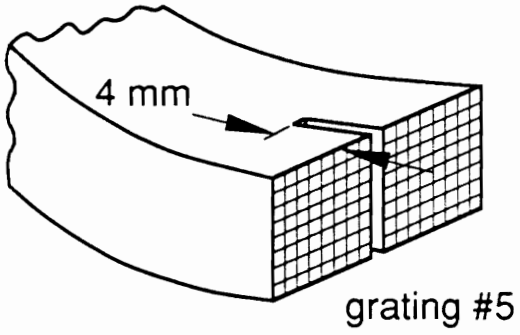

(c)

Figure 2.1 Specimen configuration and details of the cuts.
(a) Stage 1 (b) Stage 2 (c) Stage 3

The cylinder had a stacking sequence of $[90_2/0]_{28}/90_2$ and was cured in four stages at 1/4t, 1/2t, 3/4t and t. For this specimen, strain gages were not used. The preparation procedure was the same as for the first specimen.

2.3 Experimental Procedure

Suppose a piece of material is stress-free. A diffraction grating is replicated on one of the surfaces of the specimen. At this point the lines of the grating are perfectly straight and uniformly spaced. Now imagine that the specimen is cut into two pieces with a saw that does not introduce any machining stresses. Since the specimen was initially stress free, the stress distribution on the surface of the cut would not change. If the specimen were positioned in a moire interferometer, the resulting interference patterns would show no fringes. A preliminary test was performed on a piece of thick composite cylinder to see how far from the state of stress-free the actual specimen was. The measured deformation was a combined effect of all the different components of the residual stresses. As such it was very difficult, if not impossible, to analyze. In order to separate the complicated effect of different stress components, measurements were performed in three stages. In each stage, a cut was made in a relevant direction in order to release the stress in the direction perpendicular to the cut. The same procedure was used for both specimens.

The purpose of the first stage of the experiment was to measure the effect of residual stresses on a global scale. Three crossed-line diffraction gratings were replicated on the surface perpendicular to the axis of the ring, among

which two gratings were backups for the other in case of damage. For the first specimen two strain gages were also attached, one onto the inside and the other onto the outside surface of the specimen, providing additional check points. Then the optical system was tuned for the undeformed grating after positioning the specimen in the system, and a set of patterns was recorded for reference. A small section of the ring was removed in order to release any bending in the plane of the cross-section that could exist in the wall of the cylinder. The specimen was then repositioned in the optical system and the resulting patterns were recorded. Figure 2.1(a) shows the details of the stage 1.

In the second stage (see Figure 2.1(b)), residual deformations associated with the normal stresses in the hoop direction were measured. A piece of the ring about 80 mm long was removed. A new grating was then replicated on the surface of the specimen perpendicular to the axis of the cylinder and a set of patterns was recorded for reference. An approximately 3 mm deep cut perpendicular to the grating and parallel to the radial direction was introduced to release the hoop stresses. The cut was made through the specimen grating.

Figure 2.1(c) illustrates the details of the third stage. The experiment was done in order to measure the residual deformations associated with the normal stresses in the axial direction. A section about 80 mm long was removed from the ring by making a cut along the radial plane parallel to the axis of the cylinder. A grating was replicated on the surface of the cut. As before, a set of patterns was recorded for reference and a cut perpendicular to the grating and the axis of the cylinder was introduced through the grating to a depth of about 4 mm to release the axial stresses.

In order to capture all the important information, measurements were made at every single step of the experiments. Additional measurements were performed to provide additional check points in the analysis of the results. The patterns were recorded both with and without appropriate carrier patterns to make the data reduction procedure more accurate and effective. In order to avoid thermal effects and assure a clean cut with well-defined edges, a slow rpm precision diamond saw was used throughout the whole experiment.

2.4 Results and Discussion

For the analysis of the results, the thickness of each ply in both specimens was measured. While the thickness is given as constant by the manufacturer, it was found to be variant from ply to ply. The measured thickness of each ply is included in the plots for easy interpretation of the results. For stages 2 and 3, data were collected along the cuts at the centers of the plies for the normal strains and at the interfaces for the shear strains. These points corresponded to the local extremum values of the measured parameters.

In the first and the second stages of the experiment, gratings with straight lines were replicated on the surface perpendicular to the axis of the cylinder such that theoretically only one grating line coincides with the radial direction. The cuts were made along, or very close to, this line. Whereas the measured displacements U and V at the edges of the cuts correspond to the displacements in the radial and the hoop directions, they do not at the regions away from the cuts. Consequently, in this work, the fringe patterns are called U

and V patterns instead of the displacement patterns in the radial and the hoop directions.

When tensile residual stresses in a structure are released, compressive strains are measured. In other words, if compressive residual strains are measured after the release of residual stresses, then it can be said that those residual stresses which existed in that structure before the release were tensile. The same thing is true for compressive stresses and tensile strains. In this section the results are presented in terms of "residual" strains which have the same magnitudes and the opposite signs as the "measured" strains. Consequently, if the word "measured" is omitted, then the word "strains" means residual strains.

2.4.1 Specimen #1

The first set of patterns shown in Figure 2.2 represents the state of deformation due to bending after a small section was removed. Those patterns are typical for structures loaded in bending except for the zigzags in the U field pattern. Those zigzags represent the oscillation of the normal strain in the r-direction between the local tension and local compression due to different material properties in different plies. The residual moment introduced tension in the hoop direction on the inner surface and compression on the outer surface. A critical effect of this type of loading is interlaminar tension through the thickness of the cylinder. Combined with the stresses caused by a service-induced load, this stress can contribute to delaminations. The distribution of residual strains corresponding to the pattern shown in Figure 2.2 through the

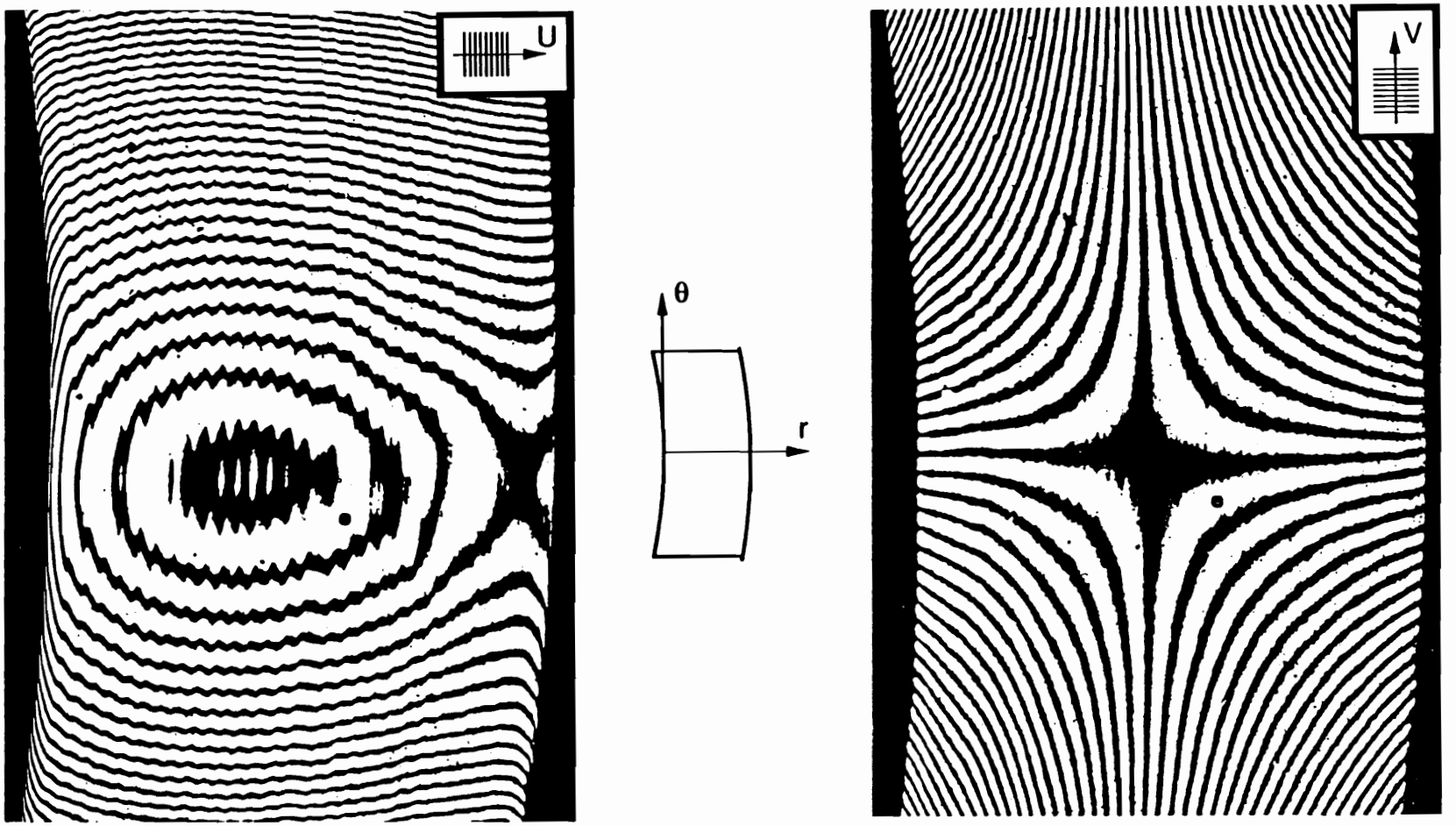

Figure 2.2 U and V fringe patterns representing the deformation of the first specimen due to the bending produced by cutting it open.

thickness of the wall of the cylinder is illustrated in Figure 2.3. In this figure the local variations of residual strains were neglected. The normal residual strain in the hoop direction varied from 700 μm/m on the inner wall to -900 μm/m on the outer one. These values agreed with those obtained by using strain gages. The normal strain in the radial direction ranged from -1000 μm/m to 200 μm/m. As expected for a curved beam loaded in bending, the neutral axis does not coincide with the central axis. Global shear strain was negligible.

Figure 2.4 shows the displacement patterns related to the release of the hoop stresses. Easily noticed in the patterns is high level interlaminar shear strain in the vicinity of the plies where the curing stops took place. These are indicated by the concentration of fringes in V field pattern. This indicates that large stresses will develop in the material if an opening in the plane perpendicular to the axis of the specimen is introduced in the cylinder. Figures 2.5(a) and 2.5(b) demonstrate the distributions of residual normal strains and residual shear strain, respectively, through the thickness of the cylinder wall. The extremum values in the center of each ply for normal strains and between the plies for shear strain were connected by straight lines to show the trend of deformation. The normal strains in the radial direction obtained at the edge of the cut varied from -2500 μm/m to 600 μm/m and in the hoop direction from -1000 μm/m to 2000 μm/m. The magnitudes of shear residual strain varied from -8500 μm/m up to 6000 μm/m. The maximum values correspond to about 25% for normal strain and 40% for shear strain of the failure strain, and it is obvious that the corresponding stresses can cause premature failure when superposed with service-induced stresses. It is

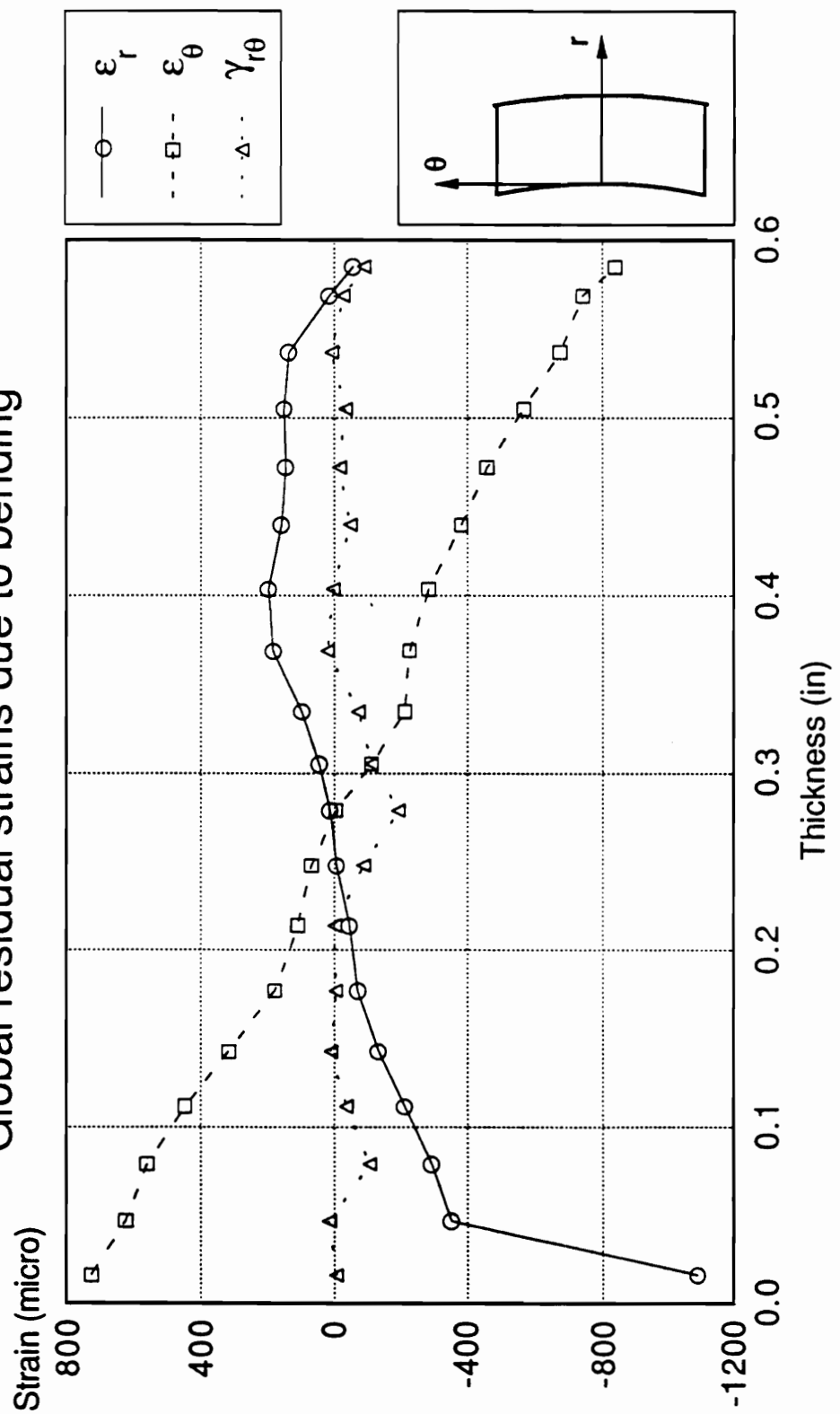

Figure 2.3 Residual strain distribution in the first specimen due to the open cut.

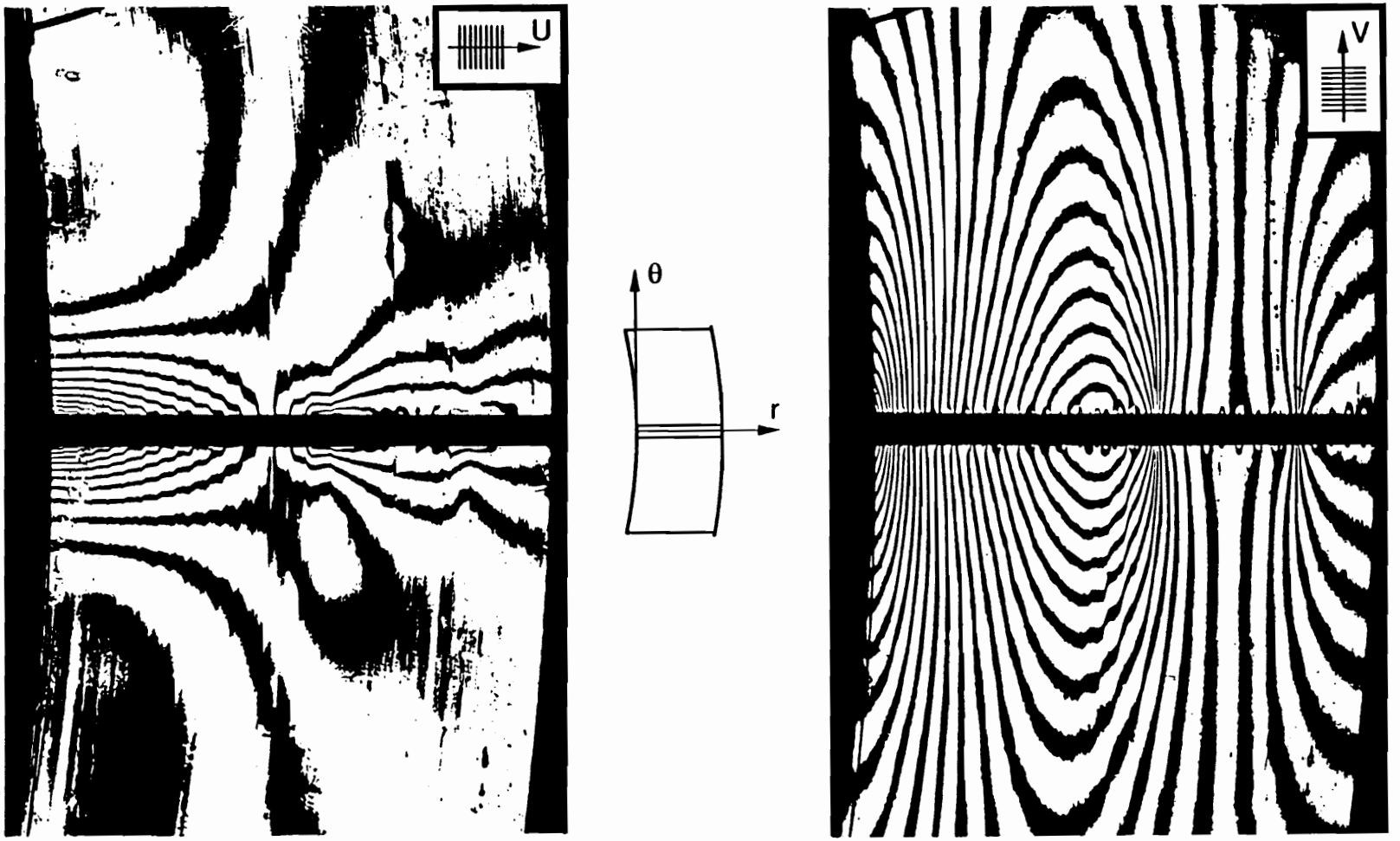

Figure 2.4 U and V displacement fields of the first specimen due to the release of the hoop stresses. The concentration of fringes on the V pattern corresponds to high shear zone near the edge of the cut.

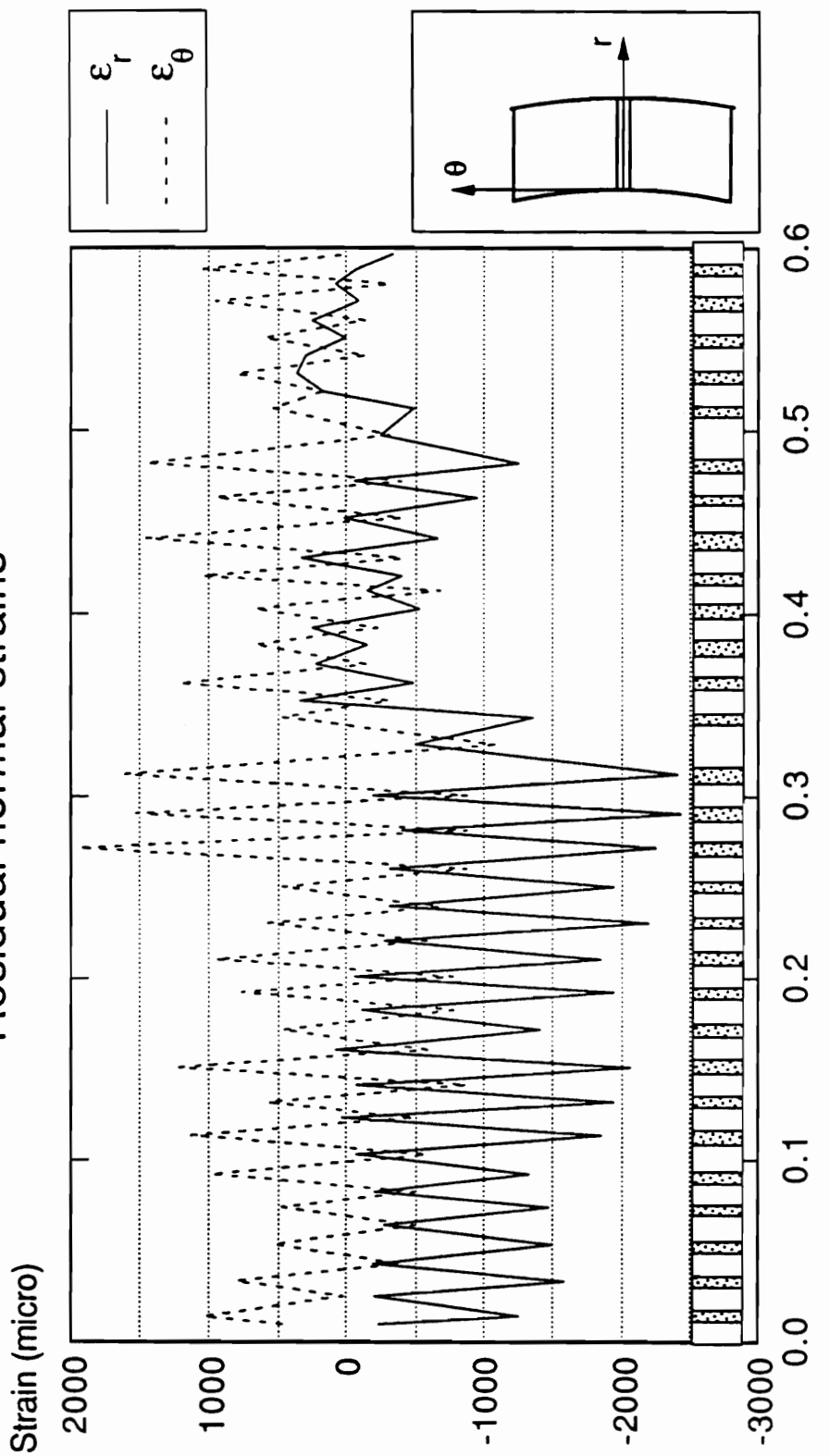

Figure 2.5 (a) Normal strain distribution in specimen #1 due to the release of the hoop stresses. The blank and the shaded rectangles represent 90° and 0° plies, respectively.

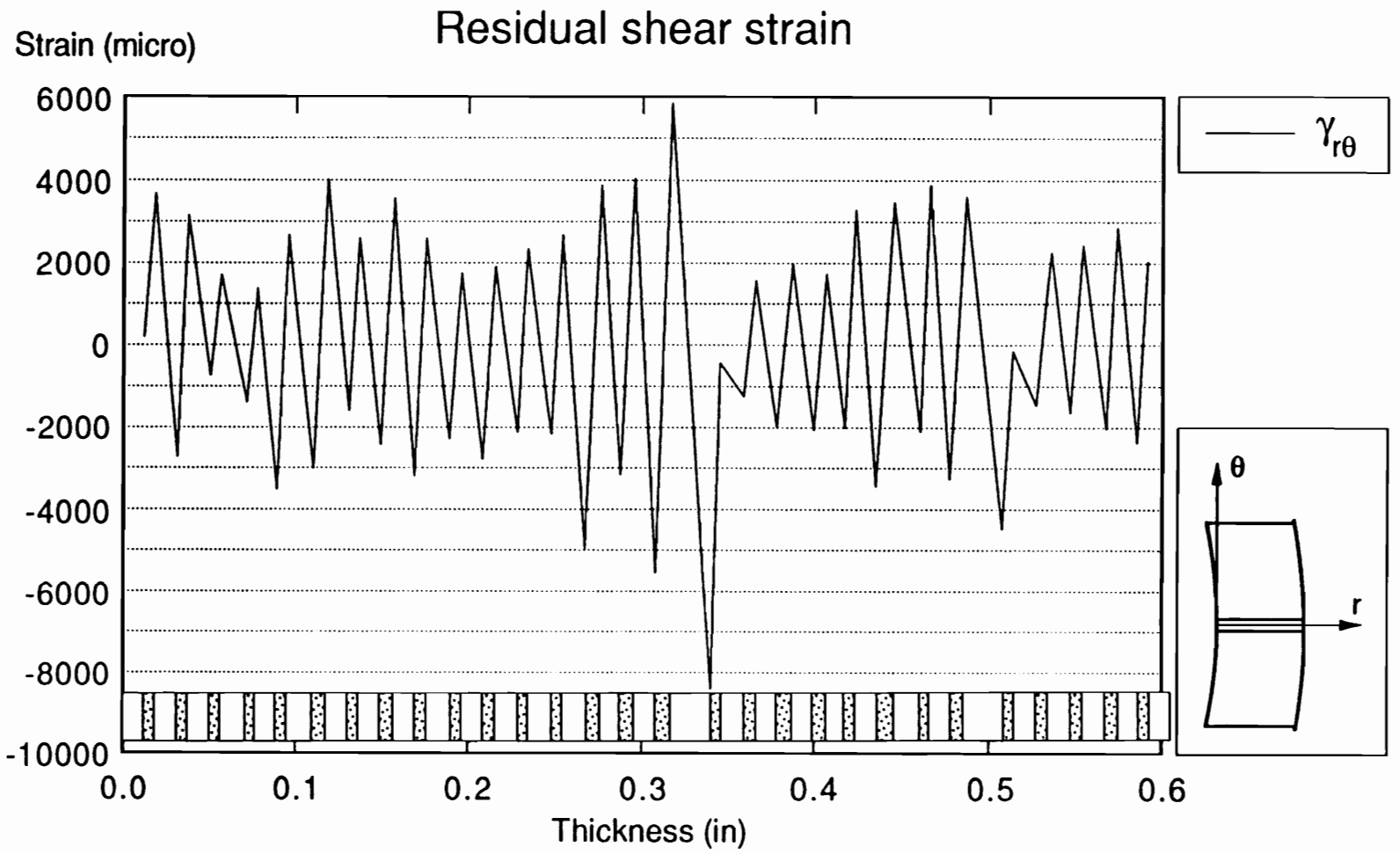

Figure 2.5 (b) Shear strain.distribution in specimen #1 due to the release of the hoop stresses. The blank and the shaded rectangles represent 90° and 0° plies, respectively.

interesting to note that both normal and shear strain concentrations exist at the curing stops.

In Figure 2.5(a) and Figure 2.5(b), both normal and shear strains oscillate between local extremum values. There are two major factors that produce this oscillation. One is the different CTE's of a lamina in the directions parallel and perpendicular to the fibers, which are attributed to the different CTE's between the fibers and the matrix materials. Upon curing, a single ply tends to contract more in the direction perpendicular to the fibers than in the fiber direction. However, a ply in a cross-ply laminate, for instance a 90° ply, cannot deform freely because it is bonded to the adjacent 0° plies. Rather it deforms together with those 0° plies. Since, when a laminate is seen from the x-direction in Figure 2.6(a), 0° plies contract less in the y-direction than 90° plies, they exert shear stresses and, therefore, effectively tension in that direction to the neighboring 90° plies (see Figure 2.6(b)). Conversely 90° plies compress the adjacent 0° plies. When these residual stresses are released by making a straight cut, the edge of the cut would not remain straight due to the interaction of the plies. An exaggerated shape of the final deformation is shown in Figure 2.7(b).

The other factor is the tension that exists in the fiber tows used in the filament winding process. This tension produces tensile residual stresses in the fiber direction of filament wound plies, the ones in the hoop direction in this case. It is interesting to note that the signs of the residual stresses are opposite to those mentioned in the previous paragraph. The fiber tows also produce, when wound in the hoop direction, outward bending moment in the cylinder,

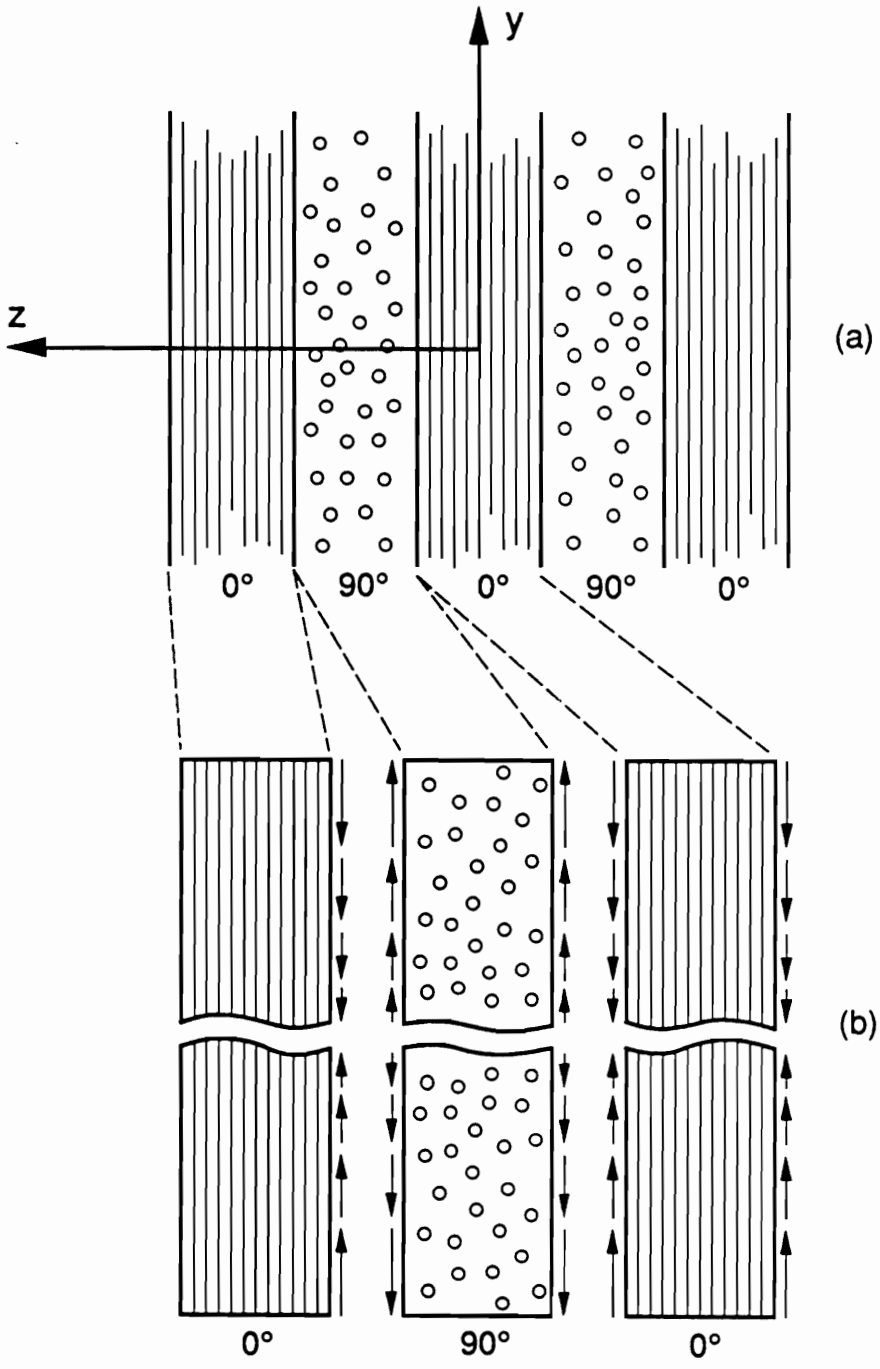

Figure 2.6 (a) Coordinate system of a laminate. (b) The interaction of plies near the edge of a cut.

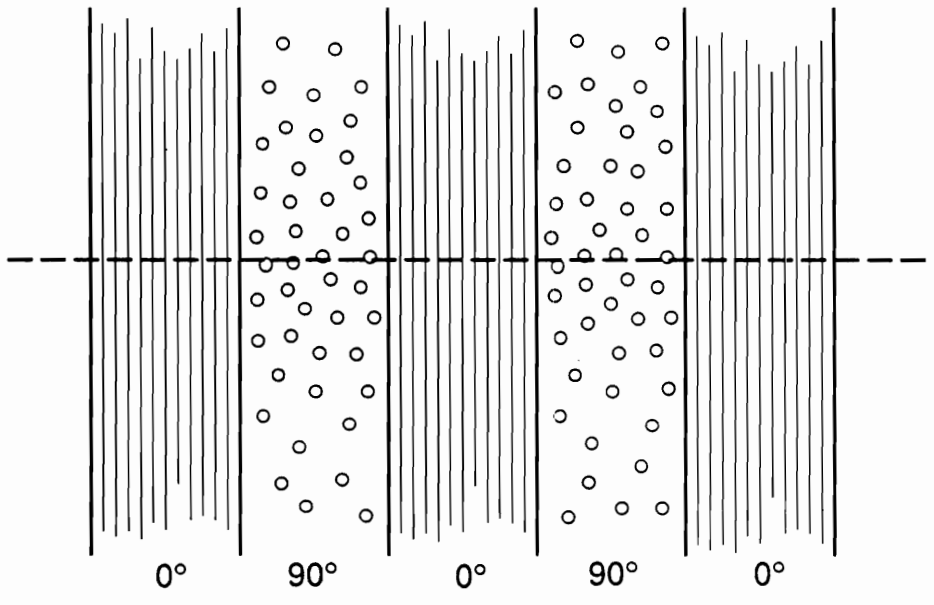

(a)

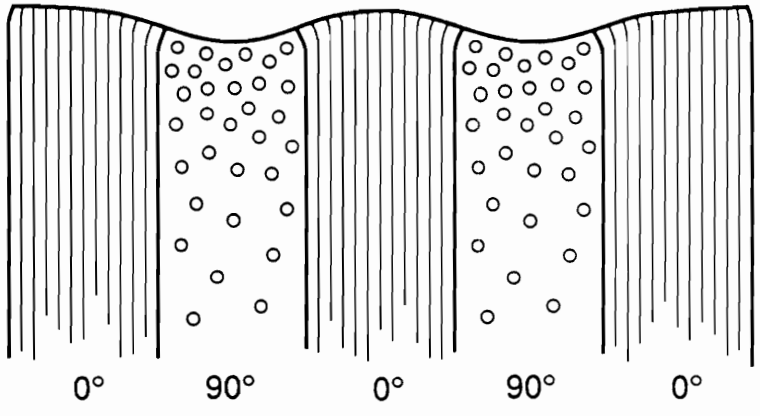

(b)

Figure 2.7 Shapes of a laminate (a) before and (b) after a cut was made. The deformed shape is exaggerated.

resulting tension in the inner portion and compression in the outer portion of the cylinder. This explanation agrees with the result obtained after cutting the ring open; that is, a small piece had to be removed because the ring deformed inward after the outward bending moment was released.

The two factors mentioned above affect residual stresses (or strains) not independently but interactively. The first is definitely dominant in the first ring, in which compressive hoop strain in the axial plies and tensile hoop strain in the hoop plies were measured. In the results of the second cylinder presented in the next section, however, the residual strains are apparently shown as a combined effect of the two factors. The details are discussed in the next section.

The deformation patterns of the specimen due to the release of the axial stresses are shown in Figure 2.8. As in the previous patterns, high interlaminar shear strains between the plies were detected. The normal residual strains at the edge of the cut ranged from -1500 μm/m to 1000 μm/m in the radial direction, -1500 μm/m to 1800 μm/m in the axial direction. The maximum shear strain was 8000 μm/m which is again about 40 % of failure strain. This fact indicates that if free edges are produced by making holes and notches, the large shear strain is introduced and can cause early delamination.

2.4.2 Specimen #2

The patterns illustrated in Figure 2.9 represent the displacement fields due to the release of bending by the open cut. A 5 mm long section had to be removed from the ring in order to release all the bending moment. The

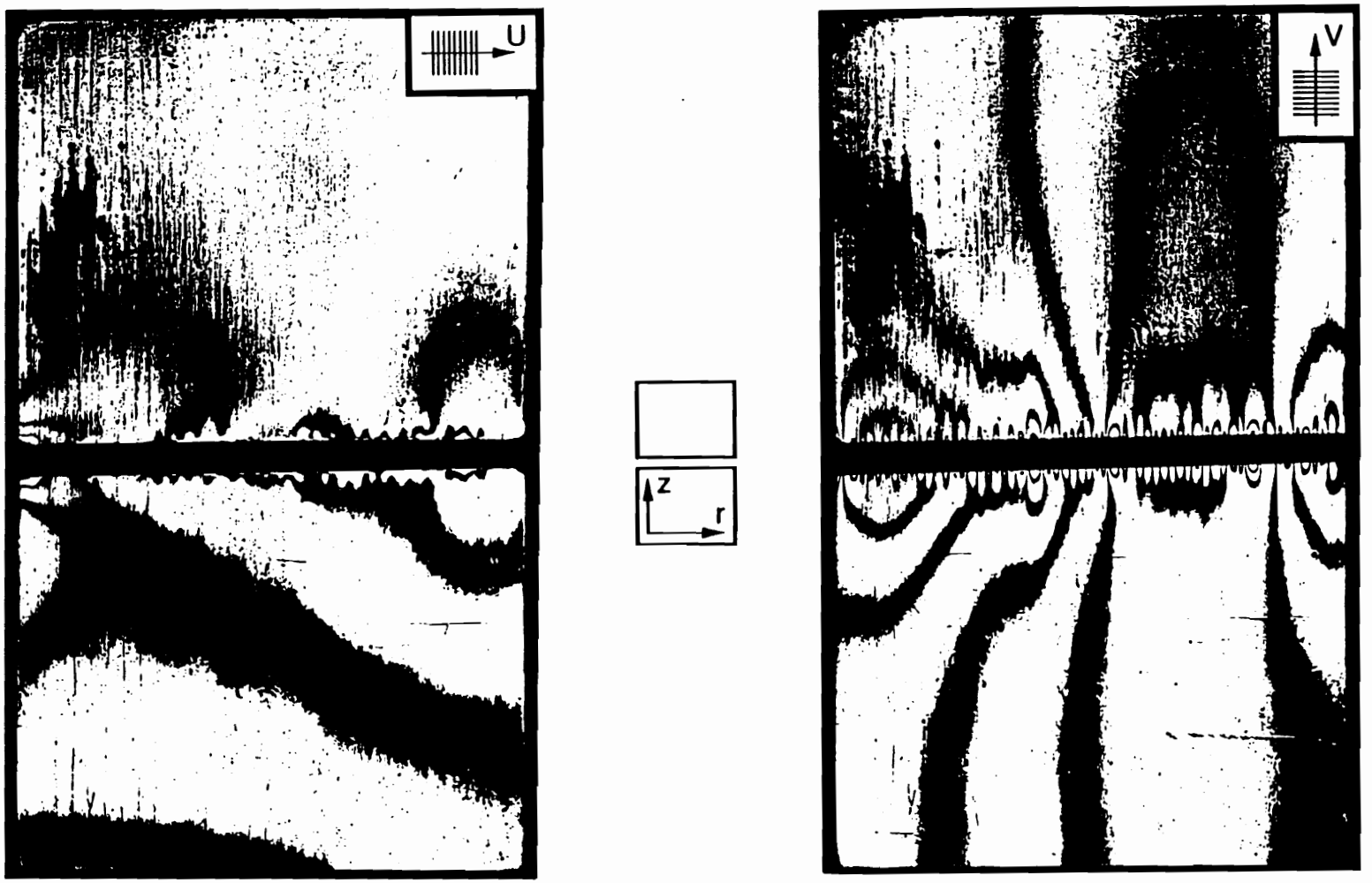

Figure 2.8 U and V displacement patterns of the first specimen due to the release of the axial stresses.

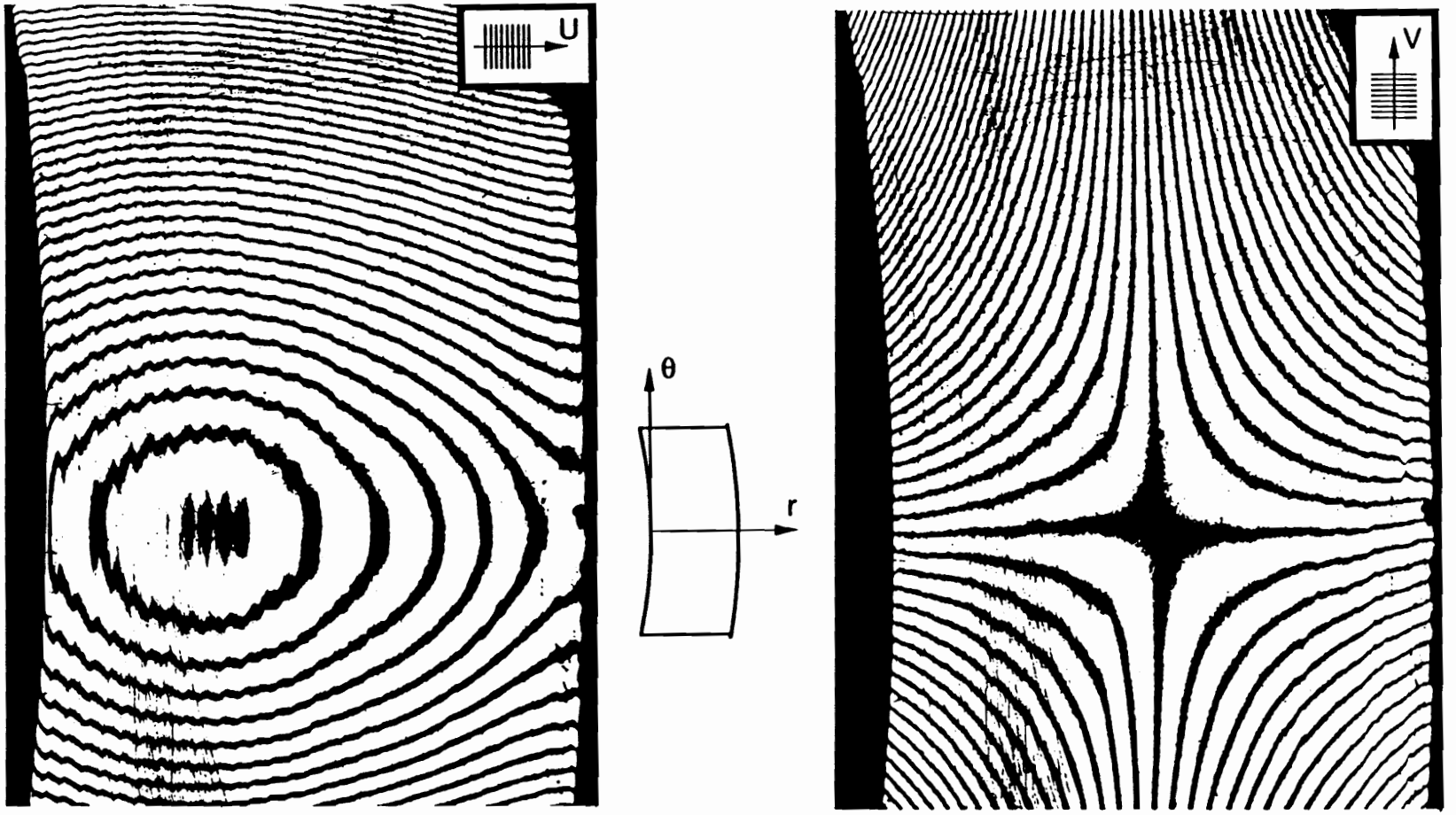

Figure 2.9 U and V patterns representing the deformation of the second specimen due to the bending produced by the open cut.

displacement patterns are qualitatively the same as those for the first specimen. The normal strains varied from -700 μm/m to 900 μm/m in the hoop direction and from -600 μm/m to 350 μm/m in the radial direction. These values were about the same as those for the first specimen. Shear strain was globally negligible.

The second set of patterns presented in Figure 2.10 was obtained from the same grating as in Figure 2.9, but after a radial cut perpendicular to the grating surface and to the hoop direction was introduced to release the residual stresses in the hoop direction. The patterns represent deformation fields resulting from the combined effect of the global bending and the local hoop stress variations. The corresponding strain distribution is shown in Figure 2.11. The concentrations of shear strain are localized in the vicinity of the curing stops.

Figure 2.12 shows the deformation patterns due to the local hoop stress variation only. The data taken at the local extrema are presented in Figure 2.13. The results were plotted and as before the data points were connected by straight lines for clarity and for easy comparison. A strong correlation between the concentrations of the shear strain and the curing stops can easily be noticed. The oscillation of strains is not as significant as that of the first specimen. It seems that the effects of different CTE's in the laminae and of the tension in fiber tows are combined. The separation of these effects is not possible at this point. The normal strains in the radial direction varied from -2000 μm/m to 1500 μm/m and in the hoop direction from -500 μm/m to 1000 μm/m. The shear strain varied from -2800 μm/m to 1500 μm/m. It

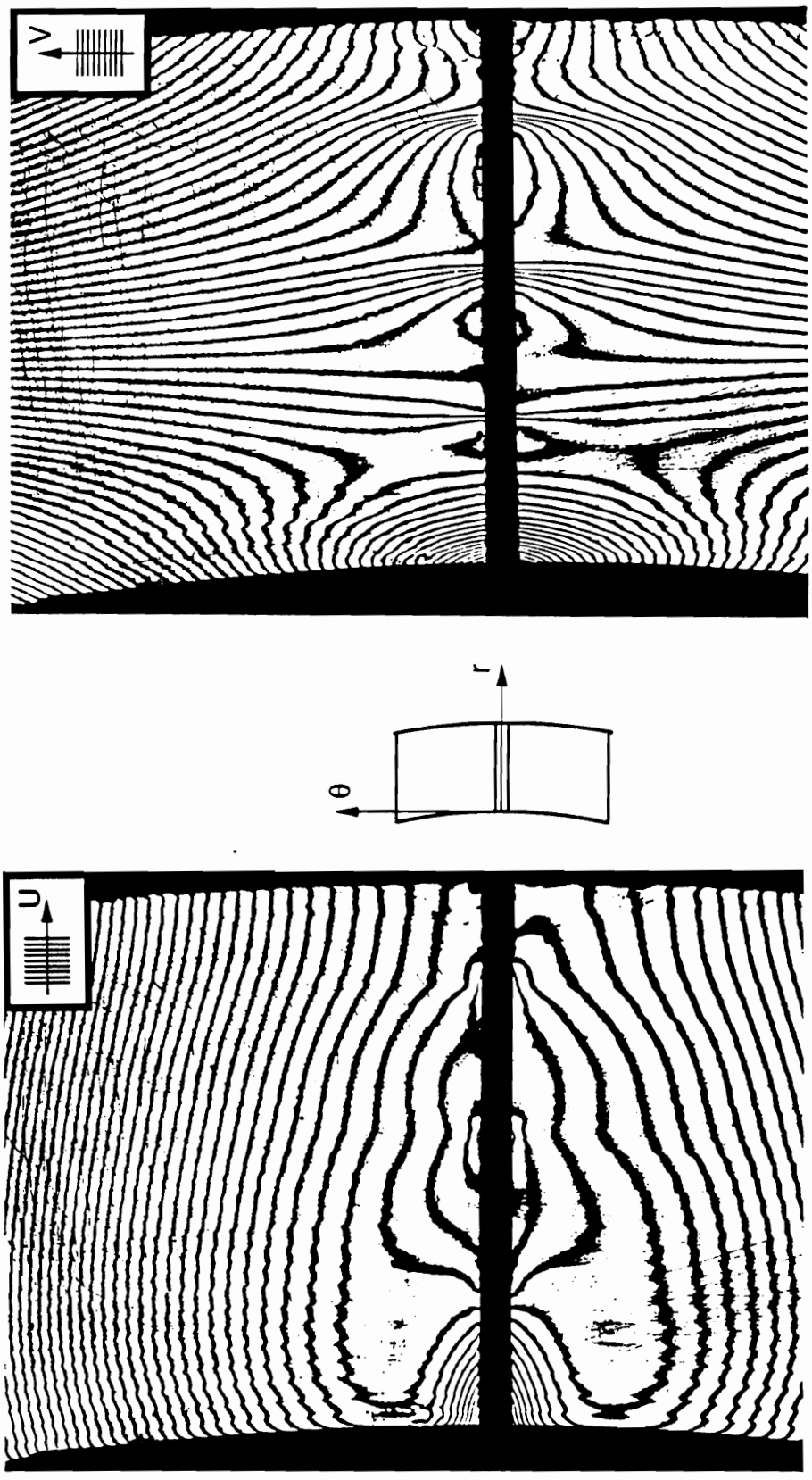

Figure 2.10 U and V patterns of the second specimen representing the deformation field resulting from the combined effect of global bending and local stress variations.

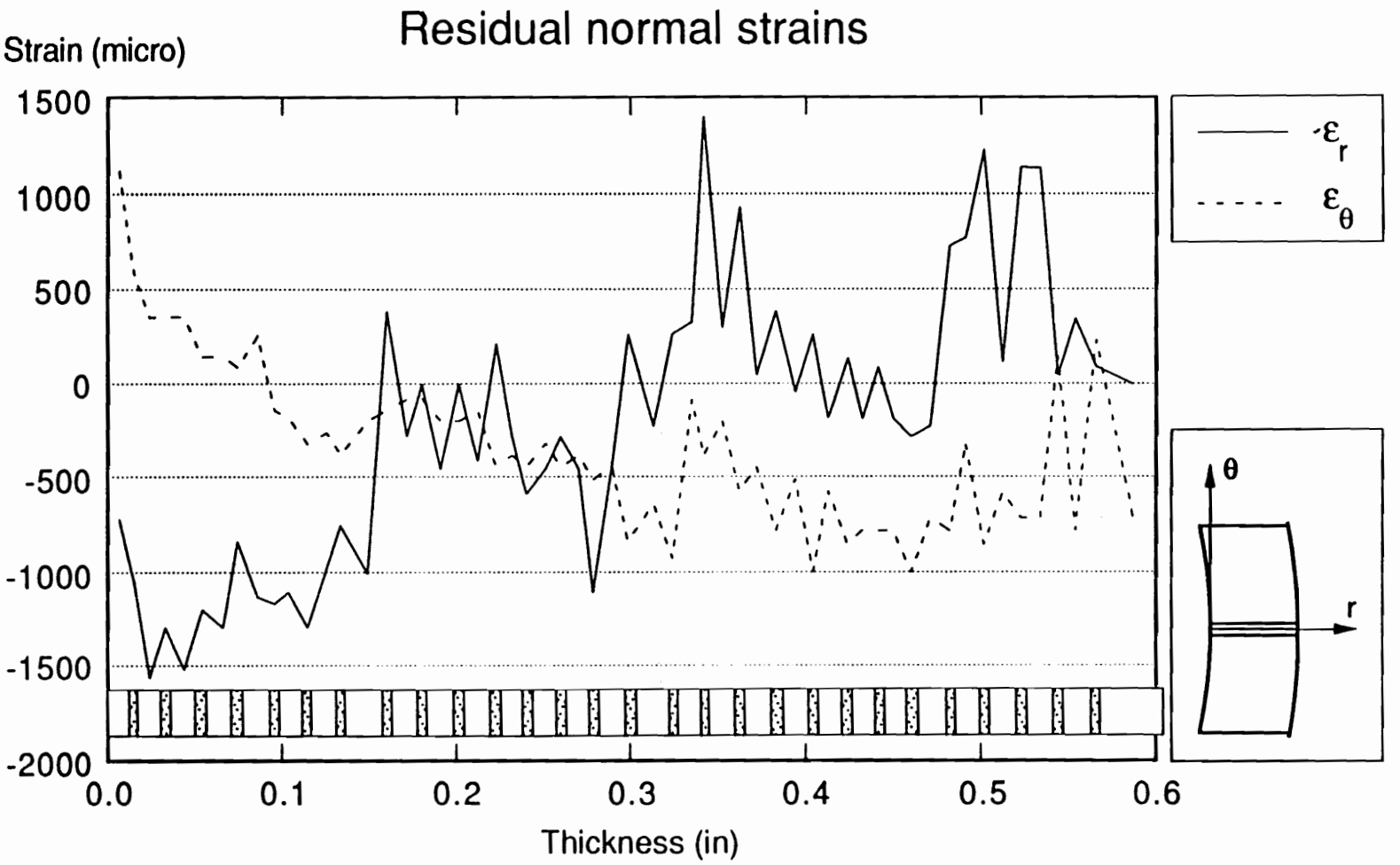

Figure 2.11 (a) Distribution of the normal strains through the thickness of the cylinder wall due to the combined effect of global bending and local stress variations. The blank and the shaded rectangles represent 90° and 0° plies, respectively.

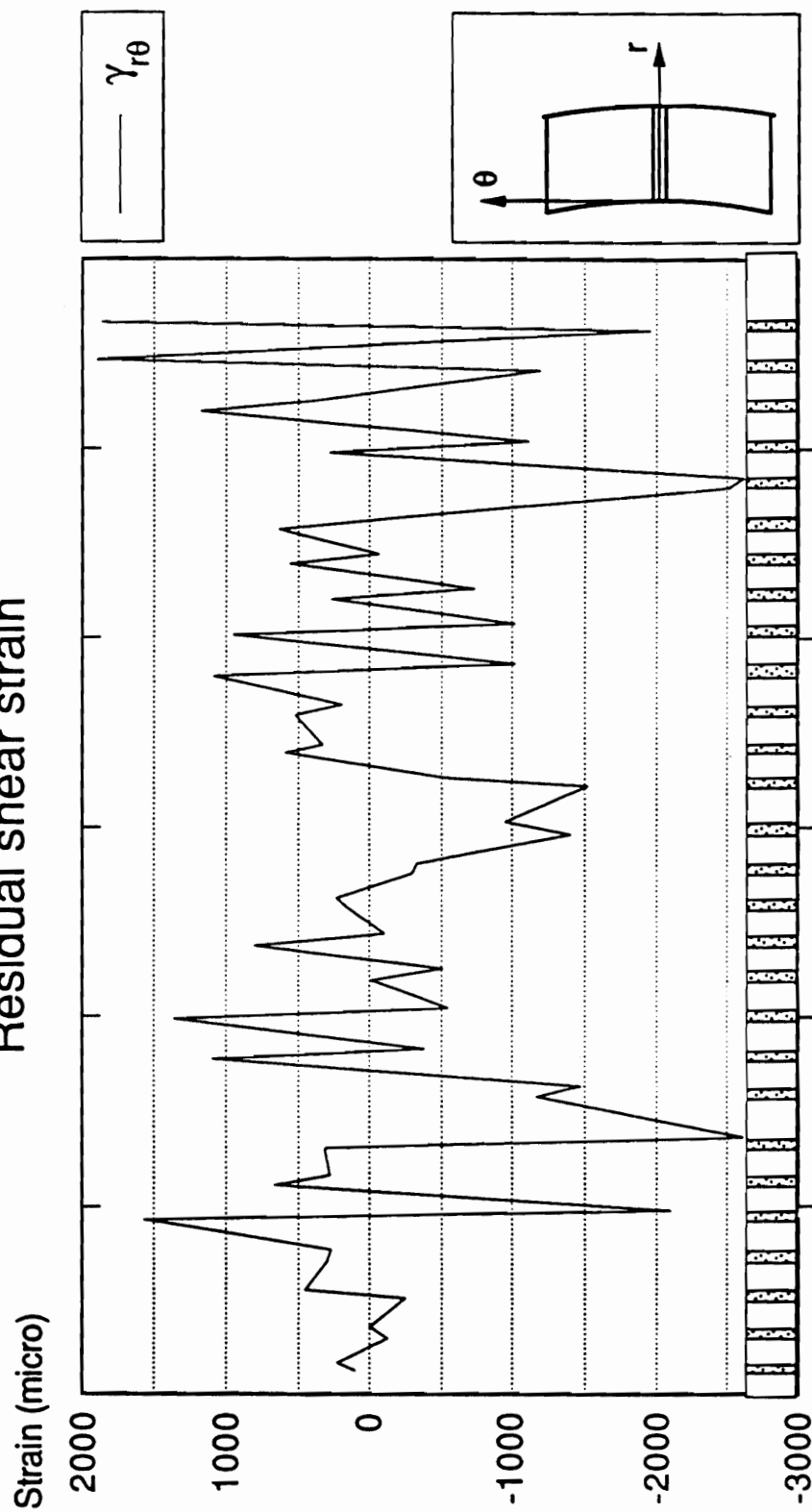

Figure 2.11 (b) Distribution of the shear strain through the thickness of the cylinder wall due to the combined effect of global bending and local stress variations. The blank and the shaded rectangles represent 90° and 0° plies, respectively.

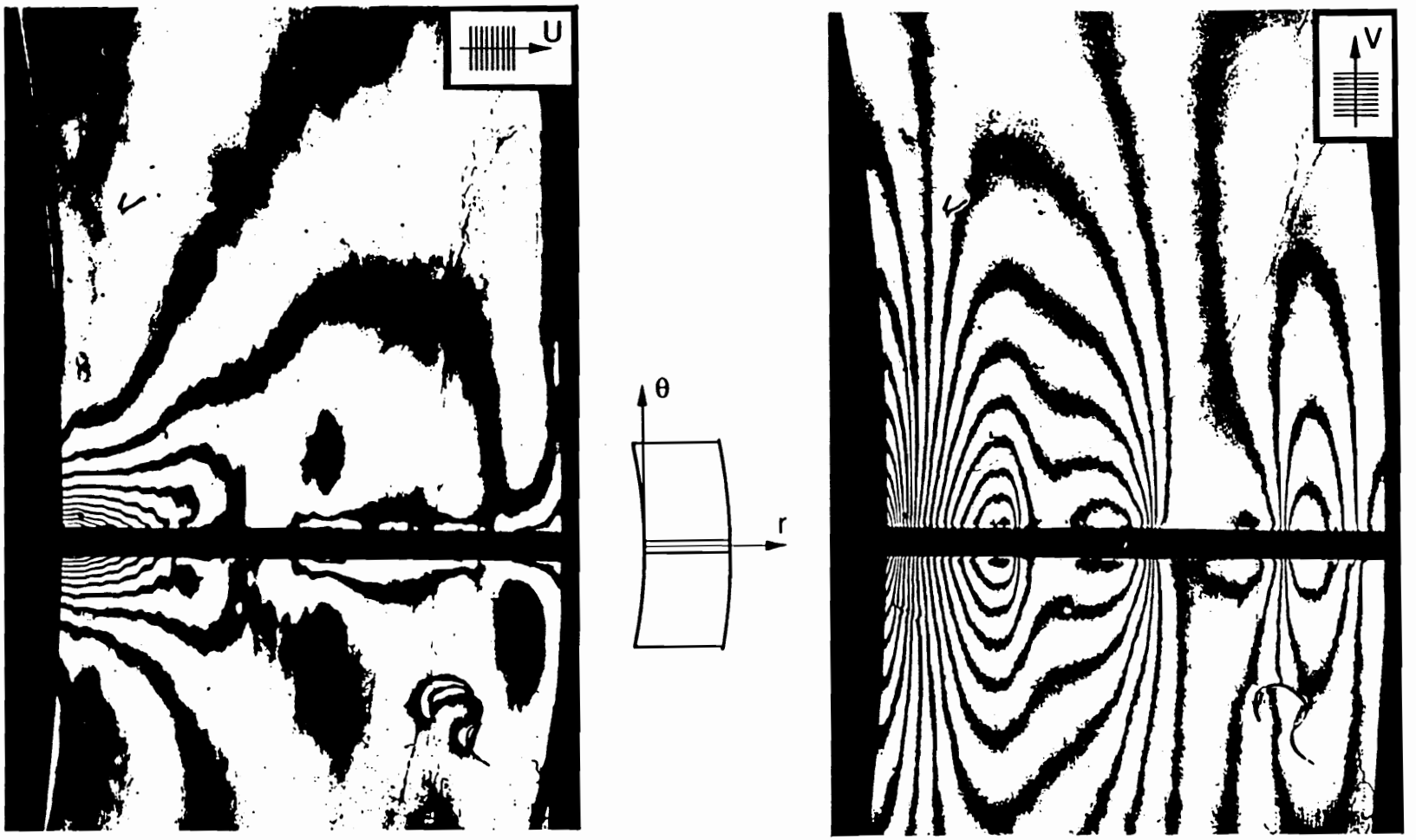

Figure 2.12 U and V patterns representing the deformation of the second specimen due to the release of the hoop stresses.

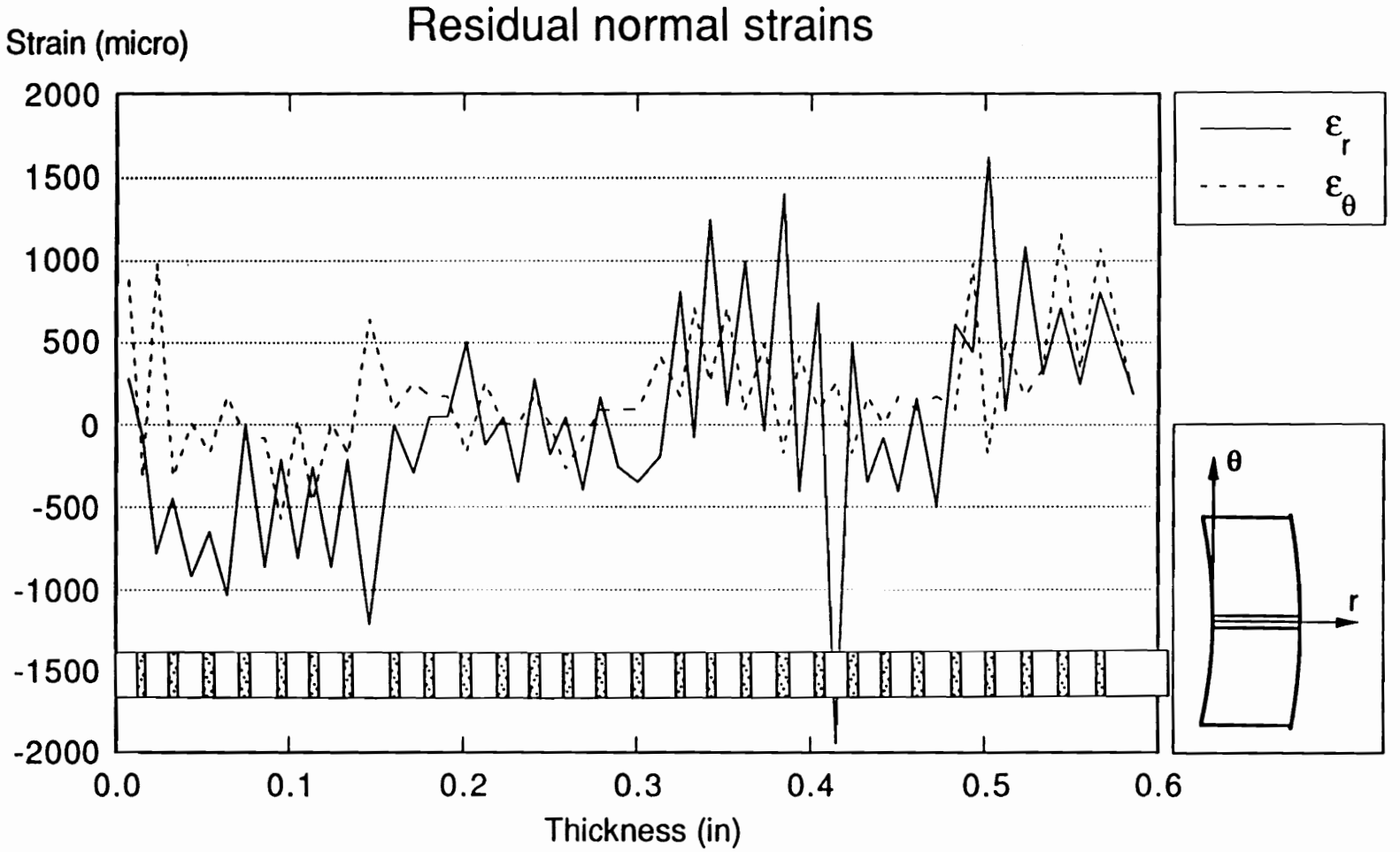

Figure 2.13 (a) Normal strain distribution through the thickness of the cylinder wall due to the release of the hoop stresses. The blank and the shaded rectangles represent 90° and 0° plies, respectively.

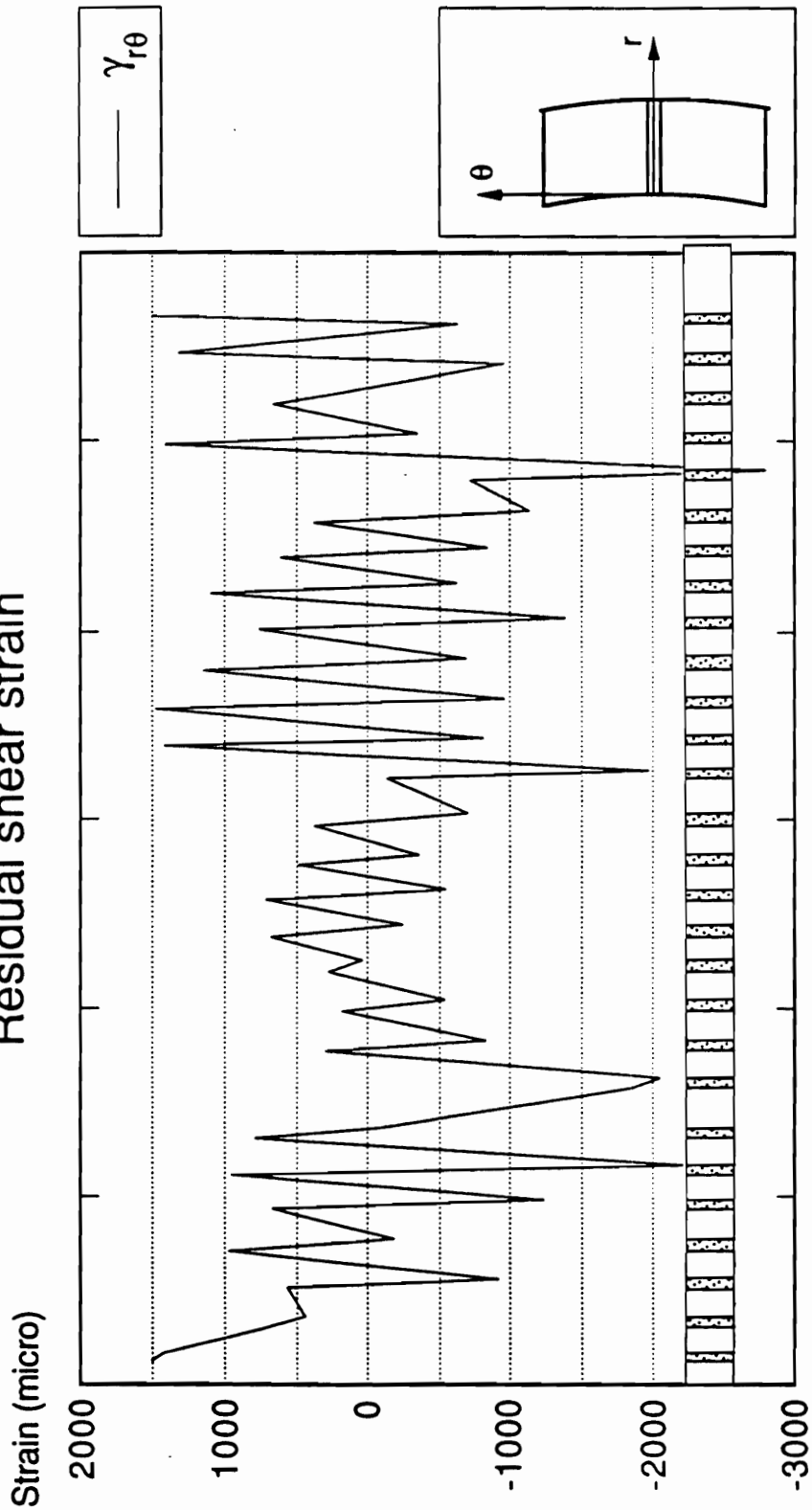

Figure 2.13 (b) Shear strain distribution through the thickness of the cylinder wall due to the release of the hoop stresses. The blank and the shaded rectangles represent 90° and 0° plies, respectively.

should be noted here that, compared with the results of the first specimen, the maximum values of the normal strain in the hoop direction and the shear strain at the curing stops were decreased by factors of 2 and 3, respectively, which is a significant improvement. In other words, although one more strain concentration was introduced by having one more curing stop, the absolute values of the maximum strains were reduced. No significant difference in normal strain in the radial direction was noticed. One more thing to note is a peculiar strain distribution at the outer layers of the cylinder. The tendency of extremum radial strain corresponding to extremum hoop strain is opposite to the tendency seen in all the other plots. The location of the point where this tendency reversed coincides with the interface where failure was detected in destructive pressure tests. The cause of this effect is not known at this time.

The last set of patterns, presented in Figure 2.14, corresponds to the deformation field measured at a cross-section parallel to the radius and the axis of the cylinder. The variation of strains along the cut is similar to that analyzed on the previous grating. The axial strain varied from -1700 μm/m up to 1600 μm/m. The radial strain varied from -1500 μm/m up to 800 μm/m. The maximum value of shear strain was 6200 μm/m. No great difference in the maximum strains was found.

2.5 Summary and Conclusions

The results of this experiment indicate several problems associated with the current methods of manufacturing thick composite cylinders. These problems are:

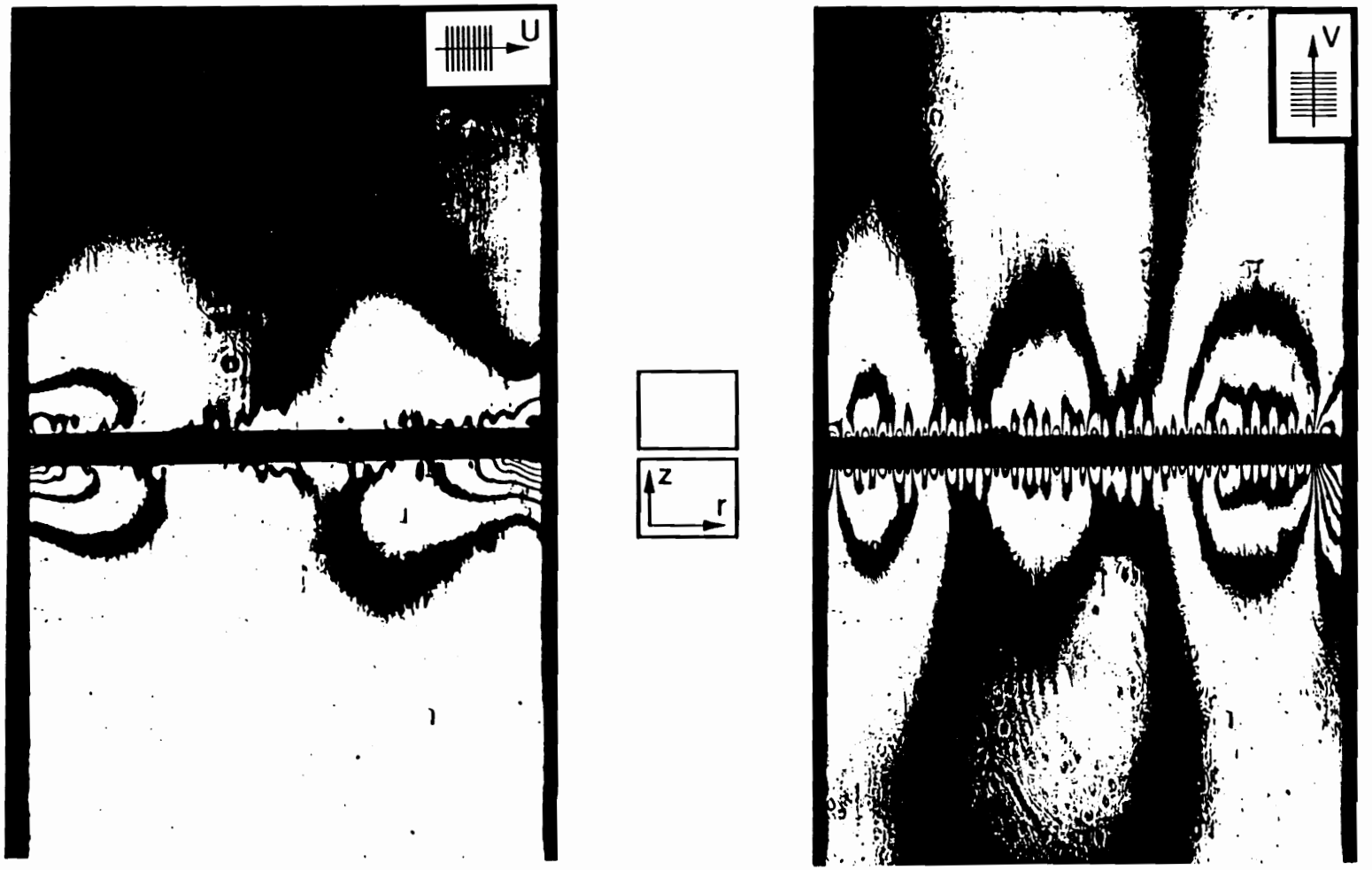

Figure 2.14 U and V patterns representing the deformation of the second specimen due to the release of the axial stresses.

— high level tensile stresses in the direction perpendicular to the direction of the fibers,
— large interlaminar tensile stresses associated with bending moments in the cylindrical wall of the specimen,
— large normal and shear strain concentrations corresponding to halts in the fabricating process,
— voids and imperfections in the zones corresponding to the halts in the manufacturing process,
— large interlaminar shear strains in the immediate vicinity of the cuts that are due to singularities in the stress field at the boundaries of any hole introduced into a thick composite cylinder.

The curing procedure has significant influence on the distribution and the magnitude of stresses in the material. By adding one more curing stop the maximum normal hoop strain and shear strain due to the release of the hoop stresses were decreased by factors of 2 and 3, respectively. No significant difference in the axial strains was detected. The results are summarized in Table 2.1.

It is expected that time-dependent relaxation and moisture expansion introduced some change in the stress field after the specimen was manufactured. Since both factors tend to reduce the magnitudes of the measured deformations, residual strains in freshly cured composite elements could be even more severe and need serious consideration.

A new procedure for measuring residual strain was developed, in which the separation of the effects of different components of the residual stresses was

Table 2.1 Comparison of residual strains for two different specimens, one with 3 curing stages and the other with 4 curing stages.* (a) After the release of the hoop stresses. (b) After the release of the axial stresses. The minimum and the maximum values of strains are separated by a slash.

	ε_r	ε_θ	$\gamma_{r\theta}$
3-stage cure	-2500 / 600	-1000 / 2000	8500
4-stage cure	-2000 / 1500	-500 / 1000	2800
ratio, 4-stage/3-stage	1	1/2	1/3

(a)

	ε_r	ε_z	γ_{rz}
3-stage cure	-1500 / 1000	-1500 / 1800	8000
4-stage cure	-1500 / 800	-1700 / 1600	6200
ratio, 4-stage/3-stage	1	1	1

(b)

ε_r : normal strain in the radial direction.

ε_θ : normal strain in the hoop direction.

ε_z : normal strain in the axial direction.

$\gamma_{r\theta}$: interlaminar shear strain in r-θ plane.

γ_{rz} : interlaminar shear strain in r-z plane.

* Strains are given in μm/m.

achieved by cutting the specimen in the relevant directions. This method allowed measurement of displacements and, therefore, strains in each ply. However, it did not give information on deformation within the plies since the already high resolution of moire interferometry was not high enough. This necessitates the development of a new data reduction method which has higher resolution than that of the current data reduction procedure.

PART 3 : A NEW PROCEDURE FOR HIGH-RESOLUTION DATA REDUCTION

3.1 Introduction

The sensitivity in moire interferometry is defined as the displacement per fringe order, or $\Delta U_i / \Delta N_i$, where U_i is the displacement and N_i is the fringe order. It is limited to half of the wavelength of the light used in the experiment per fringe order. As mentioned in Part 1, the sensitivity with the standard configuration used at VPI&SU is 0.417 μm per fringe order. This sensitivity corresponds to approximately 60% of the theoretical limit for visible light and is most common since it is a good compromise between the sensitivity, the compactness, and the light efficiency of the system. It should be mentioned that unless a more or less complicated technique such as optical multiplication [45] is used, the sensitivity is fixed as long as the frequency of the reference grating is fixed.

On the other hand, the resolution is defined as the maximum error within which we can obtain reliable data from a given fringe pattern. Depending on the methods of pattern recording and data collection, the resolution of measurements varies from about 1/4 of a fringe order down to about 1/20 of a fringe order. Usually moire patterns are analyzed in two ways. One of them is to collect the data at the center lines of the fringes. In this method, the fringe patterns are normally recorded with overexposure. This method gives the

resolution of measurements about 1/20 of a fringe order which is about 20 nm. The other method is to use fractional fringe orders in which data can be read reliably with a resolution of about 1/4 of a fringe order. This resolution corresponds to approximately 100 nm.

Although the aforementioned sensitivity and resolution are high enough for many applications, enhancement of either sensitivity or resolution is desirable to increase the number of reliable data points for the cases where the number of fringes in the field of interest is small. Examples of such cases are measurements on high stiffness materials such as ceramics that produce fewer fringes for a given load, and measurements of deformation of small fields such as within-the-ply measurement that could not be performed with the ordinary data reduction procedure presented in Part 2. While somewhat complicated procedures are required for increasing the sensitivity, it can be more efficient to enhance the resolution. The enhancement procedure for resolution is easier and simpler to use, and more amenable than that of sensitivity. It is, therefore, expedient to focus on the enhancement of resolution.

The objective of this part was to develop a procedure that enables data reduction with higher resolution than that of standard moire interferometry. A new algorithm reproducing whole-field fringe patterns with enhanced resolution and, therefore, providing qualitative as well as quantitative full field information about deformation will be presented. This new method does not require any modification to existing moire interferometers and can be used in measurements on the macro as well as the micro scale.

3.2 Fringe Pattern Recording and Data Extraction

Depending upon the frequencies of fringe patterns, the method of recording the patterns may vary. In cases of low frequency fringe patterns, it is a common practice to record them in a low contrast photographic process to allow recovery of fractional fringe orders from variations of the intensity of light. In cases of high frequency patterns it is usually sufficient to collect the data at the center lines of the fringes. In these cases, the patterns are recorded with overexposure in a high contrast photographic process.

The most common approach for extracting fractional fringes is grey level analysis which is based on a TV camera system connected to a computer. This method is, however, not only complicated and expensive but also sacrifices the quality of the results. The spatial resolution is limited by the resolution of the camera used and, because the measured intensity of light is strongly dependent on the uniformity of the diffraction efficiency of the specimen grating as well as on the uniformity of the illuminating light, the reliability of the results is questionable. The errors resulting from these factors can be easily as large as 1/4 of a fringe order and the only possible advantage is a larger number of data points.

Mainly for aesthetic reasons it has been a common procedure to record moire patterns using a high contrast photographic process and strong overexposure. The nonlinearity of this procedure can be used for threshold of the intensity of light. It has been used for many years in a more elaborate form in photoelasticity and was used to extract fractional fringes before digital image processors became available. As can be seen in Figure 3.1, once the

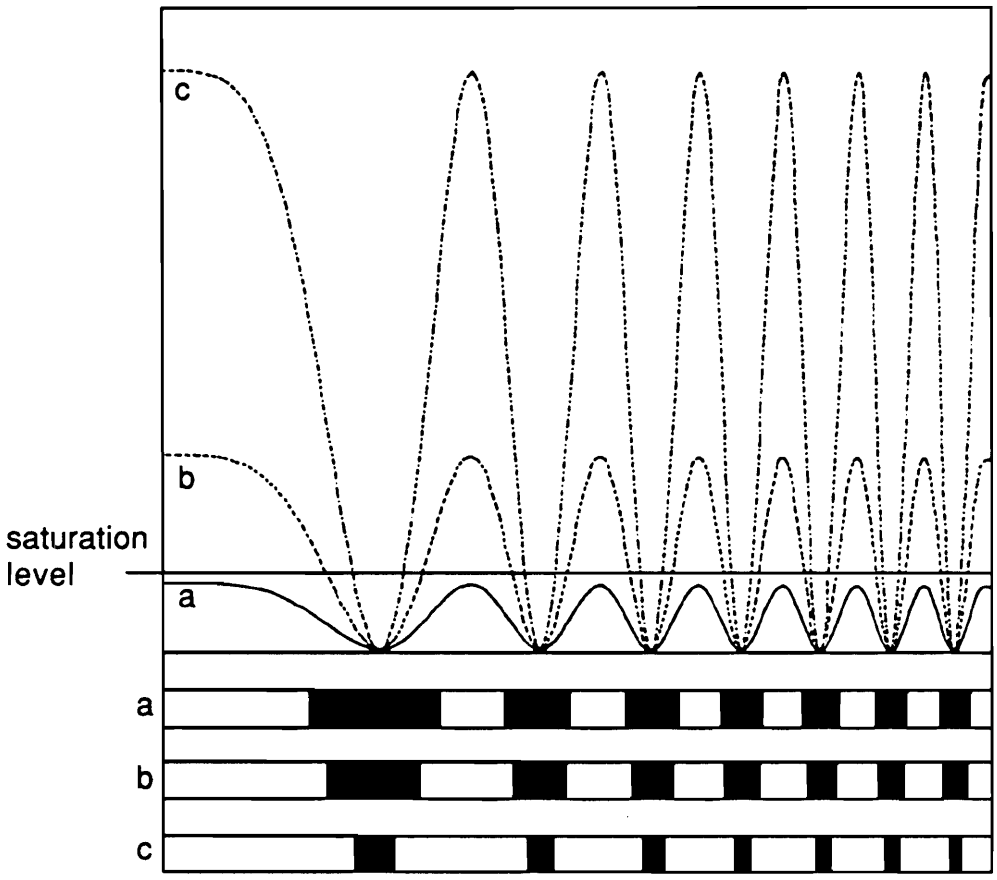

Figure 3.1 Distribution of exposure energy across an interference fringe pattern for three different exposure times. Strips at the bottom of the figure demonstrate the corresponding fringe pattern recorded in high contrast photographic process.

maximum exposure intensity exceeds the saturation point of the film the width of the unexposed or the partially exposed zone of a fringe diminishes. After the pattern is printed, the final effect of this nonlinear process is a fringe pattern consisting of black narrow fringes on a white background. In theory the width of fringes recorded this way can be reduced to a line. In practice, however, due to imperfections of interferometric systems, the ratio of the width of the black fringe to that of the white fringe is limited to approximately 1:10. The black fringe must contain the line of minimum intensity, and if the data are taken at the center of the black fringe the error is not more than 1/20 of a fringe order. At the standard sensitivity of 417 nm per fringe order the displacement data can be extracted with an accuracy of the order of 20 nm. This means an improvement of accuracy by a factor of five.

This method of image enhancement is very effective if a pattern contains a large number of fringes. In the case of small deformations or small fields of view, the total number of fringes can be as few as one or two. While the narrowing of fringes by overexposure would increase the accuracy of locating the center lines of the fringes, it would drastically reduce the number of points where high quality data can be taken. On the other hand, the number of data points can be increased by the addition of a carrier pattern. This modification, however, obstructs qualitative interpretation of fringe patterns and makes the analysis of results very difficult and time consuming. If qualitative as well as quantitative data with high resolution are desired, a different method of pattern enhancement must be considered. A new method of high resolution data

reduction without losing full-field qualitative information is presented in the next section.

3.3 A New Algorithm

Each component of the displacement field on the surface of a specimen can be represented by a function of two variables or graphically by a surface in three dimensional space. A fringe pattern is a contour map of this surface. The fringe orders depend on the amount of deviation of this surface from a horizontal plane and the contour interval. Since the latter is pretty much fixed by the frequency of the grating and the wavelength of the light used, the only factor that can be modified is the shape of the surface. The number of fringes can be increased by either increasing the warpage of the surface by a factor constant across the domain [44] or adding a linear function to the function representing the displacement field. The function describing the surface, S, can be represented by Equation (3.1):

$$S = U + C_1 x + C_2 y + C_3 \tag{3.1}$$

where U is the displacement in the direction of the x-axis and a function of both x and y,

C_1 is the apparent uniform strain,

C_2 is the angle of rigid body rotation, and

C_3 is the rigid body translation.

Since rigid body translation does not change the shape of the fringes, C_3 can be chosen arbitrarily. Usually it is convenient to set it to zero. If, however,

either C_1 or C_2 is different from zero, uniformly spaced straight fringes will be added to the fringe pattern representing the displacement field U. This type of artificially introduced pattern is called a carrier pattern. The apparent uniform strain corresponding to a nonzero C_1 (carrier pattern of extension) can be introduced by a small angular separation between the interfering beams. This separation can be produced by a small change in the angle of incidence. The rigid body rotation corresponding to a nonzero C_2 (carrier pattern of rotation) can be introduced by small in-plane rotation of the specimen with respect to the interferometer or vice versa. In Figures 3.2 are shown four patterns representing the same deformation, a longitudinal displacement field on the surface of an epoxy cantilever beam loaded in bending. The first one was recorded in the ordinary fashion, the second with strong overexposure, the third one with overexposed carrier pattern of rotation, and the last with overexposed carrier pattern of extension.

At a given contour interval, δ_x, a fringe order, N_x, can be related to the function S by the equation

$$N_x = \frac{S}{\delta_x} \tag{3.2}$$

Now Equations (3.1) and (3.2) can be combined to give

$$U = N_x\delta_x - C_1\, x - C_2\, y - C_3 \tag{3.3}$$

Once all the constants are known, the magnitudes of displacement can be calculated at every point where data is collected. In practice the carrier pattern

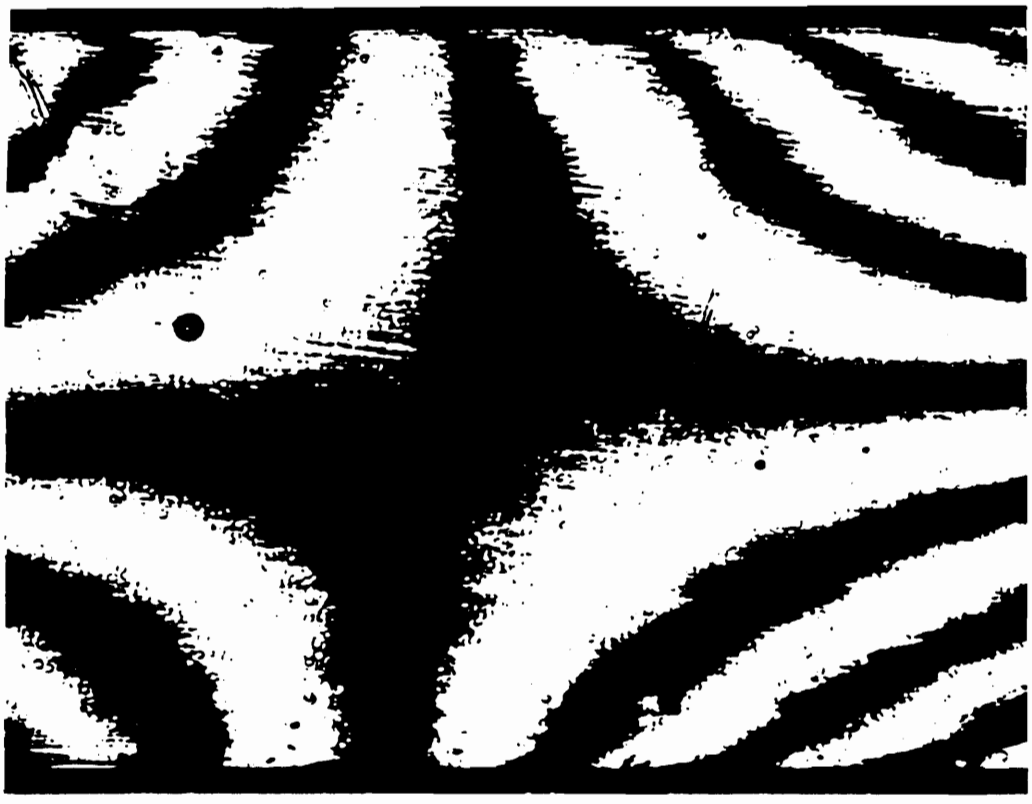

Figure 3.2 (a) Conventionally recorded moire fringe pattern representing the horizontal displacement field on a surface of a cantilever beam loaded in bending.

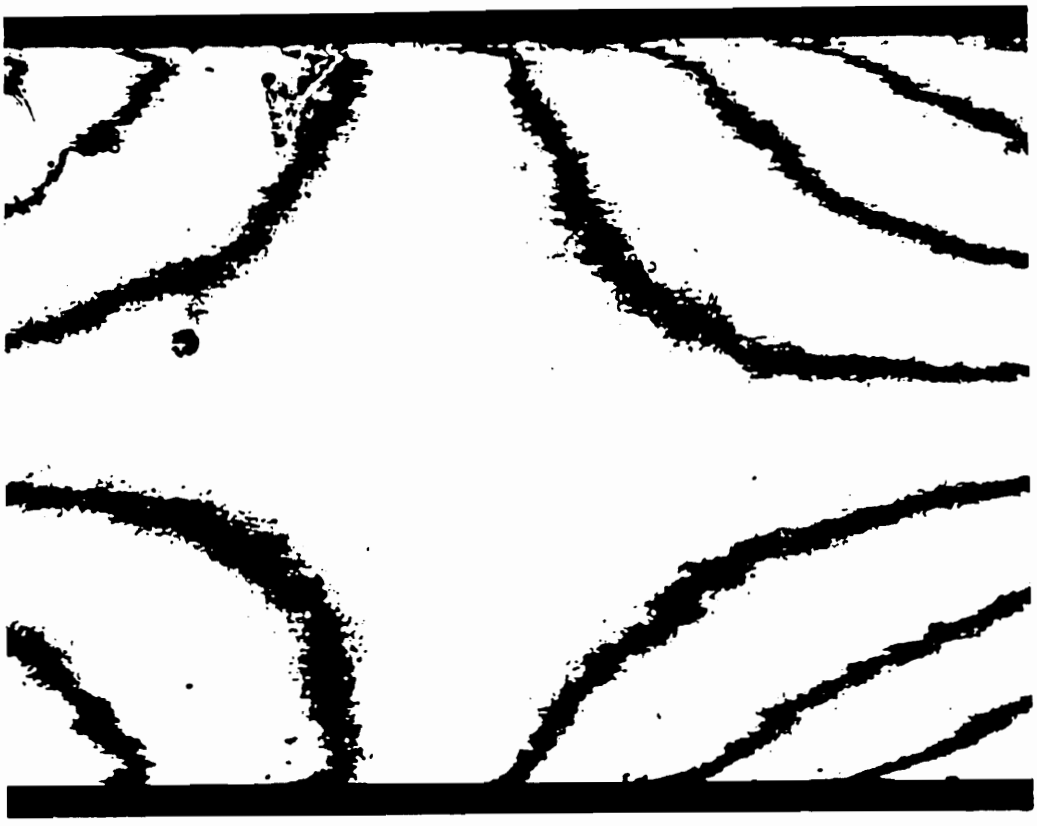

Figure 3.2 (b) Overexposed moire fringe pattern representing the horizontal displacement field on a surface of a cantilever beam loaded in bending.

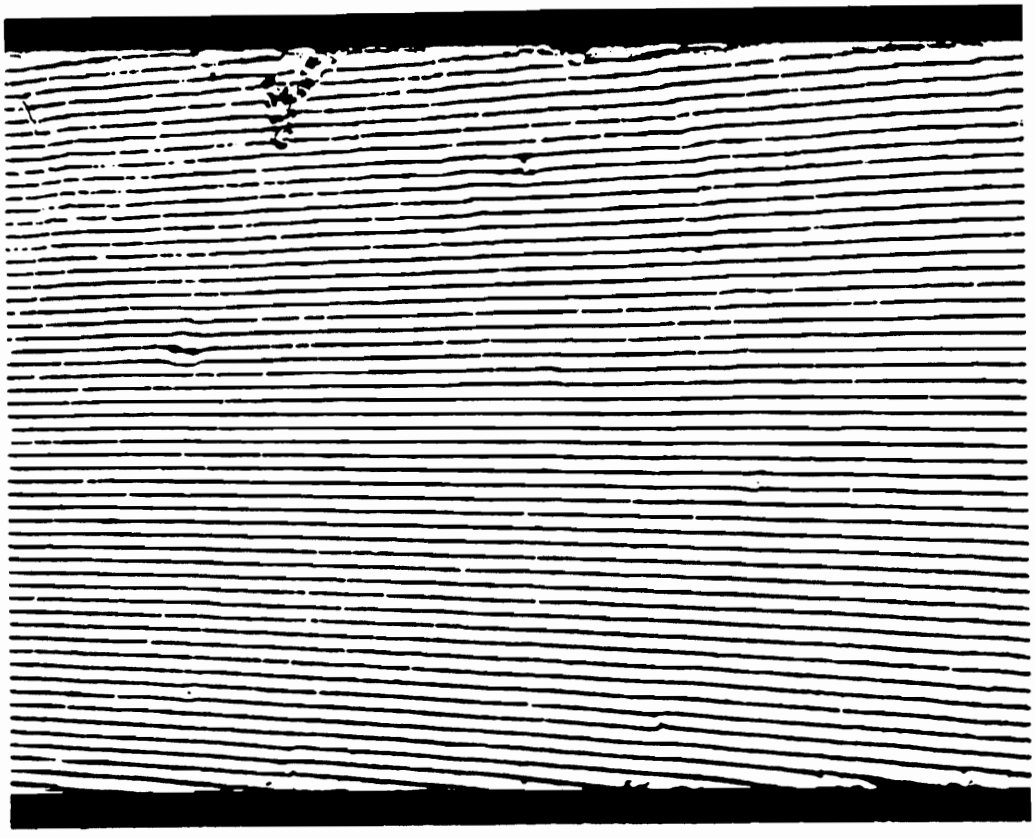

Figure 3.2 (c) Moire fringe pattern representing the horizontal displacement field on a surface of a cantilever beam loaded in bending recorded with overexposed carrier pattern of rotation.

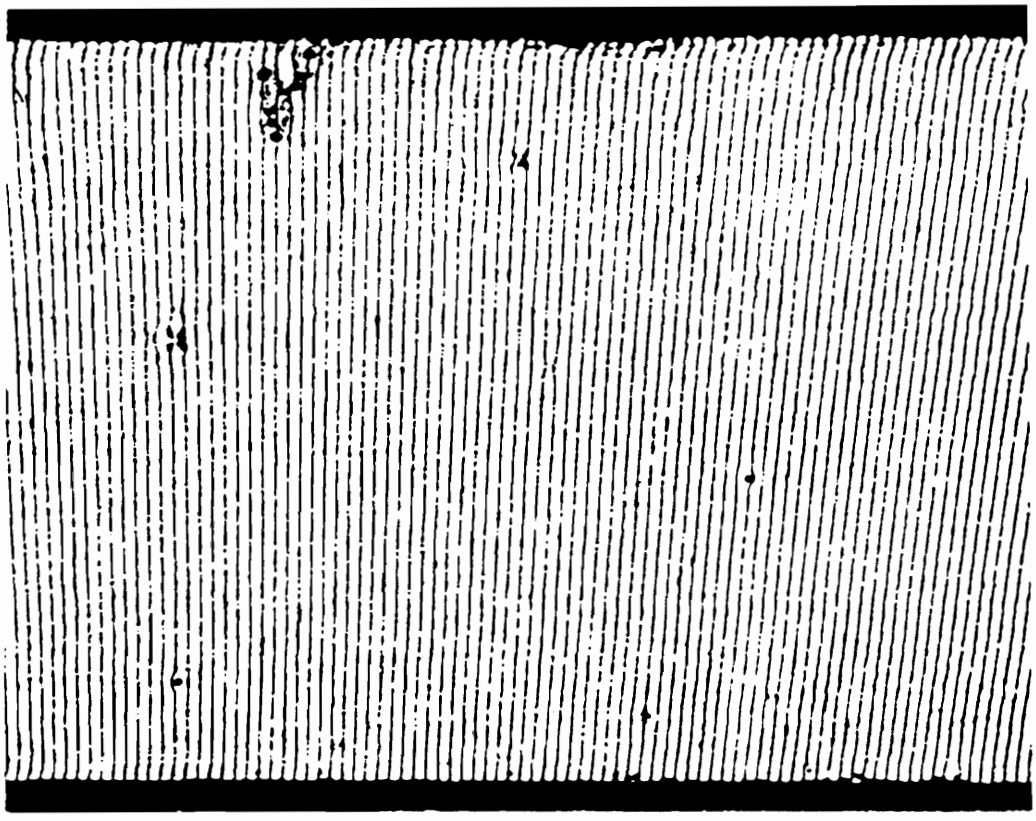

Figure 3.2 (d) Moire fringe pattern representing the horizontal displacement field on a surface of a cantilever beam loaded in bending recorded with overexposed carrier pattern of extension.

can be so fine that the data can be collected at practically any point of the field of interest. Similarly, the displacement in the y direction, V, can be expressed as

$$V = N_y\delta_y - C_4\, y - C_5\, x - C_6 \tag{3.4}$$

where C_4, C_5, C_6, N_y, and δ_y represent the same parameters for the V displacement as C_1, C_2, C_3, N_x, and δ_x do for the U displacement, respectively. The constants C_4 and C_5 are not arbitrary but related to C_1 and C_2 by the following equations:

$$C_4 = C_1 \tag{3.5a}$$

and

$$C_5 = -\,C_2 \tag{3.5b}$$

This is because, for the three-mirror system used in this work, the carrier patterns of extension with exactly the same frequency are simultaneously introduced in the displacement fields U and V, and also the rotation of the specimen with respect to the interferometer produces the carrier patterns of rotation with the same frequency but with the opposite sign in both fields. Substituting Equations (3.5a) and (3.5b) into Equation (3.4), the following equation is obtained:

$$V = N_y\delta_y - C_1\, y + C_2\, x - C_6 \tag{3.6}$$

Now Equations (3.3) and (3.6) can be used for determining both U and V displacements for the collected data points.

While both deformation patterns with carrier pattern of extension (Figure 3.2(c)) and carrier pattern of rotation (Figure 3.2(d)) can be analyzed to give the same information, the pattern with carrier pattern of extension was used in the presented example. The frequency of the carrier pattern was 9.15 lines/mm, which allowed collection of data every 0.11 mm. The data was collected using a digitizing pad connected to a personal computer. The digitizer has a resolution of 0.0254 mm (0.001 inch) and, using enlarged pictures of the fringe patterns, the data points are collected with sufficient accuracy. The longitudinal displacements were calculated at every data point using Equation (3.3) and a contour map of them illustrated in Figure 3.3 was electronically generated with the same contour interval as in the original fringe pattern, i.e., 417 nm. A comparison between the overexposed original pattern (Figure 3.2(b)) and the one generated electronically shows a good agreement between the two. An electronically generated pattern with multiplication factor of 10 is illustrated in Figure 3.4 with original fringes highlighted by thicker lines for easy comparison. The corresponding contour interval was 41.7 nm. It was reasonable to choose a multiplication factor of 10 since, when data are collected at the center of the fringes, the resolution is about 20 nm. As shown in the figure, easy analysis of the deformation state is achieved. In other words, qualitative as well as quantitative information about deformation was obtained. It should be emphasized here that those lines between the original fringes were obtained not by direct interpolation of the original fringes but by collecting high quality data with maximum resolution. The amount of error is, therefore, minimized.

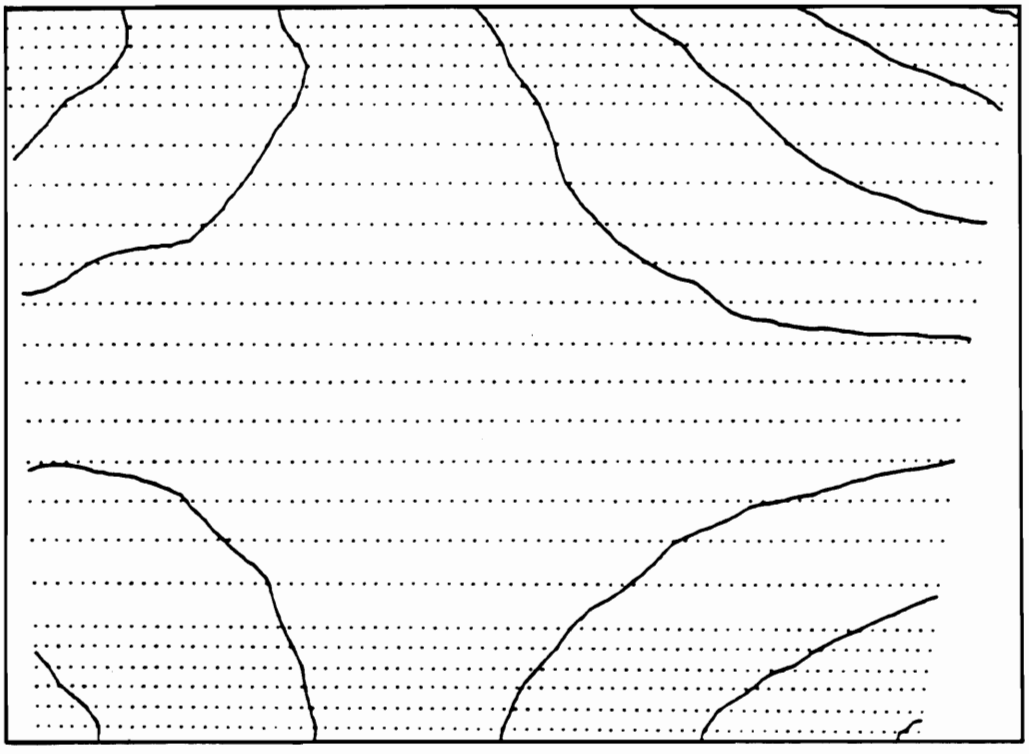

Figure 3.3 Electronically generated contour map of U displacement field with standard contour interval of 417 nm.

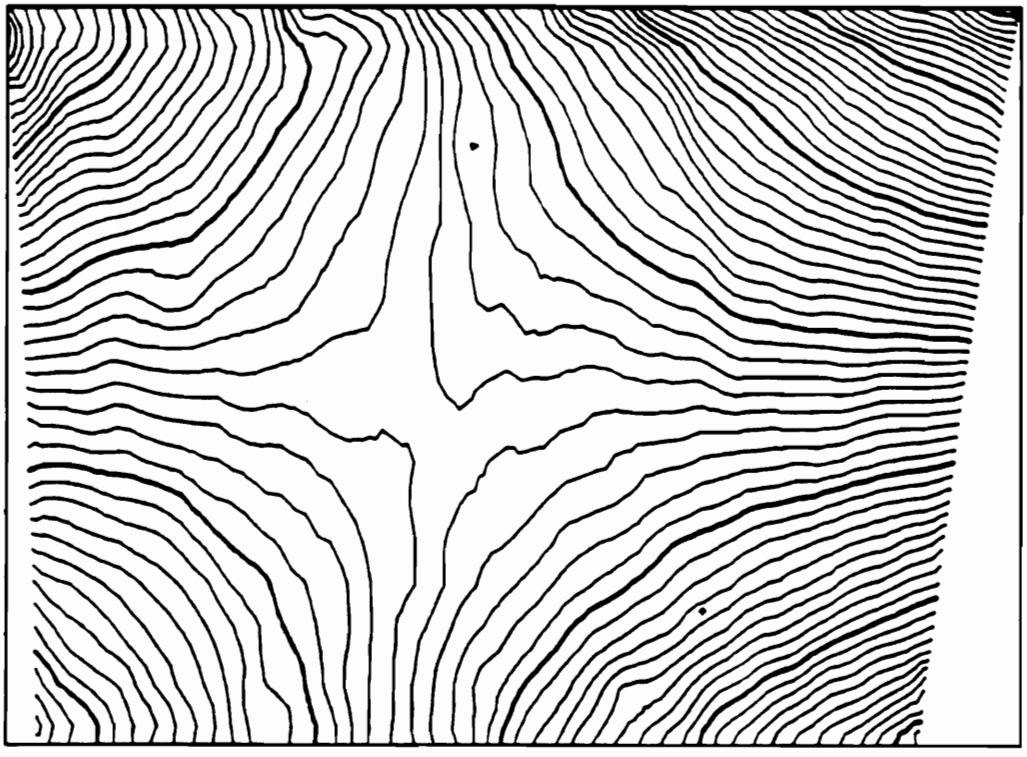

Figure 3.4 Electronically generated contour map of U displacement field with contour interval of 41.7 nm.

3.4 Nonuniform Mesh Generator

In order to produce the patterns in Figure 3.3 and 3.4, a relatively uniform grid was used for collecting data and for plotting contours. It may not be efficient to use uniform grids for highly nonuniform fringe patterns which fibrous composite materials usually show, or for various shapes of boundaries such as those with stress raisers. A nonuniform mesh-generating routine was developed in which a totally nonuniform mesh can be generated to study local nonuniformities more efficiently. The mesh-generating program uses the digitized data points as the nodes and produces a nonuniform mesh by connecting them. Triangular elements are used to make the mesh very effective for the analysis of nonuniform deformation. Since a mesh with acutely shaped triangles produces large errors when it is used for finite element analysis, the program was written to produce only non-acute triangles. For demonstration, the data were collected again from Figure 3.2(c) with a digitizing pad connected to a personal computer. Figure 3.5 shows the mesh generated by the program for the previously mentioned epoxy cantilever beam loaded in bending. The displacement pattern was digitized densely around the boundaries where some anomalies existed and less densely on the center portion where the pattern was smooth. This significantly reduces the number of data points to be digitized and hence the computing time.

The mesh-generating routine can be combined with finite element method (FEM) to provide a hybrid technique for data analysis. A hybrid method where two different methods are combined provides a more efficient means of analyzing various engineering problems than either of them does alone. An

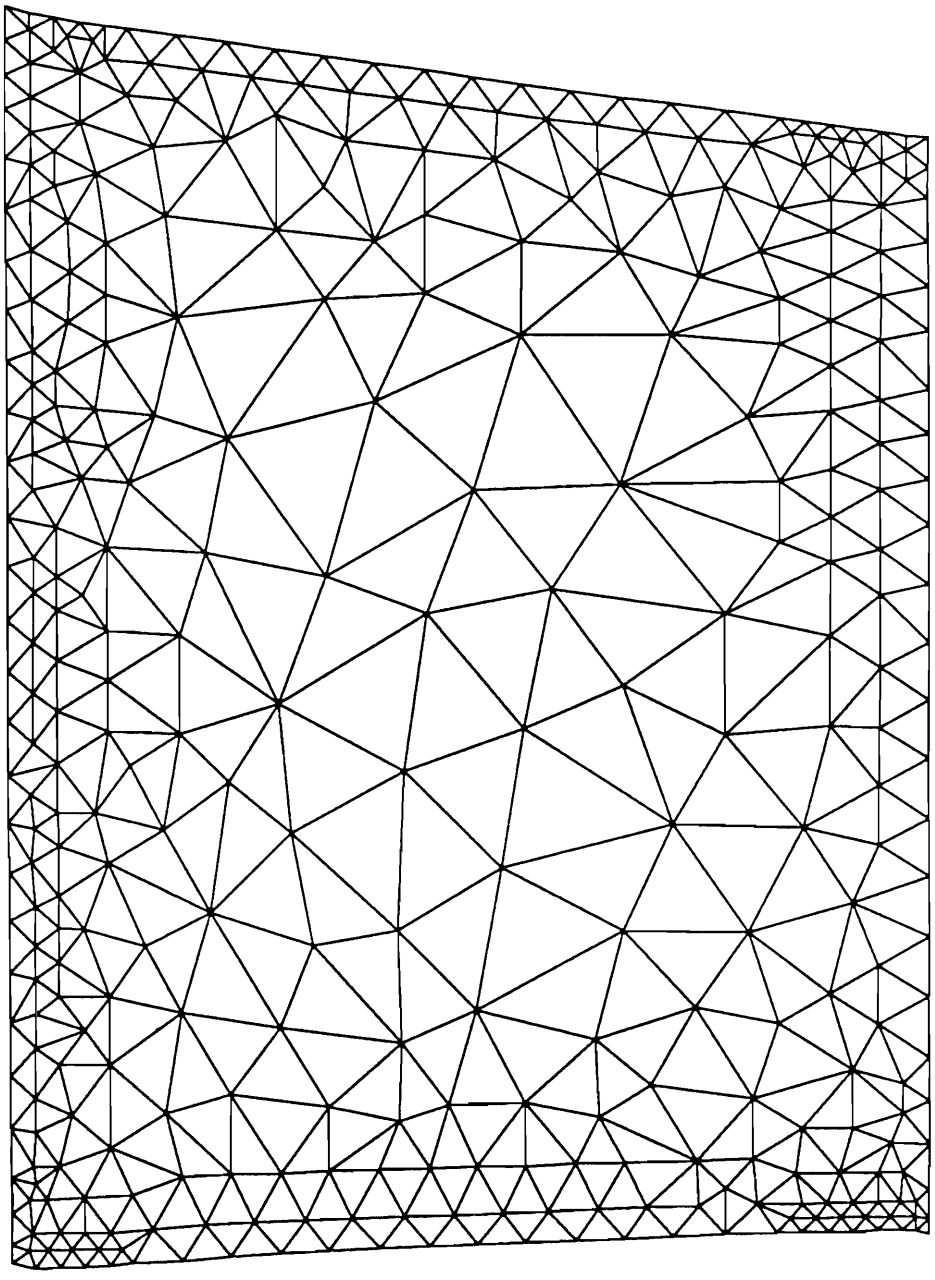

Figure 3.5 Electronically generated mesh for the epoxy cantilever beam.

existing hybrid method of analyzing moire data consists of getting displacement data along the boundary of a region of interest from a fringe pattern and using them as boundary conditions in finite element analyses [46]. The deformation parameters such as displacements and strains inside the region are then determined. This method requires precise knowledge of the material properties of the test specimens. In another hybrid method, the displacement data are obtained inside the region as well as along the boundary [46]. Such a method does not require material properties for the determination of strains. However, in both methods, a mesh is first generated and then the displacement data are obtained at the nodes from a fringe pattern. In such a case fringe lines do not necessarily pass through the nodes, and the displacements must be approximated at the nodes by interpolation. The error can be large, especially when localized nonuniform deformations are analyzed. With the mesh-generating routine and the new algorithm presented previously, a mesh is generated based on the digitized points such that the nodal points are at the fringe lines, and no interpolation is involved. Since the data can be collected practically everywhere in the entire region of interest from a pattern with high-frequency carrier fringes, the displacements are known at the interior nodes as well as at the nodes on the boundary. This means that strains can be determined without knowledge of material properties. Also the known displacements in the entire region of interest on a surface can be used as boundary conditions for three dimensional finite element analyses.

3.5 Summary

The new method of high-resolution data reduction was developed. It has the following features:

— It does not require any modification to interferometric systems already in use,

— The spatial resolution of the measurements is not sacrificed,

— Since only one exposure is needed for a given displacement component and the new method is employed not during the experiment but in the analysis of the data, it can be applied to dynamic as well as static measurements,

— The presented algorithm applies not only to moire interferometry but also to any experimental technique based on two beam interference as long as the fringe pattern has good contrast,

— While it was used in this work for the measurements of residual deformation, it can be applied to any kind of deformation measurements as long as the fringe patterns have high contrast.

It should be emphasized that no matter what the number of electronically generated fringes is, the sensitivity is the same as in ordinary moire interferometry. The improvement is in the increase of the number of points where the data can be collected with the maximum resolution; therefore overall resolution of measurements increases.

The mesh-generating routine was also developed for effective analysis of nonuniform deformation, which can be combined with FEM for determination of strains and stresses. The new procedure combined with the mesh routine

presented in the previous section would be very efficient especially when it is applied to composite materials that often show complex mechanical and/or thermal behavior. This new method will be applied, in the next part, to graphite/epoxy composite plates for measuring residual strains introduced during the curing process.

PART 4 : HIGH RESOLUTION MEASUREMENT OF RESIDUAL STRAINS IN COMPOSITE PLATES

4.1 Introduction

The new method, moire interferometry combined with the cut-and-sectioning techniques presented in Part 2, provided an excellent tool for releasing the residual stresses and measuring the resulting residual strains effectively in composite materials. However, the standard data reduction technique of moire interferometry is not able to provide the residual strain distribution within a single ply and, hence, allow for investigation of the physical phenomena in more detail. A new data reduction method which is capable of providing a qualitative as well as quantitative within-the-ply analysis was developed and described in Part 3. Its usefulness was demonstrated for an epoxy beam loaded in bending. Now the goal is to combine both new methods and to apply them to composite materials. The combined method applied to composite materials and its results are presented in this part. Flat composite plates were chosen as test materials since their behavior is simpler and more predictable than that of composite cylinders.

As mentioned previously, the residual stresses in fiber-reinforced composite materials are a function of many parameters such as constituent material properties, stacking sequence and orientation of plies, fiber content, and curing temperature. In addition to the capability and effectiveness of the new method,

the effects of size and stacking sequence of plies in flat composite panels on resulting residual strains are also studied. The analysis of results is focused on the in-plane transverse stresses and the corresponding strains, because they are very large relative to the transverse strength and, thus, critical to the failure of structures.

4.2 Specimens and Experimental Procedure

4.2.1 Specimens

Specimens with three different stacking sequences were tested in this work to study the effect of stacking sequence of composites on residual strains. They were cross-ply graphite/epoxy composite plates with stacking sequences of $[0_2/90_2/0_2/90_2/0_2]$, $[0_2/90_2/0_2/90_2/0_2]_s$, and $[0_4/90_4/0_4/90_4/0_4]$. They were made of AS4 graphite fibers and 3502 epoxy system. The thickness of a single ply was about 0.125 mm.

As for the tests for cylindrical specimens described in Part 2, they were stored in the laboratory for a few weeks where the tests were performed to minimize the instability of the specimens due to moisture and temperature changes during the experiment. Additionally all the gratings were replicated in the same testing laboratory.

4.2.2 Experimental Procedure

The experimental procedure was the same as that for the composite cylinders, i.e., a crossed-line diffraction grating was replicated on the surface

perpendicular to the plane of the plates, and a cut was made through the grating in the plane perpendicular to both the grating and the plane of the plates to release the residual stresses. The deformation patterns were recorded with and without proper carrier fringes in order to apply the new data reduction method in the analysis of the results. Again, as for the ring test, a slow rpm precision diamond saw was used throughout the experiment in order to avoid thermal effects and assure a clean cut with well-defined edges. Additionally, for cutting, small scrap pieces of composites were placed on both sides of the plates to minimize the damage to the gratings. Time-dependent deformations were negligible since the test for each specimen was completed in about an hour after the cut was made.

4.3 Results and Discussion

The mesh-generating routine combined with the high-resolution data reduction procedure described in Part 3 was used in the analysis of the results. Data were collected by digitizing the displacement patterns with high-frequency carrier fringes. Then a commercial FEM program was used to determine strains and stresses at those data points. The word "transverse" used in the next two sections means "in-plane transverse" and the word "in-plane" is omitted. It is important to note here that the coordinate system used in this section is not conventional; that is, the x-axis is used to represent the out-of-plane direction whereas the z-axis is used in conventional coordinate system. This is only to follow the convention of moire interferometry in which the letters U and V are used to represent in-plane displacements in the x- and the y-directions, respectively.

[0_4/90_4/0_4/90_4/0_4]

Fringe patterns shown in Figure 4.1 represent the U and V displacements after the residual stresses were released. For easy interpretation, a schematic diagram which shows the directions of fibers is added. The V displacement pattern shows large deformation in 90° plies. The semi-circular shaped fringes in those plies indicate that the V displacement varies through the thickness of the plies in such a way that it is maximum at the center of the plies and gradually decreases towards the interfaces. This is because the 90° plies are constrained by the adjacent 0° plies at the interfaces between them. The U displacement pattern does not show significant deformation, but it is not negligible. This is easily noticed in the same pattern with carrier fringes as shown in Figure 4.2(b); the fringe lines near the edge of the cut are not straight as they are in the region away from the cut. In Figure 4.2(a), the wavy fringe lines represent the continuous strain variation through the thickness of the specimen.

Figure 4.3 illustrates the nonuniform mesh for the analysis of the displacement patterns (see Figure 4.1) generated by the mesh program presented in Part 3. Approximately 400 data points were collected from the displacement patterns with high-frequency carrier fringes of rotation. They were digitized densely near the edge of the cut and less densely in the region away from the cut for more efficient analysis of the fringe patterns. Computer-generated displacement patterns with a contour interval of 83.4 nm are demonstrated in Figure 4.4. The original fringes with a contour interval of

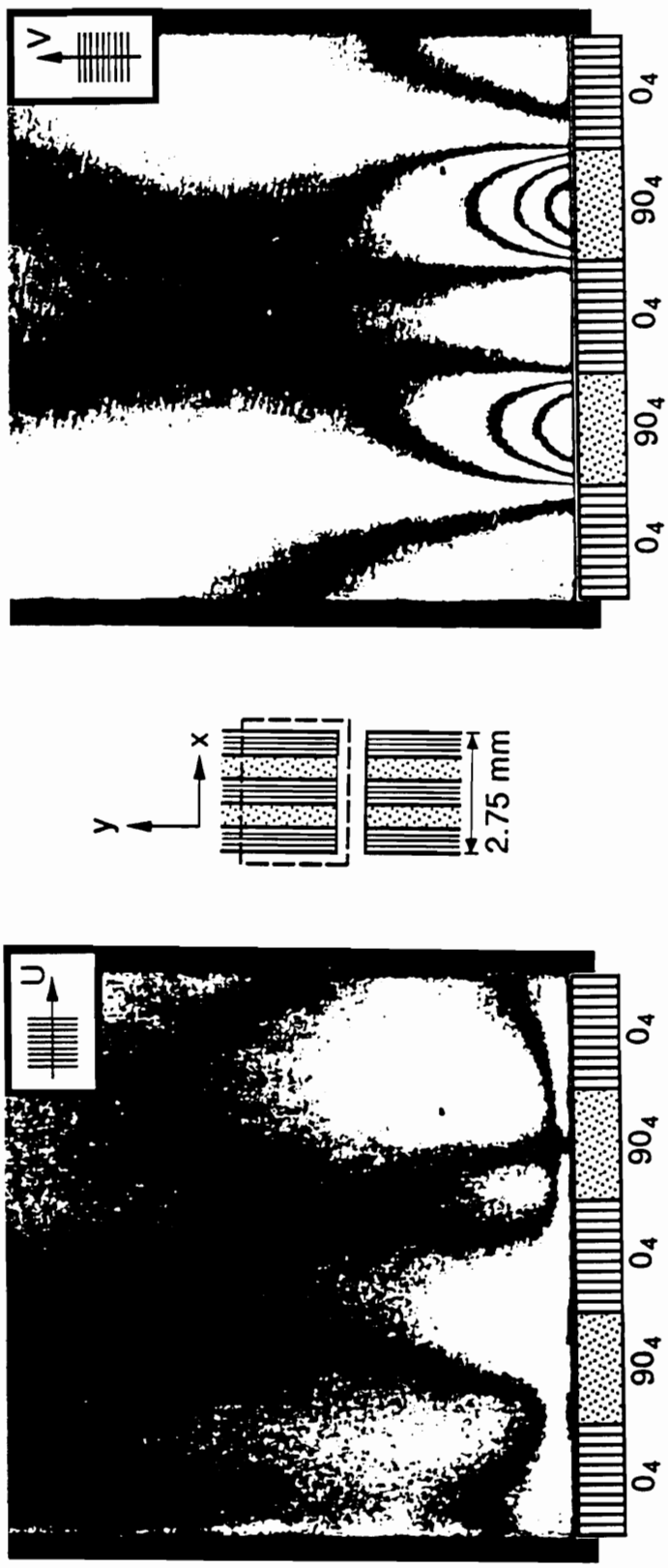

Figure 4.1 U and V displacement patterns for $[0_4/90_4/0_4/90_4/0_4]$ specimen after the residual stresses are released.

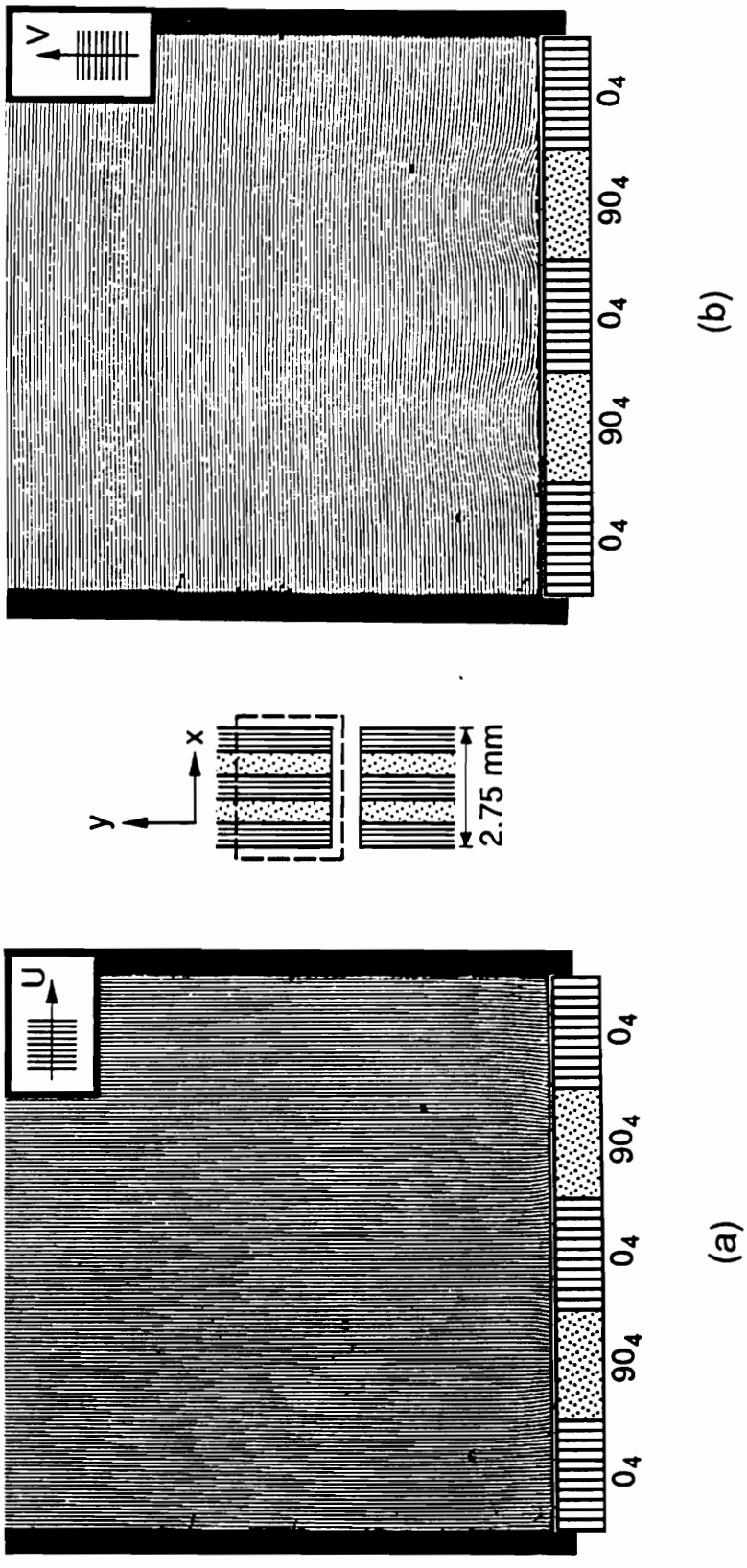

Figure 4.2 (a) U and (b) V displacement patterns for $[0_4/90_4/0_4/90_4/0_4]$ specimen after carrier fringes of extension were added.

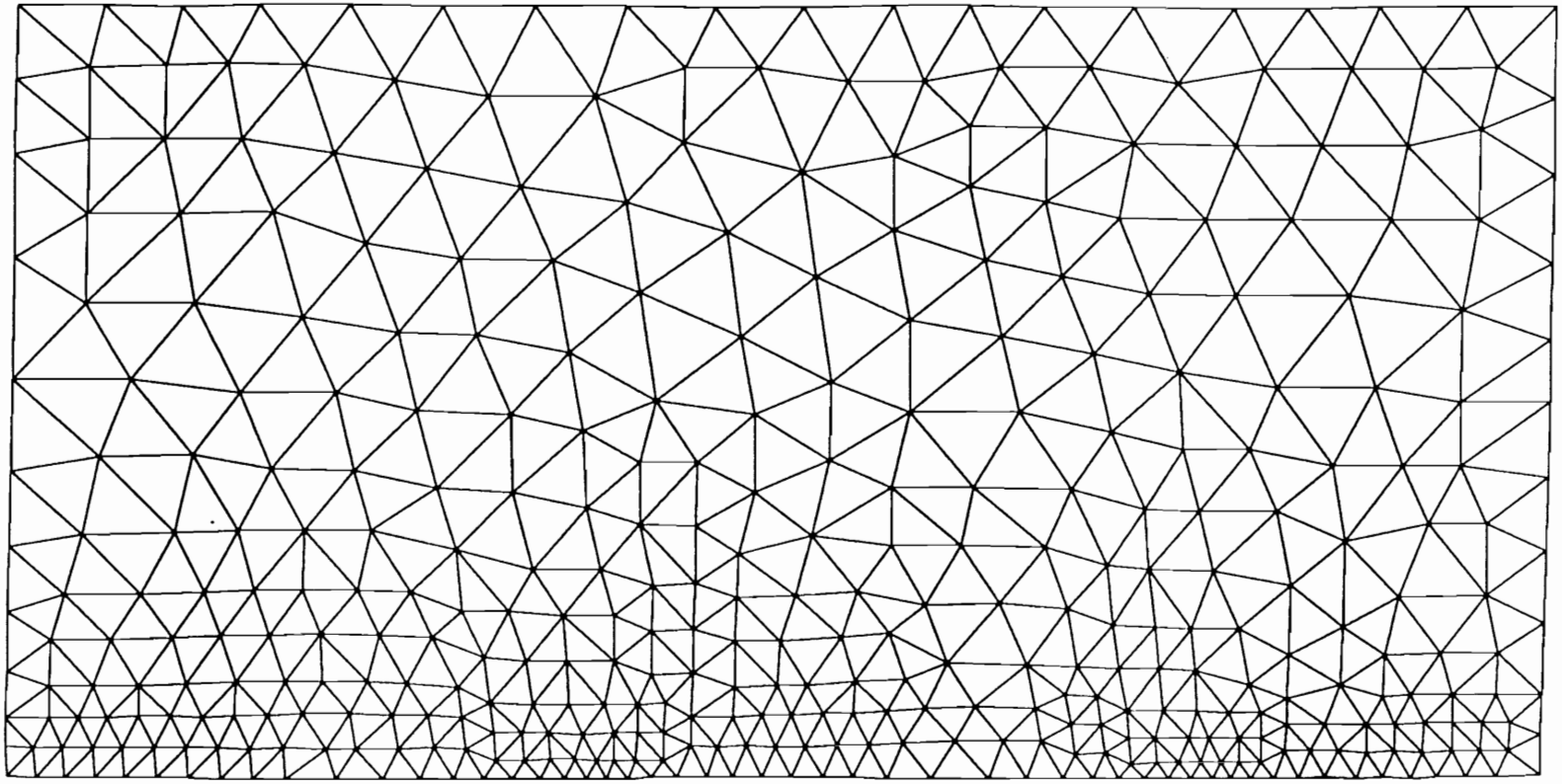

Figure 4.3 A nonuniform mesh produced for data analysis of the specimen with stacking sequence of $[0_4/90_4/0_4/90_4/0_4]$.

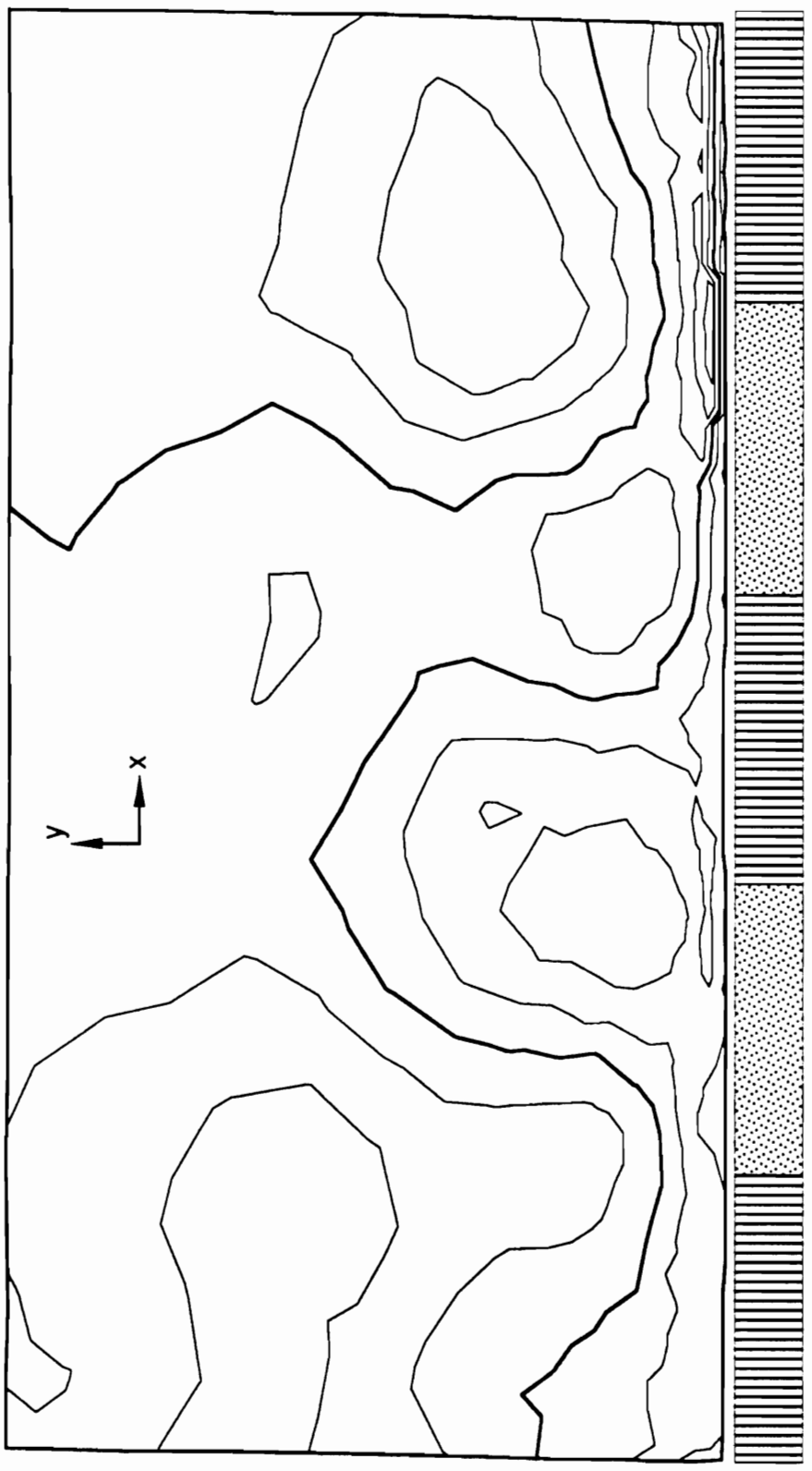

Figure 4.4 (a) Computer generated U-displacement pattern showing a good agreement with the original fringe patterns. Contour interval is 83.4 nm and the original fringes are highlighted by thicker lines.

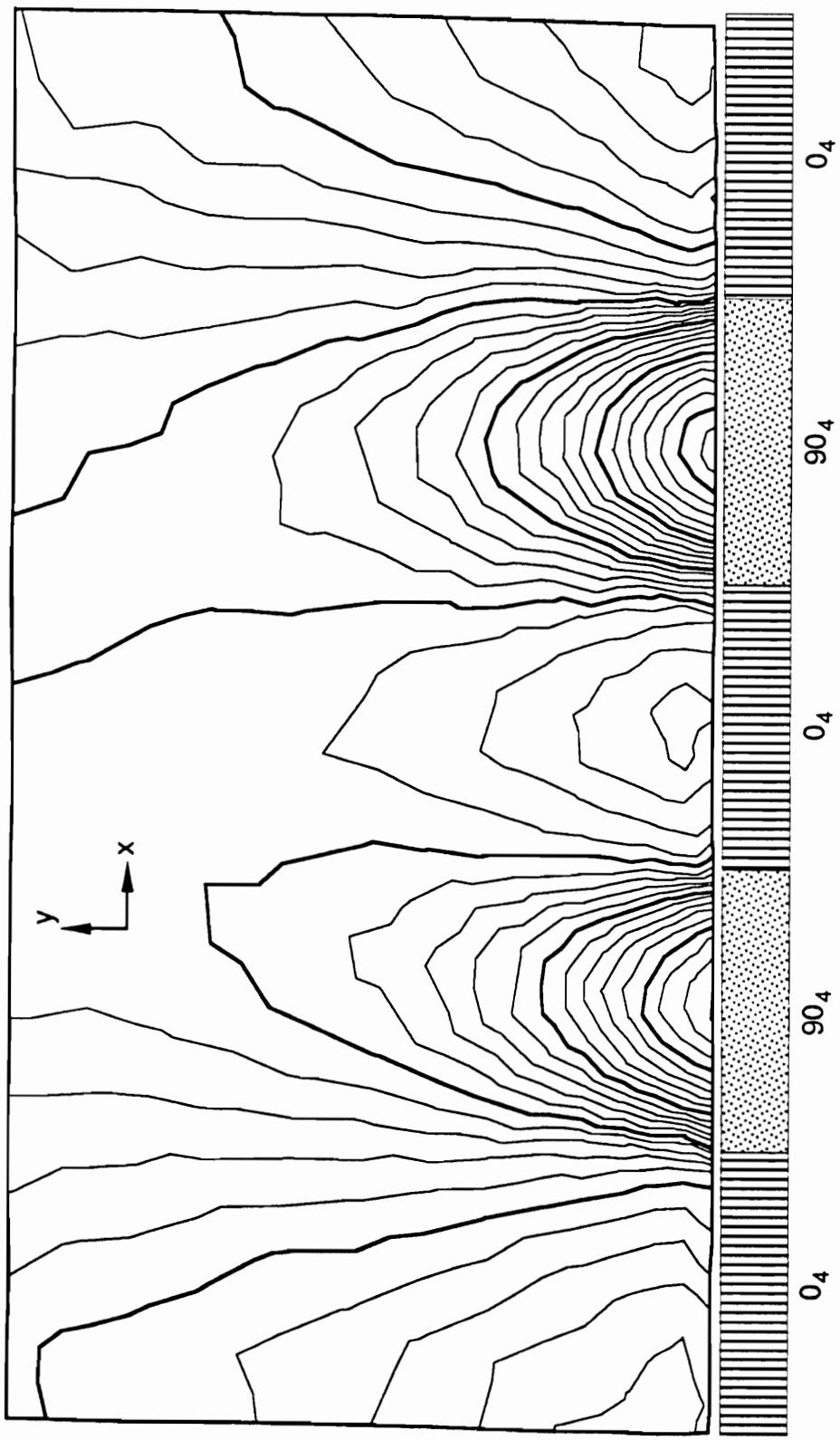

Figure 4.4 (b) Computer generated V-displacement pattern showing a good agreement with the original fringe patterns. Contour interval is 83.4 nm and the original fringes are highlighted by thicker lines.

417 nm are highlighted with thicker lines. The computer-generated patterns show a good agreement with the original patterns.

The contour maps of strain components ε_x, ε_y, and γ_{xy} are shown in Figures 4.5. They were determined using a FEM post-processor without knowledge of material properties because the displacements are known at all nodes in the mesh. A peculiar pattern noticed in the contour map of ε_y is that the maximum and minimum values were measured not at the edge of the cut but a bit inside the cut, which is against intuition. This behavior for ε_y in 90° plies, for instance, can be explained as follows. Consider small elements A and B in a deformed composite panels as shown in Figure 4.6. Element A is subject to compression in the x-direction because the deformed shape of a 90° ply causes shear stresses to act inward at the edge of the cut as shown in the figure, whereas element B has no stress component in the x-direction. Such a compressive stress produces tensile strain in the y-direction due to Poisson's effect, and reduces the magnitude of the total compressive strain in that direction. This phenomenon is easily seen from the contour map of ε_x, where ε_x in 90° plies has the negative maximum at the edge and drastically changes to positive values inside. The distance between the location of the maximum strain and the edge of the cut was about 0.15 mm. It is about 30% of the thickness of 90° layers considering the fact that the thickness of a single ply is 0.125 mm. The local nonuniformities in strain contour are possibly due to nonuniform distribution of fibers in the laminae. The measured normal strains varied from -1935 μm/m to 1515 μm/m in the x-direction, and from -2745 μm/m to 685 μm/m in the y-direction. The maximum shear strain was 5055 μm/m.

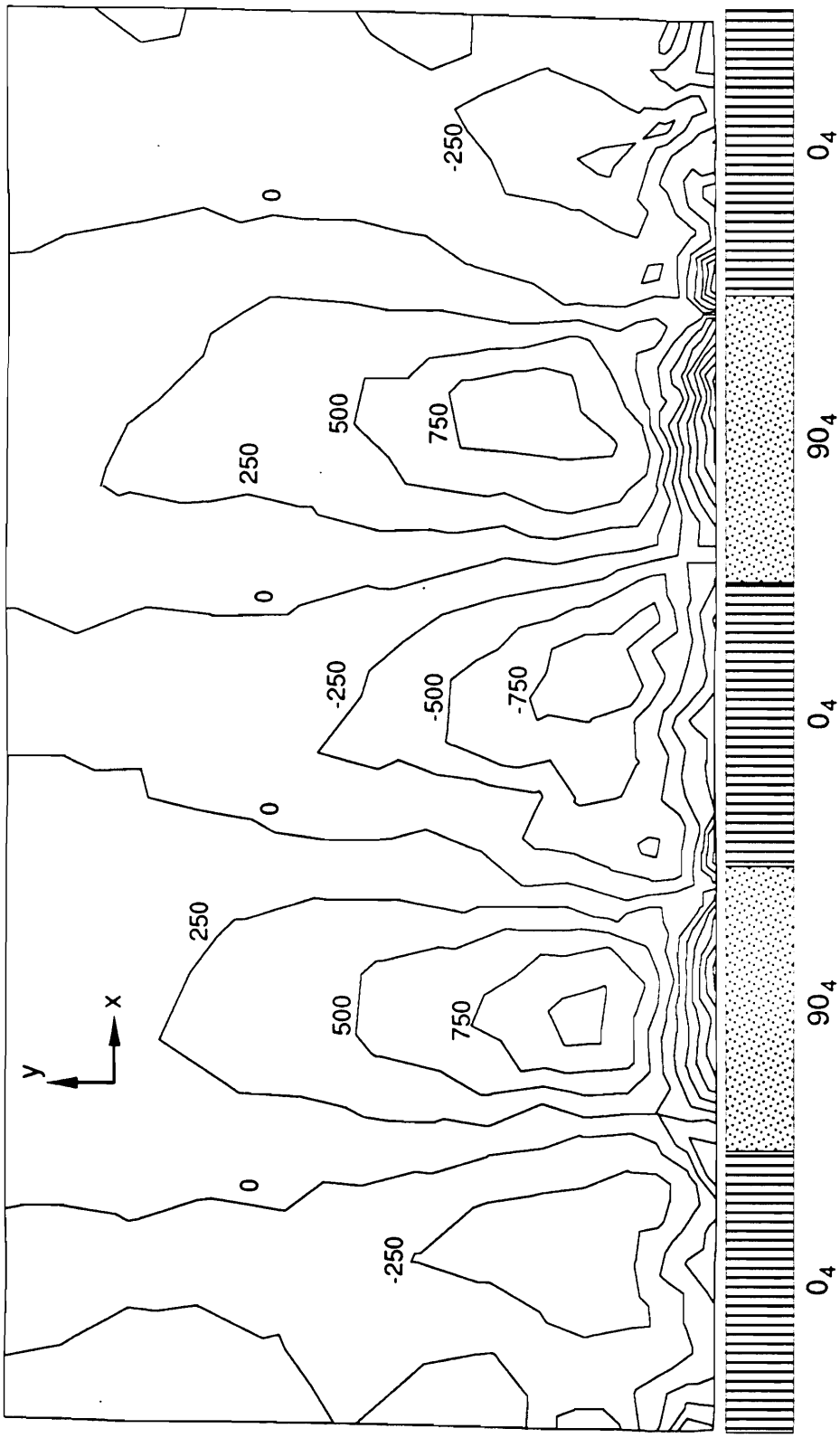

Figure 4.5 (a) Contour map of the measured normal strain ε_x for $[0_4/90_4/0_4/90_4/0_4]$ specimen with a contour interval of 250 μm/m.

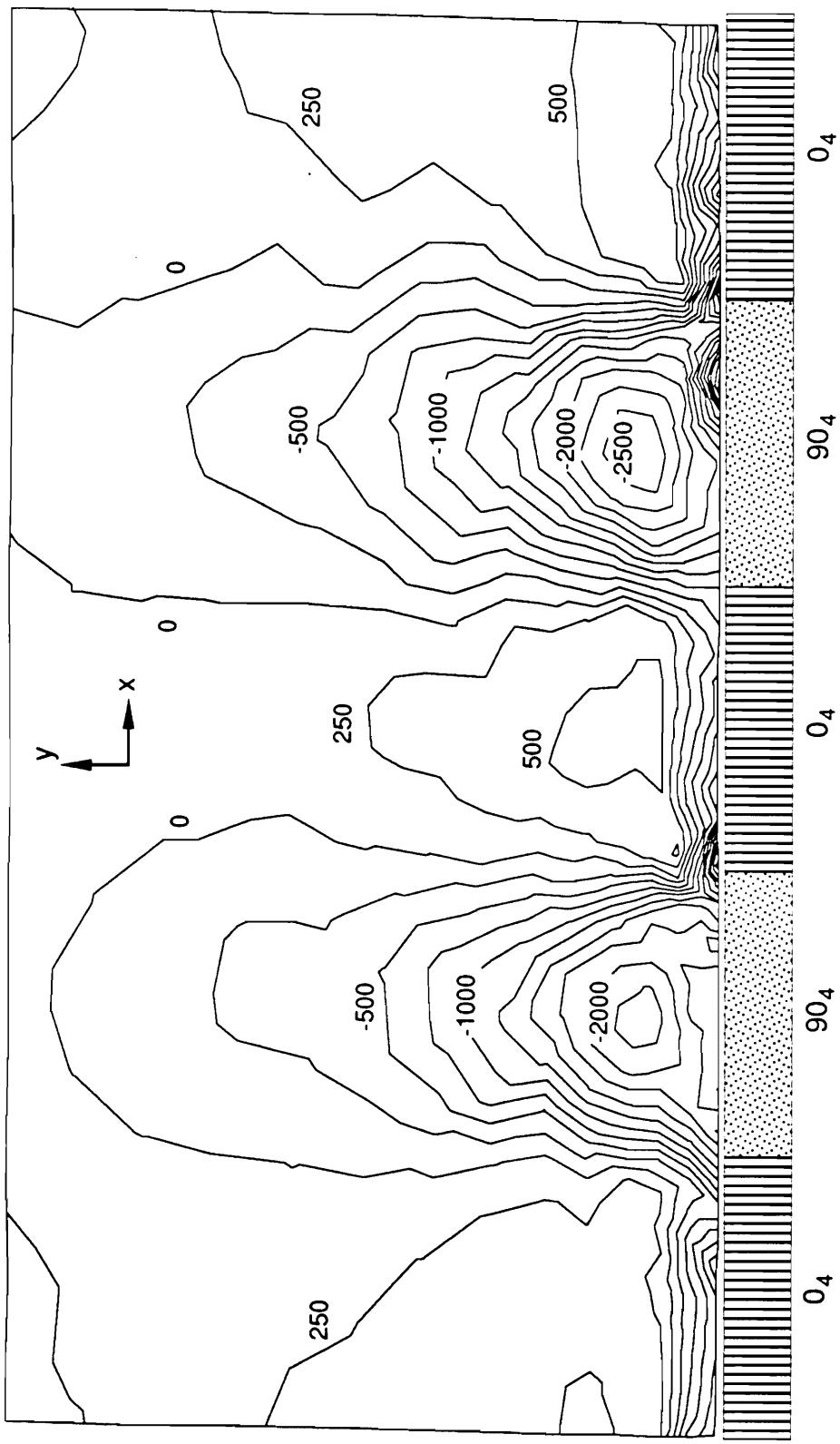

Figure 4.5 (b) Contour map of the measured normal strain ε_y for $[0_4/90_4/0_4/90_4/0_4]$ specimen with a contour interval of 250 μm/m.

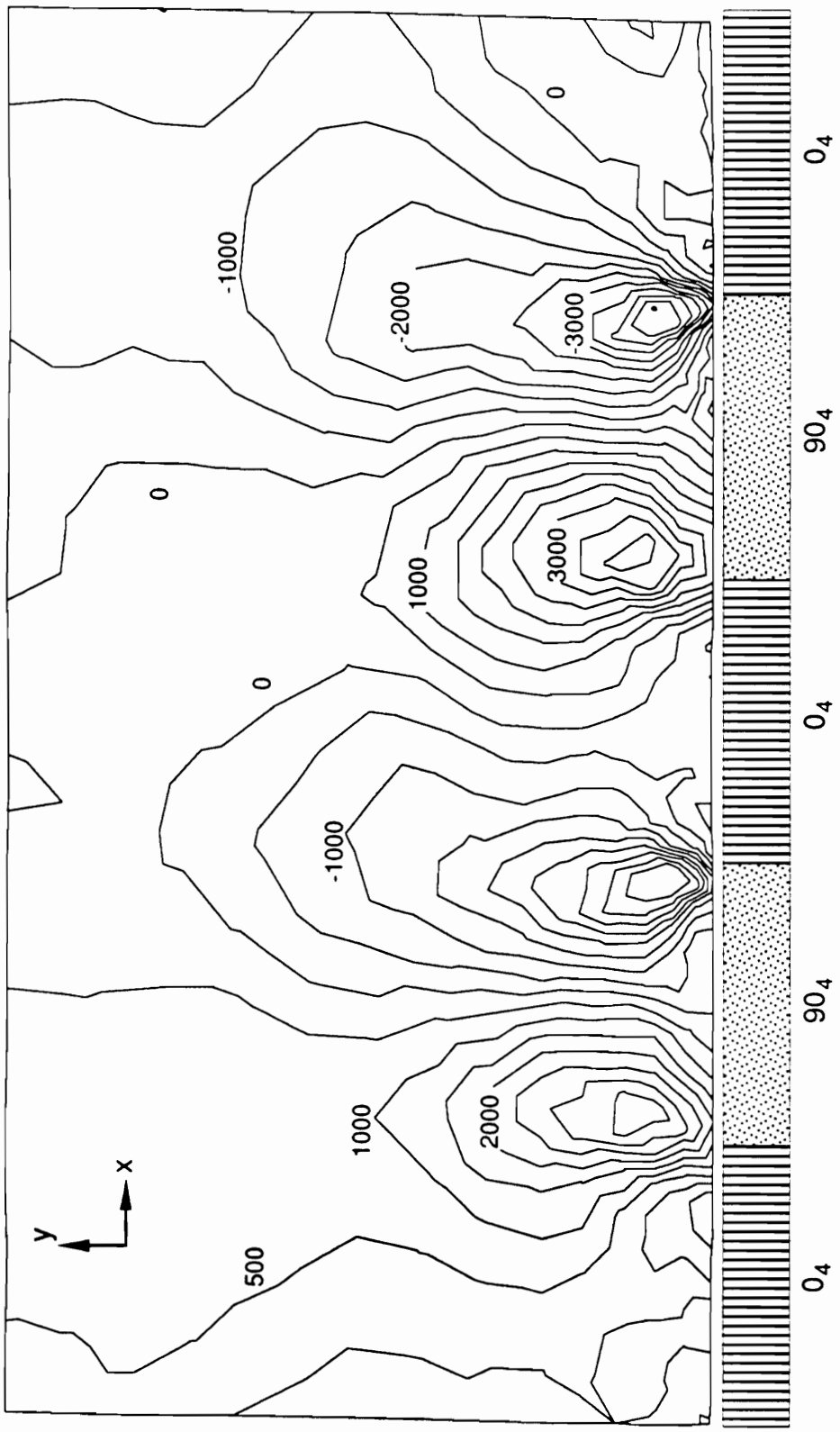

Figure 4.5 (c) Contour map of the measured interlaminar shear strain γ_{xy} for $[0_4/90_4/0_4/90_4/0_4]$ specimen with a contour interval of 500 μm/m.

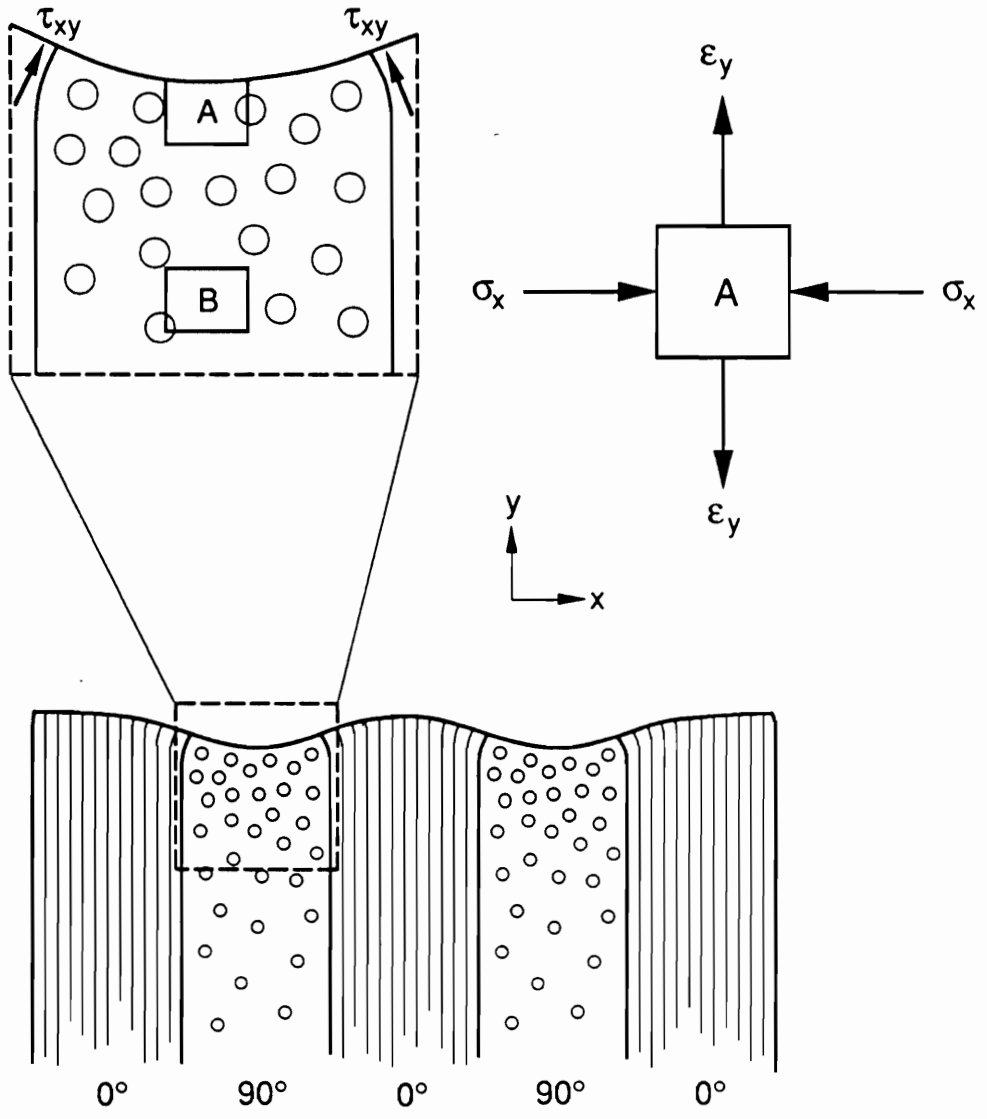

Figure 4.6 Formation of σ_x at the edge of a cut.

Figure 4.7 shows the contour map of transverse stress σ_y in a 90° ply and its distribution along A-A' in the same ply. Whereas the maximum strain was measured a little bit off the edge of the cut, the maximum value of stress was obtained at the edge, which is physically correct. The maximum magnitude of σ_y was 50.3 MPa (7.3 ksi) and this value is comparable to the transverse strength. It agrees with the analytical results obtained by Chamis [2], in which he concluded that the transverse residual stresses in a layer can reach values comparable to the transverse strength of that layer. The large transverse residual stress can cause matrix cracking, and the corresponding interlaminar shear stress can result in delamination.

$[0_2/90_2/0_2/90_2/0_2]_s$

The fringe patterns representing U and V displacements due to the release of the residual stresses are shown in Figure 4.8. It is easy to see that the qualitative behavior is the same as for $[0_4/90_4/0_4/90_4/0_4]$; that is, large compressive deformation in 90° plies and small deformation in 0° plies were detected.

Figure 4.9 represents the corresponding strain contours in which again the maximum strain was measured inside the cut. The distance between the location of the maximum strain and the edge of the cut was about 0.1 mm, which is about 40% of the thickness of 90° plies. The measured normal strain varied from -985 μm/m to 1190 μm/m in the x-direction and from -2600 μm/m to 300 μm/m in the y-direction. The maximum shear strain was 4130 μm/m.

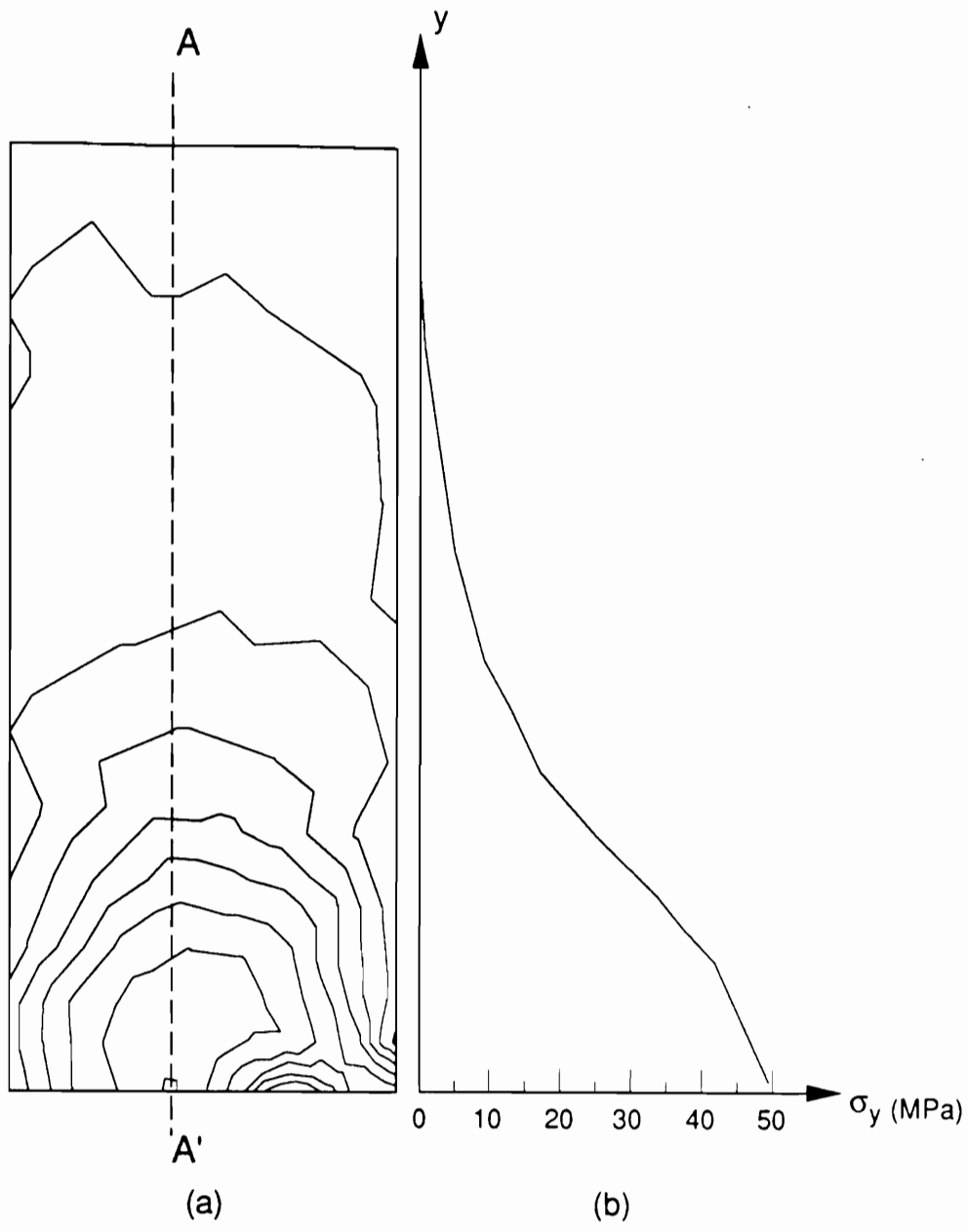

Figure 4.7 (a) Contour map and (b) the distribution along A-A' of the transverse stress in a 90° ply. The maximum value was obtained at the edge of the cut.

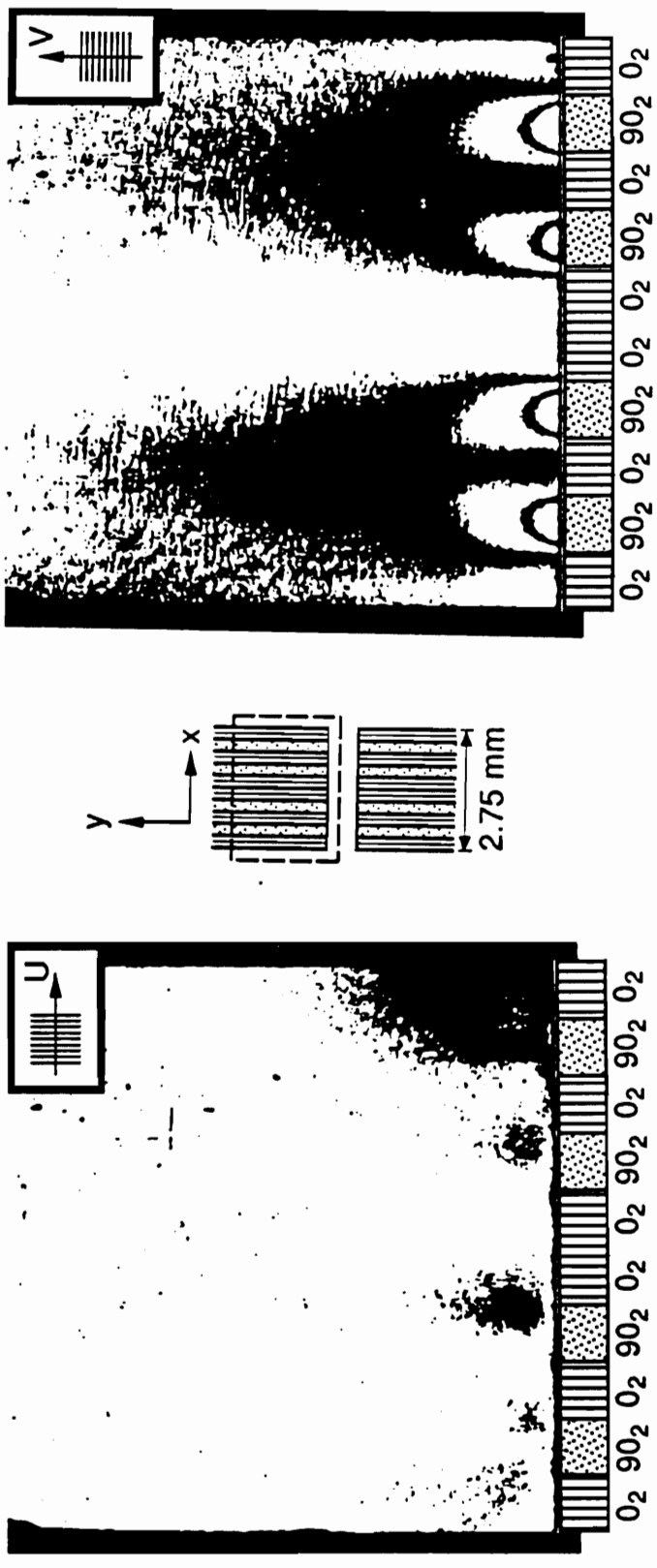

Figure 4.8 U and V displacement patterns for $[0_2/90_2/0_2/90_2/0_2]_s$ specimen after the residual stresses are released.

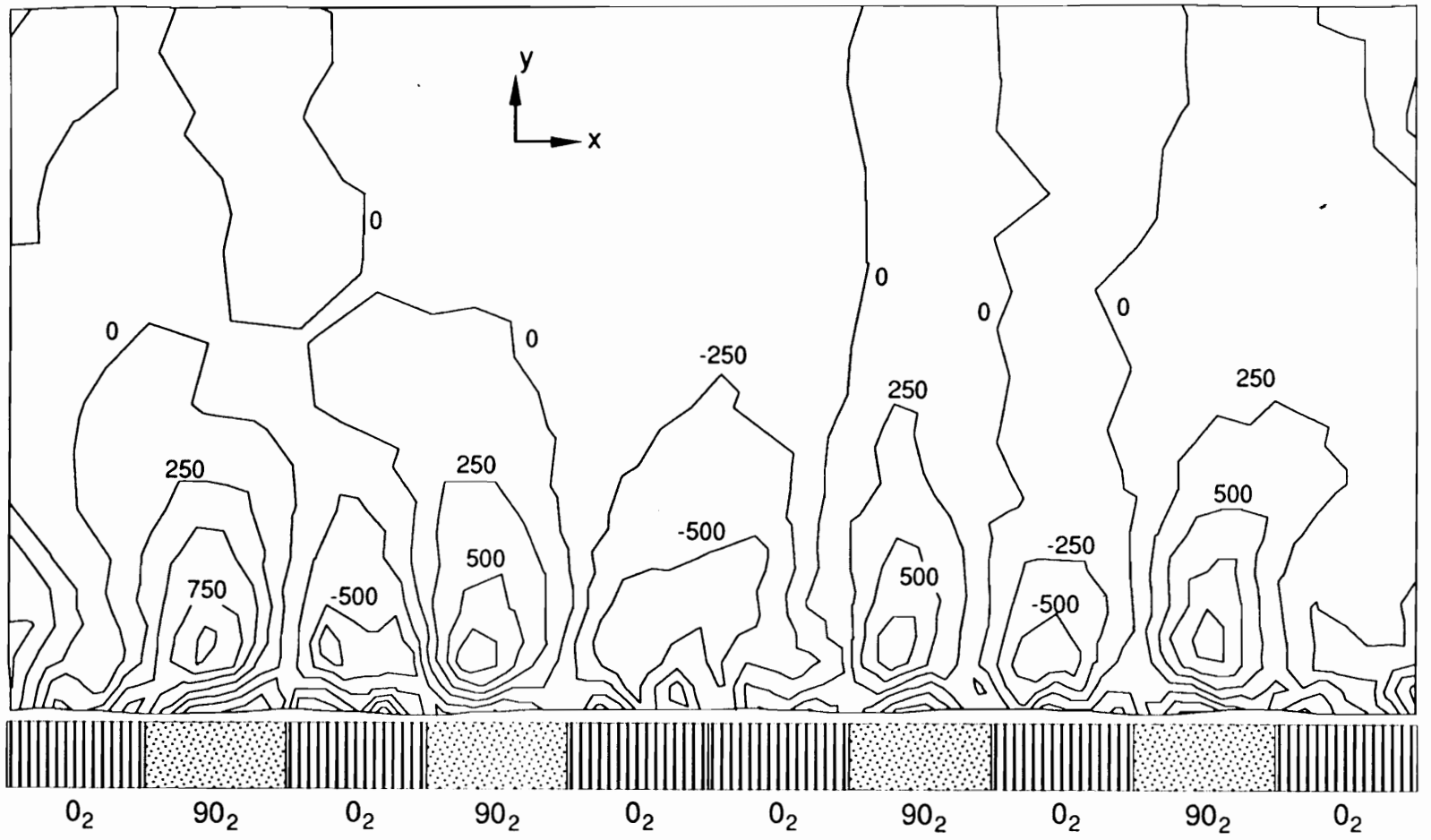

Figure 4.9 (a) Contour map of the measured normal strain ε_x for $[0_2/90_2/0_2/90_2/0_2]_s$ specimen with a contour interval of 250 μm/m.

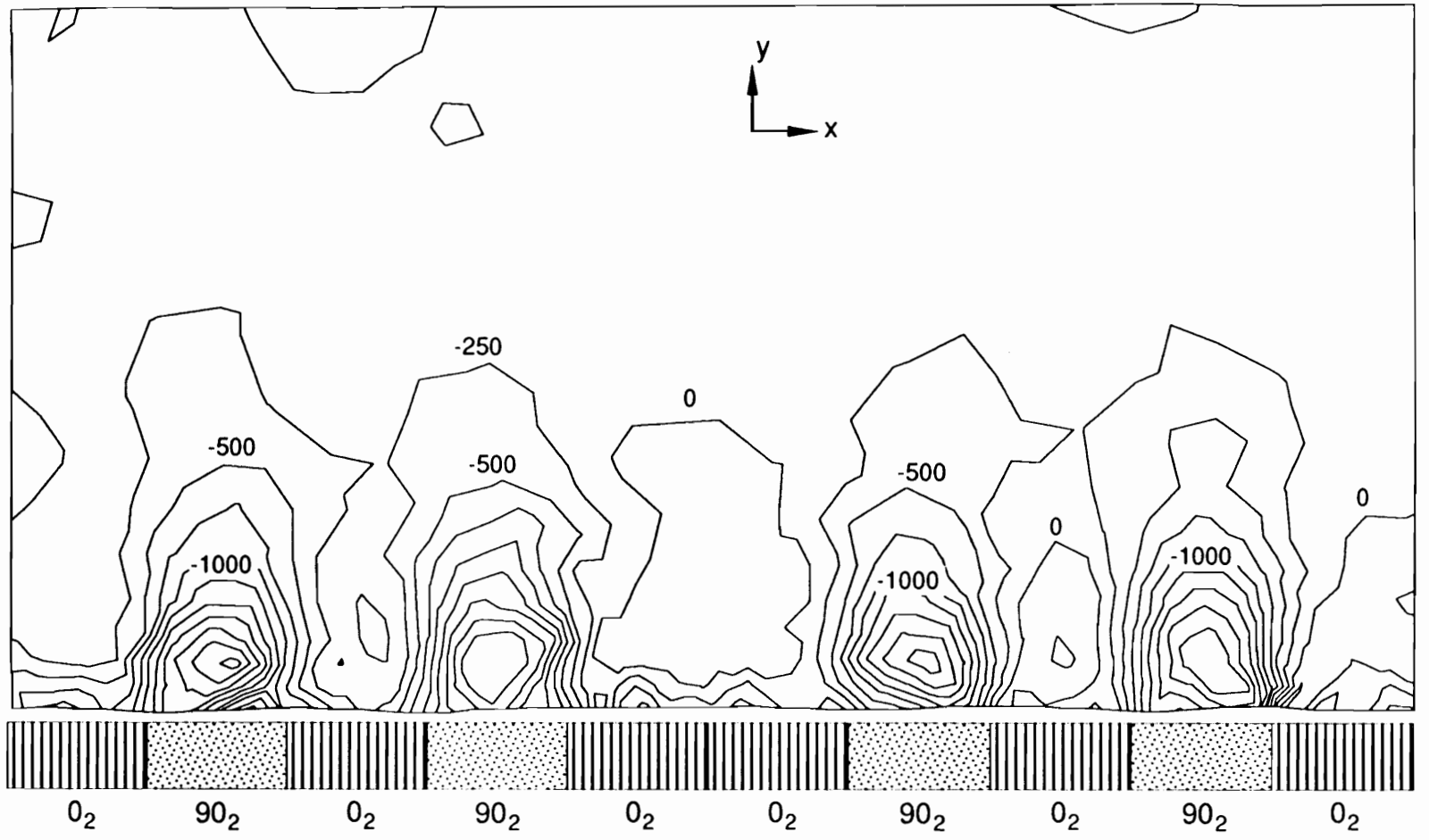

Figure 4.9 (b) Contour map of the measured normal strain ε_y for $[0_2/90_2/0_2/90_2/0_2]_s$ specimen with a contour interval of 250 μm/m.

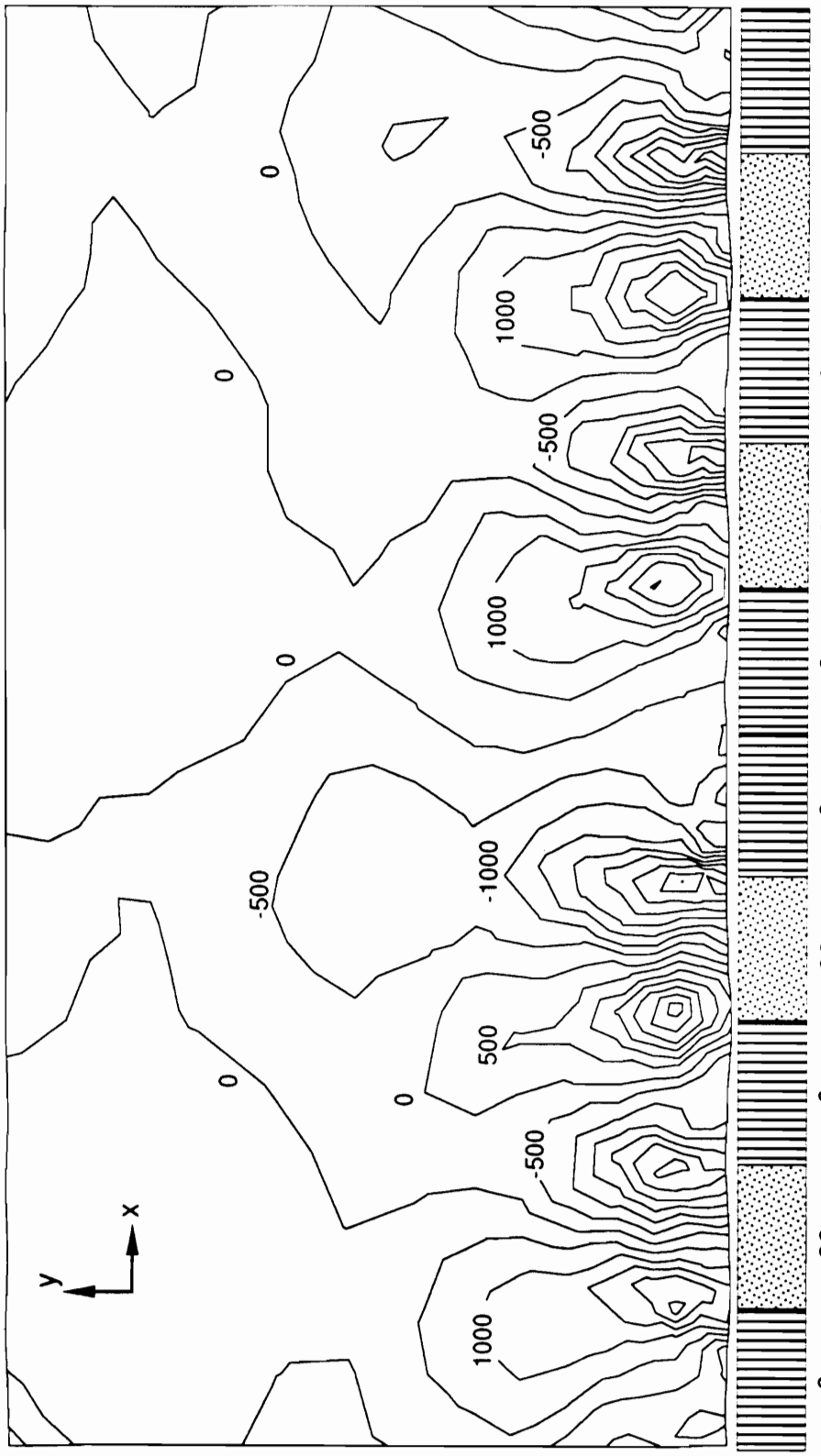

Figure 4.9 (c) Contour map of the measured interlaminar shear strain γ_{xy} for $[0_2/90_2/0_2/90_2/0_2]_s$ specimen with a contour interval of 500 μm/m.

The maximum value of the transverse stress σ_y in 90° plies was 42.1 MPa (6.1 ksi) which is about 80% of the transverse strength.

$[0_2/90_2/0_2/90_2/0_2]$

Figure 4.10 shows U and V residual displacement patterns, and the corresponding strain contour maps are given in Figure 4.11 The deformation pattern was the same as for $[0_2/90_2/0_2/90_2/0_2]_s$. The distance between the location of maximum strain and the edge of the cut was about 0.1 mm, and is the same as that for $[0_2/90_2/0_2/90_2/0_2]_s$ specimen. The measured normal strains varied from -800 μm/m to 1210 μm/m in the x-direction and from -2795 μm/m to -45μm/m in the y-direction. The maximum shear strain was 3620 μm/m. The maximum transverse stress σ_y in 90° plies was 46.0 MPa (6.67 ksi) which is about 90% of the transverse strength.

Comparison

The maximum values of transverse residual strains and stresses in all three specimens were about the same. This agrees with classical lamination theory (CLT) in a sense that, in CLT, strains and stresses are independent of stacking sequence (between $[0_4/90_4/0_4/90_4/0_4]$ and $[0_2/90_2/0_2/90_2/0_2]_s$) and size (between $[0_2/90_2/0_2/90_2/0_2]_s$ and $[0_2/90_2/0_2/90_2/0_2]$). A significant difference is that even though, in CLT, strains and stresses are considered to be constant through the thickness of a layer, they varied continuously, having the maximum value on the center of the layer. The maximum transverse stresses in all three cases reached about 80 to 95% of the transverse strength. These

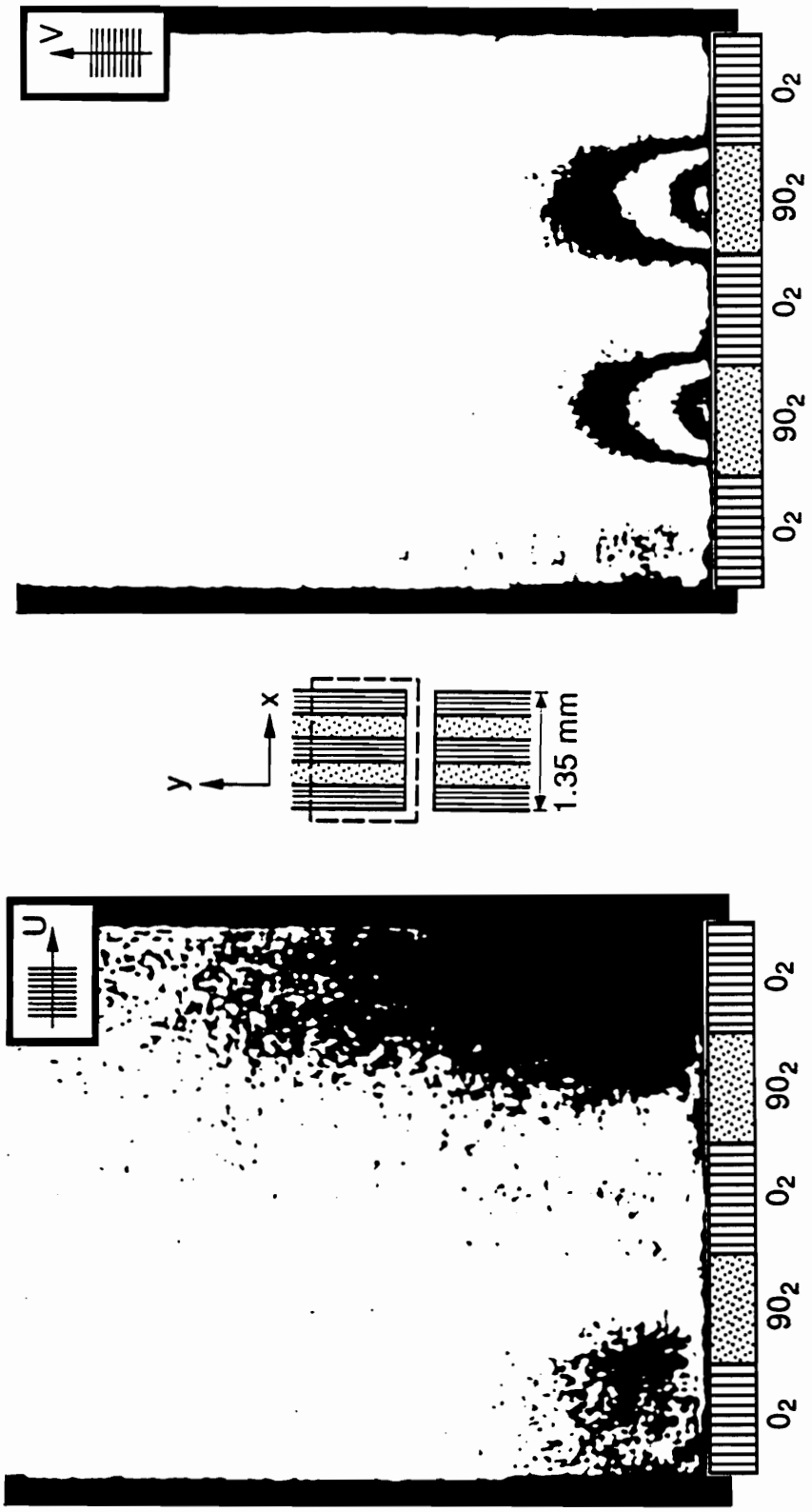

Figure 4.10 U and V displacement patterns for $[0_2/90_2/0_2/90_2/0_2]$ specimen after the residual stresses are released.

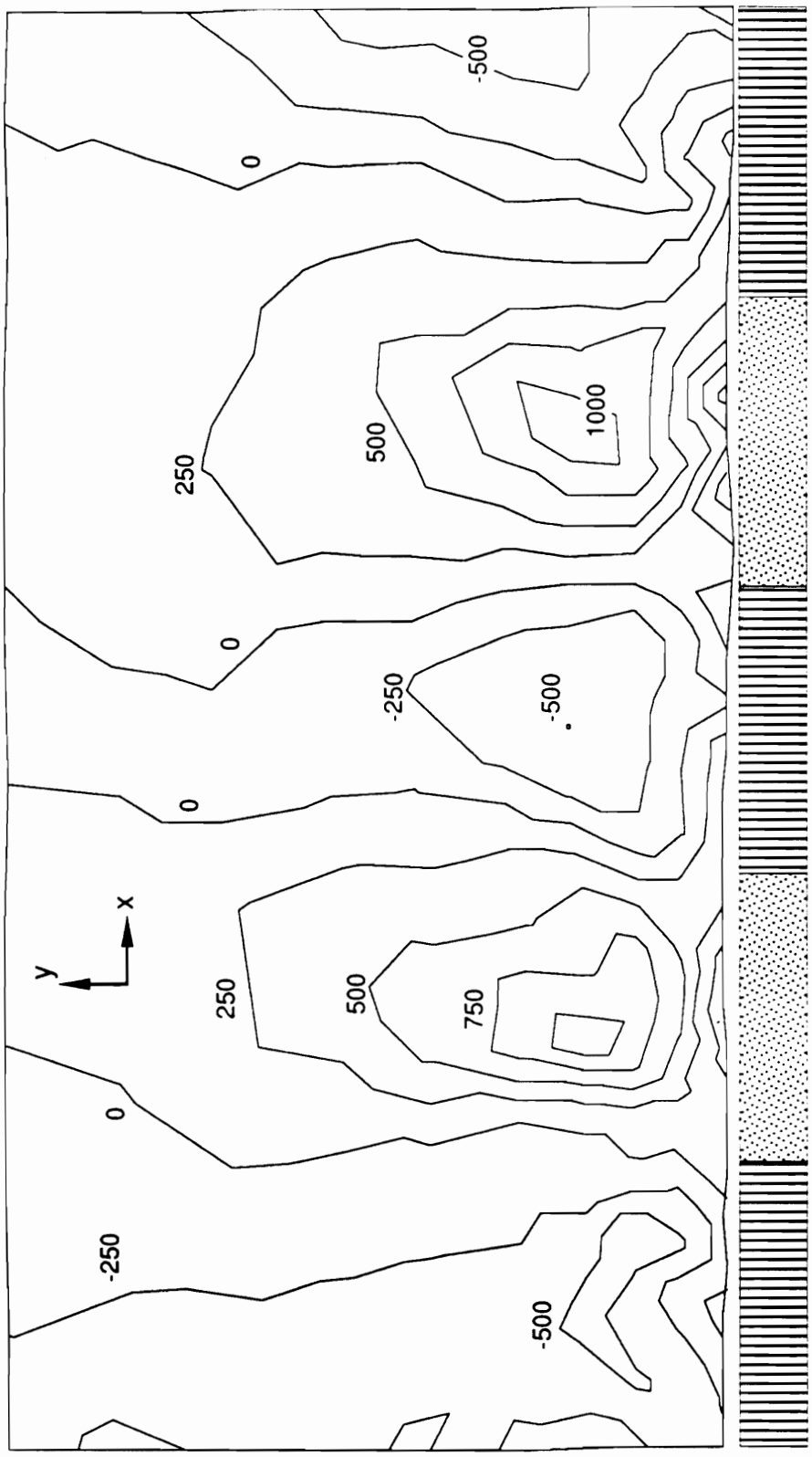

Figure 4.11 (a) Contour map of the measured normal strain ε_x for $[0_2/90_2/0_2/90_2/0_2]$ specimen with a contour interval of 250 μm/m.

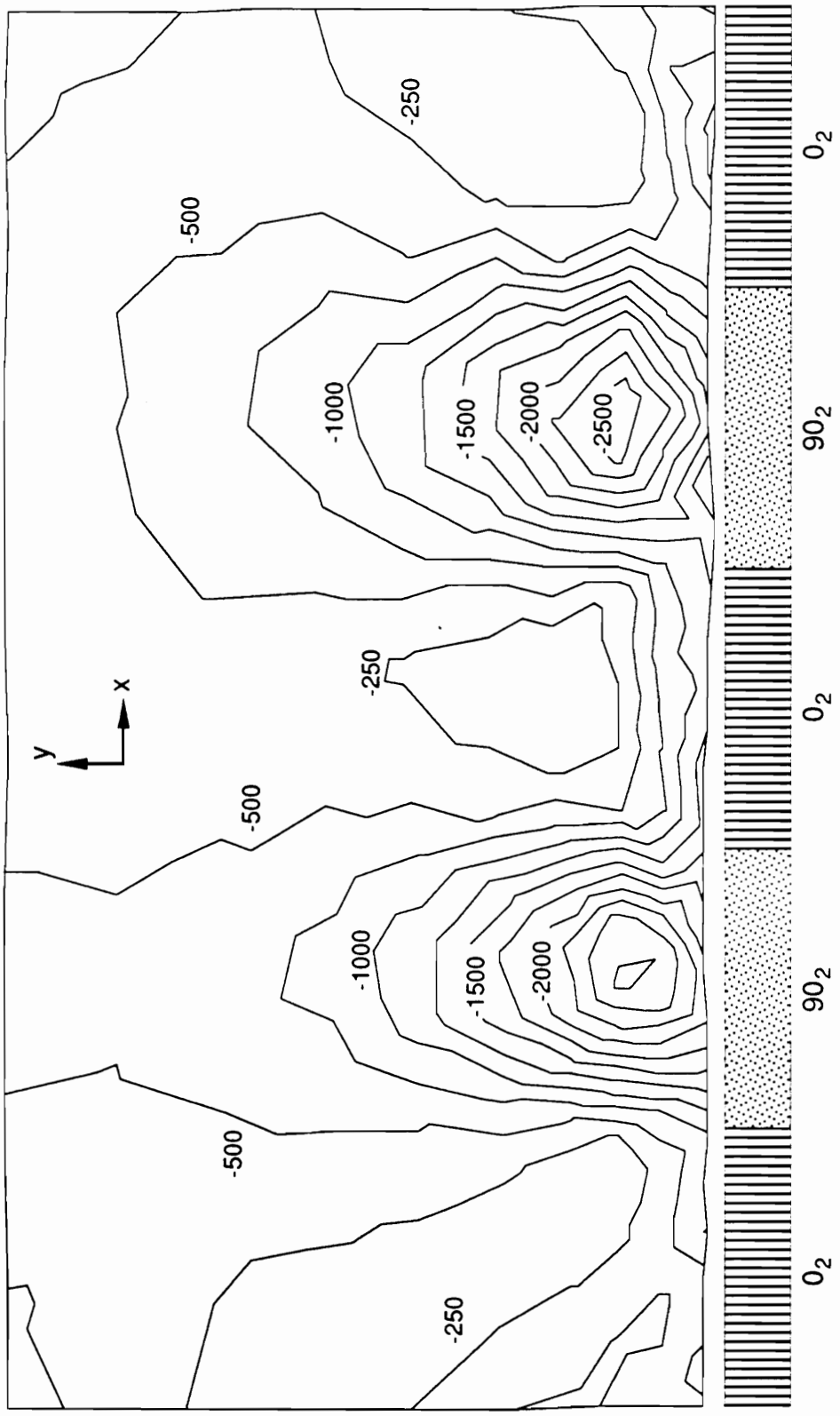

Figure 4.11 (b) Contour map of the measured normal strain ε_y for $[0_2/90_2/0_2/90_2/0_2]$ specimen with a contour interval of 250 μm/m.

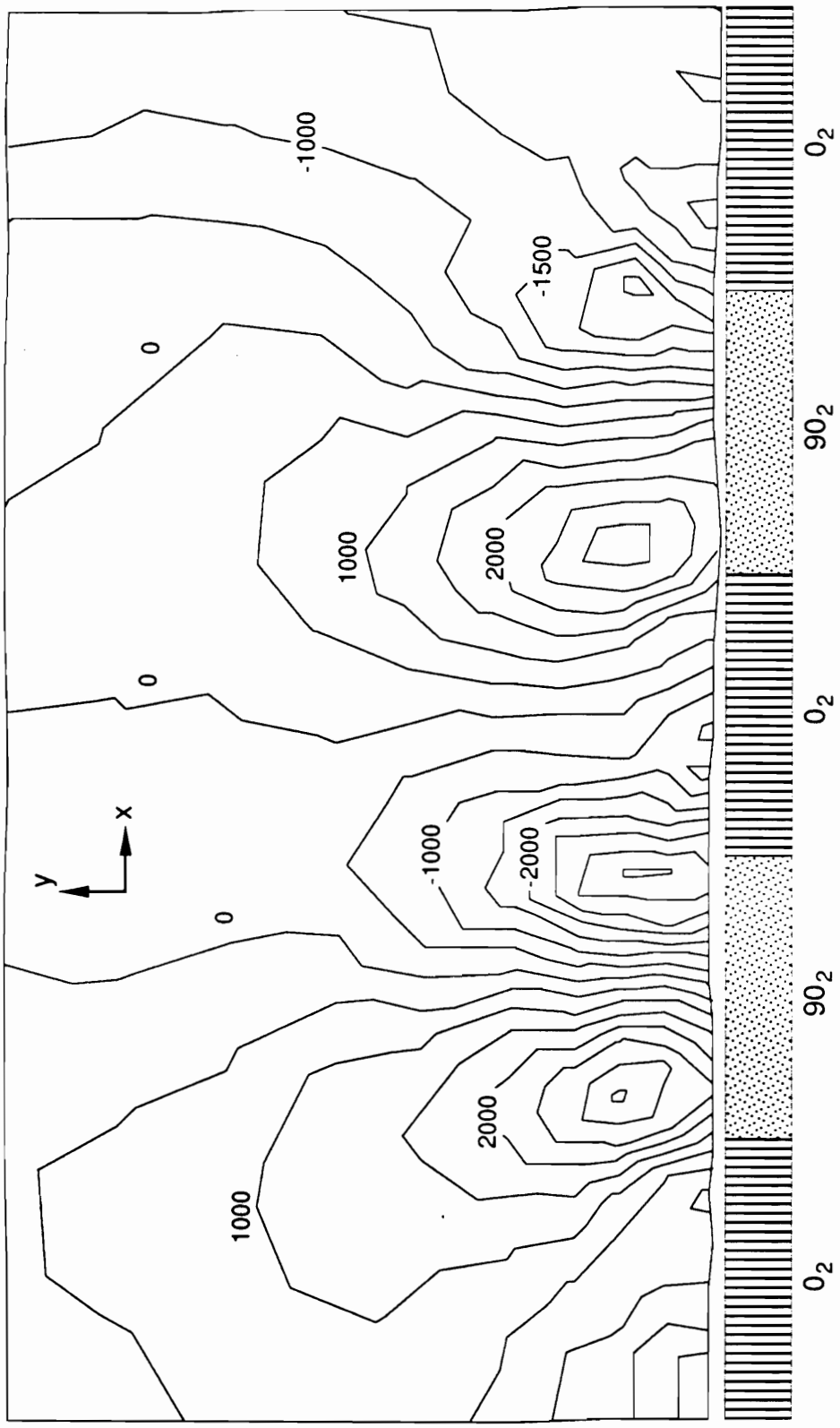

Figure 4.11 (c) Contour map of the measured interlaminar shear strain γ_{xy} for $[0_2/90_2/0_2/90_2/0_2]$ specimen with a contour interval of 500 μm/m.

large stresses, of course, must be taken into account in designing structures because they may cause premature failure of the structures. The values of residual strains and the maximum transverse stresses were listed in Table 4.1.

The distance between the edge of the cut and the location of the maximum transverse strain varied depending on stacking sequence. They were the same for $[0_2/90_2/0_2/90_2/0_2]_s$ and $[0_2/90_2/0_2/90_2/0_2]$, and $[0_4/90_4/0_4/90_4/0_4]$ had different values. The ratios of the distances and the thicknesses of layers with the same fiber direction, however, were about the same, i.e., 0.3 to 0.4.

4.4 Summary

The residual deformations in graphite/epoxy composite panels were measured using the new technique described in Part 2. The residual displacements were obtained with enhanced resolution by digitizing the fringe patterns with high-frequency carrier fringes. The corresponding strains and stresses were then determined by utilizing a FEM package. The contour maps of residual displacements and strains were generated.

The results showed that the transverse stresses in all three cases reached values comparable to the transverse strength. These large values of stresses indicate that the failure of structures is expected below the designed load or prior to the designed life of the structure. The residual stresses, therefore, should be carefully taken into account in the design of structural members. More research must be done in the area of development of the matrix materials and processing of the composite structures in order to eliminate or at least reduce these undesirable effects.

Table 4.1 Comparison of (a) residual strains and (b) the maximum transverse stresses for specimens with different stacking sequences.* Note that the residual strains have signs opposite to the measured strains. The minimum and the maximum values of strains are separated by a slash.

	ε_x	ε_y	γ_{xy}
$[0_4/90_4/0_4/90_4/0_4]$	-1515 / 1935	-685 / 2745	5055
$[0_2/90_2/0_2/90_2/0_2]_s$	-1190 / 985	-300 / 2600	4130
$[0_2/90_2/0_2/90_2/0_2]$	-1210 / 800	45 / 2795	3620

(a)

	σ_y (MPa / ksi)
$[0_4/90_4/0_4/90_4/0_4]$	50.3 / 7.3
$[0_2/90_2/0_2/90_2/0_2]_s$	42.1 / 6.1
$[0_2/90_2/0_2/90_2/0_2]$	46.0 / 6.67

(b)

* Strains are given in μm/m.

The new data-reduction procedure provided an effective way of analyzing the results. Qualitative as well as quantitative interpretation of fringe patterns was performed. A phenomenon which is intuitively not obvious was detected, that is, the maximum transverse strain was measured off the edge of the cut. This phenomenon is not detected by other deformation-measurement methods.

PART 5 : CLOSURE

5.1 Summary and Conclusions

The main objectives of the presented work were to develop a new technique for effective high-resolution measurement of residual strains and to measure residual strains using the new technique.

A new method of residual strain measurement was developed, in which the cut-and-sectioning procedure was combined with moire interferometry. The cut-and-sectioning method was chosen for the separation of the combined effect of different stress components, and moire interferometry for high-sensitivity, high-resolution and full-field measurements. The separation of the combined effect of different stress components was accomplished by dividing the experiment into a few steps and cutting the specimens in the relevant direction in each step.

Two specimens cut from thick walled composite cylinders were tested using the new technique. The results indicated a few serious problems associated with the current techniques of manufacturing the thick composite cylinders. These problems are:

— large interlaminar shear strains in the vicinity of the cuts which may cause early delaminations,

— large strain concentration at the locations corresponding to the curing stops,

— voids and imperfections in the region near the curing stops.

The curing procedure has been found to have very significant influence on the distribution and the magnitude of residual stresses. Specimens with several different numbers and locations of curing stops should be tested and analyzed before any definite conclusion can be assessed.

The time-dependent relaxation and moisture expansion that may occur after the specimens were manufactured are expected to introduce some change in the residual stress field. Consequently, residual strains in freshly cured composites can be more severe and need serious consideration.

The time-dependent deformation during the experiment seems to be negligible. No noticeable change in the deformation field was measured during the tests. It took several weeks in an uncontrolled environment to introduce measurable changes. It is anticipated that these changes were mostly related to moisture absorption in the vicinity of the stress releasing cuts.

The test of thick composite cylinders demonstrated the limitations of current data-reduction methods and the need for higher resolution measurement technique. A new procedure for high-resolution data reduction was developed to enhance resolution. It has the following features:

— preserves the full-field qualitative information of fringe patterns,
— can be used for dynamic measurements,
— can be applied to any interferometric technique based on two beam interference as long as the fringe patterns have high contrast.

This new procedure offered an order of magnitude higher resolution of measurements but at the price of very elaborate data collection process. In

order to make it efficient and attractive for practical applications, a new data processing routine was required.

The nonuniform mesh generating routine was created for efficient data reduction. Fringe patterns can be digitized nonuniformly and the total number of data points to be digitized significantly decreases. This is very efficient especially for highly nonuniform deformation patterns that composite materials often show. Also displacement patterns may be digitized separately and the digitized data points can be combined to produce a mesh. The mesh routine produces nonuniform mesh with triangular elements based on the digitized data points.

The mesh routine allows a hybrid analysis where moire interferometry and FEM are combined. Using a FEM processor, unknown displacements can be determined. If all displacements are known, the corresponding strains can be obtained, without knowledge of material properties, using a post-processor. Also the known displacements in the entire region of interest on a surface can be used as boundary conditions for three-dimensional finite element analyses.

The new methods mentioned above were used for the measurement of residual strains in flat composite panels. The methods were shown to be very useful, in that a phenomenon which is not intuitively obvious and detectable with other techniques was detected. The new methods were a useful step for better understanding of the complexity of residual stresses.

5.2 Recommendations

Even though there are more factors which have effects to some extent on the residual stresses, listed here are a few items which should be extensively studied for better understanding of residual stresses:

— time dependent (viscoelastic) behavior,

— moisture effects,

— effect of fiber volume fraction,

— various combination of the fiber and the matrix materials with different CTE's.

REFERENCES

1. R. M. Jones, Mechanics of Composite Materials, McGraw-Hill Book Company, New York, 1975.

2. C. C. Chamis, "Lamination Residual Stresses in Cross-Plied Fiber Composites," Paper No. 17-D, *Proceedings of 26th Annual Technical Conference of the Society of the Plastics Industry*, Reinforced Plastics/Composites Division, (Feb. 1971).

3. Y. M. Tarnopolskii and T. Kincis, Static Test Methods for Composites, Van Nostrand Reinhold Company, New York, 1985.

4. J. Mathar, "Determination of Initial Stresses by Measuring the Deformation Around Drilled Holes," *Transactions to ASME*, Vol. 56, No. 4, pp. 249-254 (1934).

5. W. Soete and R. Vancrombrugge, "An Industrial Method for the Determination of Residual Stresses," *Proceedings of SESA*, Vol. 8, No. 1, pp. 17-28 (1950).

6. R. A. Kelsey, "Measuring Non-uniform Residual Stresses by the Hole Drilling Method," *Proceedings of SESA*, Vol. 14, No. 1, pp. 181-194 (1956).

7. C. W. Bert and G. L. Thompson, "A Method for Measuring Planar Residual Stresses in Rectangularly Orthotropic Materials," *Journal of Composite Materials*, Vol. 2, No. 2, pp. 244-253 (1968).

8. B. R. Lake, F. J. Appl and C. W. Bert, "An Investigation of the Hole-Drilling Technique for Measuring Planar Residual Stress in Rectangularly Orthotropic Materials," *Experimental Mechanics*, Vol. 10, No. 6, pp. 233-239 (1970).

9. N. J. Rendler and I. Vigness, "Hole-Drilling Strain-Gage Method of Measuring Residual Stresses," *Experimental Mechanics*, Vol. 6, No. 12, pp. 577-586 (1966).

10. A. M. Nawwar, K. McLachlan and J. Shewchuk, "A Modified Hole-Drilling Technique for Determining Residual Stresses in Thin Plates," *Experimental Mechanics*, Vol. 16, No. 6, pp. 226-232 (1976).

11. A. M. Nawwar and J. Shewchuk, "On the Measurement of Residual-Stress Gradients in Aluminum-alloy Specimens," *Experimental Mechanics*, Vol.18, No. 7, pp. 269-276 (1978).

12. "Standard Test Method for Determining Residual Stresses by the Hole-Drilling Strain-Gage Method," E837-89, *Annual Book of ASTM Standards*, ASTM, Philadelphia, PA.

13. "Measurements of Residual Stresses by the Blind Hole Drilling Method," Technical Data Bulletin T-503-3, Photolastic Division, Measurements Group, Wendell, NC.

14. A. Ajovalasit, "Measurement of Residual Stresses by the Hole-Drilling Method: Influence of Hole Eccentricity," *Journal of Strain Analysis*, Vol. 14, No. 4, pp. 171-178 (1979).

15. J. P. Sandifer and G. E. Bowie, "Residual Stress by Blind-Hole Method with Off-Center Hole," *Experimental Mechanics*, Vol. 18, No. 5, pp. 173-179 (1978).

16. A. McDonach, J. McKelvie, P. MacKenzie and C. A. Walker, "Improved Moire Interferometry and Applications in Fracture Mechanics, Residual Stress and Damaged Composites," *Experimental Techniques*, Vol. 7, No. 6, pp. 20-24 (1983).

17. D. V. Nelson and J. T. McCrickerd, "Residual-Stress Determination Through Combined Use of Holographic Interferometry and Blind-Hole Drilling," *Experimental Mechanics*, Vol. 26, No. 4, pp. 371-378 (1986).

18. G. Sachs, "The Determination of Residual Stresses in Rods and Tubes," *Zeitschrift fur Metallkunde*, Vol. 19, pp. 352-357 (1927).

19. J. W. Lambert, "A Method of Deriving Residual Stress Equations," *Proceedings of SESA*, Vol. 12, No. 1, pp. 96-99 (1954).

20. R. Srinivasan, C. S. Hartley and R. Bandy, "Residual Stress Determination in Inconel-600 Tubes Using Electrochemical Machining," Novel Techniques in Metal Deformation Testing, ed. R. Wagoner, TMS-AIME, Warrendale, PA, pp. 163-174 (1983).

21. J. Rasty and C. S. Hartley, "Experimental Measurement of Residual Stresses in Nuclear Fuel Cladding," *Proceedings of the 1986 SEM Spring Conference on Experimental Mechanics*, pp. 39-46, New Orleans, LA (June 1986).

22. W. A. Olson and C. W. Bert, "Analysis of Residual Stresses in Bars and Tubes of Cylindrically Orthotropic Materials," *Experimental Mechanics*, Vol. 6, No. 9, pp. 451-457 (1966).

23. G. Z. Voyiadjis, P. D. Kiousis and C. S. Hartley, "Analysis of Residual Stresses in Cylindrically Anisotropic Materials," *Experimental Mechanics*, Vol. 25, No. 2, pp. 145-147 (1985).

24. G. Z. Voyiadjis and C. S. Hartley, "Residual-Stress Determination of Concentric Layers of Cylindrically Orthotropic Materials," *Experimental Mechanics*, Vol. 27, No. 3, pp. 290-297 (1987).

25. Y. T. Toombes, M. G. Abdallah and A. K. Johnson, "An Assessment of Residual Stresses in Graphite/Epoxy Tubes," *Proceedings of the 1989 SEM Spring Conference on Experimental Mechanics*, pp. 27-32, Boston, MA (May 1989).

26. J. W. Dally and W. F. Riley, Experimental Stress Analysis, McGraw-Hill Book Company, 2nd ed., New York, 1978.

27. Y. Miyano, S. Nakamura, S. Sugimor, T. Kunio and T. C. Woo, "A Simplified Optical Method for Measuring Residual Stress by Rapid Cooling in Thermosetting Resin Strip," *Experimental Mechanics*, Vol. 26, No. 2, pp. 185-192 (1986).

28. L. E. Hornberger and K. L. DeVries, "Measurement of Favorable Residual Stresses in Polycarbonate," *Experimental Mechanics*, Vol. 27, No. 1, pp. 94-98 (1987).

29. C. P. Burger, T. H. Baek, V. Marzen and D. Tarudji, "The Study of Thermal Stresses Induced During the Production of Encapsulated Ceramics," *Proceedings of the 1986 SEM Spring Conference on Experimental Mechanics*, pp. 59-64, New Orleans, LA (June 1986).

30. T. Tokuoka and Y. Iwashimizu, "Acoustical Birefringence of Ultrasonic Waves in Deformed Isotropic Elastic Materials," *International Journal of Solids and Structures*, Vol. 4, pp. 383-389 (1968).

31. H. Fukuoka, H. Toda and T. Yamane, "Acoustoelastic Stress Analysis of Residual Stress in a Patch-welded Disk,".*Experimental Mechanics*, Vol. 18, No. 7, pp. 277-280 (1978).

32. H. Fukuoka, H. Toda and H. Naka, "Nondestructive Residual-stress Measurement in a Wide-flanged Rolled Beam by Acoustoelasticity," *Experimental Mechanics*, Vol. 23, No. 3, pp. 120-128 (1983).

33. P. J. Noronha and J. J. Wert, "An Ultrasonic Technique for the Measurement of Residual Stress," *Journal of Testing and Evaluation*, Vol. 3, No. 2, pp. 147-152 (1975).

34. G. C. Johnson, "On the Applicability of Acoustoelasticity for Residual Stress Determination," *Journal of Applied Mechanics*, Vol. 48, No. , pp. 791-795 (1981).

35. G. C. Johnson, "Acoustoelastic Theory for Elastic-Plastic Materials," *Journal of the Acoustical Society of America* , Vol. 70, No. 2, pp. 591-595 (1981).

36. W. Y. Lu, "Residual Stress Evaluation by Ultrasonics in an Elastic-Plastic Material," *Proceedings of the 1983 SESA Spring Conference on Experimental Mechanics*, pp. 77-83, Cleveland, Ohio (May 1983).

37. I. M. Daniel, J. L. Mullineaux, F. J. Ahimaz and T. Liber, "The Embedded Strain Gage Technique for Testing Boron/Epoxy Composites," *ASTM STP* 497, pp. 257-272 (1972).

38. I. M. Daniel, T. Liber and C C Chamis, "Measurement of Residual Strains in Boron-Epoxy and Glass-Epoxy Laminates," *ASTM STP* 580, pp. 340-351 (1975).

39. I. M. Daniel and T. Liber, "Lamination Residual Strains and Stresses in Hybrid Laminates," *ASTM STP* 617, pp. 330-343 (1977).

40. I. G. Zewi, I. M. Daniel and J. T. Gotro, "Residual Stresses and Warpage in Woven-Glass/Epoxy Laminates," *Experimental Mechanics*, Vol. 27, No. 1, pp. 44-50 (1987).

41. I. M. Daniel and T. Liber, "Effect of Laminate Construction on Residual Stresses in Graphite/Polyimide Composites," *Experimental Mechanics*, Vol. 17, No. 1, pp. 21-25 (1977).

42. J. Guild, The Interference Systems of Crossed Diffraction Gratings; Theory of Moire Fringes, Clardendon Press, Oxford (1956).

43. R. Czarnek, "New Methods in Moire Interferometry," *Ph.D. Dissertation*, VPI&SU (Dec. 1984).

44. R. Czarnek, "Three-Mirror, Four-Beam Interferometer and Its Capabilities," *Optics and Lasers in Engineering* (in press).

45. R. Czarnek, "Super High Sensitivity Moire Interferometry with Optical Multiplication," *Optics and Lasers in Engineering* (in press).

46. M.-Y. Tsai, "Application of Localized Hybrid Methods of Stress Analysis to Some Problems in the Mechanics of Composites," *Ph.D. Dissertation*, VPI&SU (Nov. 1990).

VITA

Joosik Lee

Joosik Lee was born on November 23, 1960 in Seoul, Korea to Jo Won, an architect, and Soon-bin Hong Lee.

His college education began in 1979 when he was admitted to the engineering college of Hanyang University in Seoul, Korea, where he received his B.S. degree in Mechanical Engineering in 1983. He continued his graduate study at the same school until he went to the Mechanical and Aerospace Engineering Department of Syracuse University in Syracuse, New York in 1984 as an M.S. candidate. After completing course work and performing analytical research on high-temperature creep behavior of metals there, he found himself to be interested in experimental work and transferred to Virginia Polytechnic Institute and State University as a Ph.D. candidate in 1986. Since then, he has conducted his research work on experimental mechanics under the guidance of Prof. Czarnek. His current research area includes development of experimental methods, emphasized on moire interferometry, and their application to mechanics of high performance structural materials such as fiber-reinforced composites.